The Pennsylvania State University

The Graduate School

Department of Chemistry

BARCODED METAL NANOWIRES FOR

MULTIPLEXED DNA HYBRIDIZATION ASSAYS

A Thesis in

Chemistry

by

Rebecca L. Stoermer

Submitted in Partial Fulfillment
of the Requirements
for the Degree of

Doctor of Philosophy

December 2006

The thesis of Rebecca L. Stoermer was reviewed and approved* by the following:

Christine D. Keating
Assistant Professor of Chemistry
Thesis Advisor
Chair of Committee

Thomas E. Mallouk
DuPont Professor of Chemistry and Physics

Paul S. Weiss
Distinguished Professor of Chemistry and Physics

Ming Tien
Professor of Biochemistry

Ayusman Sen
Professor of Chemistry
Head of the Department of Chemistry

*Signatures are on file in the Graduate School

ABSTRACT

This thesis work was aimed towards developing multiplexed DNA hybridization assays using barcoded metal nanowires. These nanowires are typically several microns in length and ~300 nm in diameter, having segments of different metals along their lengths. They are promising for multiplexed bioanalysis due to the large number of striping patterns that can be synthesized, and the ease of optical read-out using simple reflectance microscopy. Oftentimes silver is used as one of the metals in the striped wires due to its high reflectivity at all visible wavelengths and large reflectance contrast to other metals. Since Ag metal is susceptible to oxidation, the long-term stability of Ag-containing wires in aqueous buffers was investigated and is reported in Chapter 2. It was found that wires stored in hybridization buffer for longer than two weeks began to show significant degradation of Ag segments. When agitated with continuous vortexing, the Ag oxidation progressed more rapidly, rendering the barcoded metal nanowires stored in hybridization buffer unidentifiable in less than one week. Addition of 40 mM citrate as a mild reducing agent increased Ag stability by 17 weeks over those stored in hybridization buffer. Nanowires subjected to continuous vortexing in 40 mM citrate buffer retained Ag segment stability for longer than 2 weeks. Derivatization of the wires with biomolecules such as are used in bioassays affords some additional protection against Ag degradation. Also, it has been discovered that wires coated with rhodamine-tagged DNA oligonucleotides attached via neutravidin-biotin chemistry are stable for 12 days in hybridization buffer and for at least 63 days when 40 mM citrate is added as a reducing

agent. Ag deterioration in these experiments was coupled to loss of fluorescence from the labeled DNA, as well as wire breakage.

When fluorescently-tagged oligonucleotides are located near metal surfaces, their emission intensity is impacted by both electromagnetic effects (i.e., quenching and/or enhancement of emission) and the structure of the nucleic acids (e.g., random coil, hairpin, or duplex). In Chapter 3, experiments are presented that explore the effect of label position and secondary structure in oligonucleotide probes as a function of hybridization buffer, which impacts the percentage of double-stranded probes on the surface after exposure to complementary DNA. Nanowires containing identifiable patterns of Au and Ag segments were used as the metal substrates in this work, which allowed for direct comparison of different dye positions in a single multiplexed experiment and differences in emission for probes attached to the two metals. The observed metal-dye separation dependence for unstructured, surface-bound oligonucleotides is highly sensitive to hybridization efficiency, due to substantial changes in DNA extension from the surface upon hybridization. In contrast, fluorophore-labeled oligonucleotides designed to form hairpin secondary structures analogous to solution-phase molecular beacon probes are relatively insensitive to hybridization efficiency, since the folded form is quenched and therefore does not appreciably impact the observed distance-dependence of the response. Differences in fluorescence patterning on Au and Ag were noted as a function of not only chromophore identity, but also metal–dye separation. For example, emission intensity for tetramethylrhodamine (TAMRA)-labeled oligonucleotides changed from brighter on Ag for 24-base probes to brighter on Au for 48-base probes. Fluorescence enhancement at the ends of nanowires and at surface

defects were also observed, where heightened electromagnetic fields affect the fluorescence.

For the research presented in Chapter 4, molecular beacon probes have been combined with barcoded metal nanowires to enable no-wash, sealed-chamber, multiplexed detection of nucleic acids. Probe design and experimental parameters important in nanowire-based molecular beacon assays are discussed. Loop regions of 24 bases and five-base-pair stem regions in the molecular beacon probes gave optimal performance. The results suggest that thermodynamic predictions for secondary structure stability of solution-phase MB can guide probe design for nanowire-based assays. The predicted solution phase ΔG for probes in 500 mM buffered NaCl of approximately –4 kcal/mol performed better than those with $\Delta G > -2$ or < -6 kcal/mol. Buffered 300 and 500 mM NaCl solutions were selected after comparison of several buffers previously reported for similar types of assays, and concentrations in the range of 300 to 750 mM NaCl was found to be the optimal ionic strength for the hybridization temperature (25 ^{o}C) and probe designs used here. The sensitivity of this assay was ~100 pM and was limited by incomplete quenching. Single base mismatches could be discriminated from fully complementary targets. Oligonucleotide target sequences specific for Human Immunodeficiency, Hepatitis C, and Severe Acute Respiratory Viruses were assayed simultaneously in a no-wash, sealed-chamber, multiplexed experiment in which each of three probe sequences was attached to a different pattern of encoded nanowires. Finally, demonstrated in this chapter is that probe-coated nanowires retain their selectivity and sensitivity in a triplexed assay after storage for over three months.

With the increasing interest in simultaneous detection of specific DNA hybridization events, the development of methods to measure multiple DNA interactions at one time is of great importance. Conventional microarrays allow thousands of DNA hybridization interactions to be measured at once; however, this method of detection is limited by high cost as well as the stability and characteristic properties of fluorescent dyes. In Chapter 5, barcoded nanowires were investigated as replacements for fluorophores on glass surfaces such as those used in microarrays. Potential advantages of nanowires include ease of reflectance-based optical read-out, the large number of tags available, and ability to distinguish multiple hybridizations occurring in a single DNA spot. A method of attaching DNA to glass microscope slides was employed which includes the use of a carboxy-terminated silane to derivatize glass slides for DNA attachment. Also determined here is the efficiency of using nanowires as tags in complementary DNA hybridization events. An average of ~5 % nonspecific binding was reported for nanowire attachment for all samples.

In all chapters, it has been demonstrated that barcoded metal nanowires have promising uses in multiplexed bioanalysis for the detection of multiple analytes simultaneously. The metal surfaces have provided useful information about interactions between fluorophores and metals and DNA hybridization events (as described in Chapter 3). The surfaces, however, are subject to oxidation of silver segments (Chapter 2), and occasional pits in the metal surfaces have led to fluorescence enhancements at those pits, causing non-uniform fluorescence (Chapter 3). Also, non-uniformity in signal intensity results from different underlying metals acting differently on the fluorophores, as well as the distance the fluorophores are positioned from the surface (Chapter 3). To avoid the

effects that the metal surfaces impose on fluorophores, nanowires were glass coated before use as substrates for fluorescently labeled bioassays. This work is presented in Chapter 6. Two different glass thicknesses (13.5 nm and 100 nm) were prepared and studied and 100 nm thickness provided the best surface, as the glass coating that resulted was very uniform. Also studied were the protective benefits that the silicon dioxide layers provide by shielding the silver segments from oxidative environments. We note that a 100 nm thick glass coating on the wires provided excellent resistance to dissolution of Ag segments when sonicated in nitric acid for 30 min and retained the same overall length and optical properties. Also shown in Chapter 6 is the feasibility of using glass coated nanowires as substrates in 2-plex assays where a single base mismatch in the target DNA sequence of a gene that affects the function of a tumor suppressor protein was detected.

TABLE OF CONTENTS

LIST OF FIGURES

LIST OF TABLES

LIST OF ABBREVIATIONS

APTMS	aminopropyltrimethoxysilane
BSA	bovine serum albumine
CB	citrate buffer
CEST	carboxyethylsilanetriol
DNA	deoxyribonucleic acid
DTT	dithiothreitol
DV	Dengue Virus
EDC	[1-ethyl-3-(3-dimethylaminopropyl)carbodiimide hydrochloride]
FE-SEM	field-emission scanning electron microscopy
HB	hybridization buffer
HCV	Hepatitis C Virus
HIV	Human Immunodeficiency Virus
LSPR	localized surface plasmon resonance
MB	molecular beacon
mRNA	messenger ribonucleic acid
MUA	mercaptoundecanoic acid
NA	NeutrAvidin™
NBCs	Nanobarcodes™
NHS	[sulfo-*N*-hydroxysuccinimide]
PBS	phosphate buffer saline
QE	quenching efficiency

RNA	ribonucleic acid
SA	streptavidin-Cy5
SARS	Severe Acute Respiratory Syndrome
SDS	sodium dodecyl sulfate
SEF	surface enhanced fluorescence
SEI	secondary electron imaging
SEM	scanning electron microscopy
SNP	single nucleotide polymorphism
SPR	surface plasmon resonance
SSA	succinic anhydride
TEM	transmission electron microscopy
TEOS	tetraethylorthosilicate
TMAC	tetramethyl-ammonium chloride

ACKNOWLEDGMENTS

Graduate school has taught me more valuable skills than just the ability to plan, to design, and to execute experiments. It has taught me new ways to think, to analyze, and to address things, both inside and outside of my research. It has taught me the importance of theory, hypothesis, and proof, and arguably, more importantly, has taught me to be confident in my ideas. I have discovered that the more I learn, the more I know; however, the more I learn, I learn that there is more to know.

In saying that graduate school has taught me valuable skills, what I should really say is that Dr. Christine Keating has taught me valuable skills. Without her drive and enthusiasm, this process would not have been nearly as rewarding. She has always pushed me to work hard and strive for the best. She sets a good example; she was always working hard for us. Thank you, Chris, for your guidance, motivation, and encouragement.

I would like to thank my committee, Dr. Tom Mallouk, Dr. Paul Weiss, and Dr. Marty Bollinger for all of their help and advice throughout my graduate career. Also, I would like to thank Dr. Ming Tien, for coming to the rescue and being willing to serve on my thesis defense committee on last minute notice in place of Marty. Marty, I wish you the best of success in guiding your wife and supporting her through her illness.

I would also like to thank all the members of our research group who have helped to lift my spirits when they needed lifting and for your help and support when I have needed it. To those of you who have left the group, I thank you for your help, inspiration, and guidance, and to those of you who are to follow, I also thank you, and encourage you

to “hang in there” and always strive for your best. James Sioss, thank you for your friendship, good laughs, and help with collecting SEM images and NBSee analysis for experiments presented in Chapter 2. Quis Cederquist and Sean McFarland, thank you for your help in collecting stem length and salt concentration data presented in Chapter 4.

To my family and friends who have supported my every decision (or at least pretended to!), I owe you the most. I will never forget, Dad, the words of encouragement and praise that you wrote in a card that you gave to me after my first year of undergraduate college. The line in the card that you wrote suggesting that I had the “right amount of work, play, and study to keep me going”, I have never forgotten. These words are still important to me and have helped to remind me of who I am. This balance was critical in allowing me to get through graduate school. Mom, I could not have gotten as far as I have without all of your help. Thank you for supporting my decisions throughout, and never holding me back. Anything I ever proposed, you would always try to help me make it happen. Without this kind of support, I would not be where I am today. To my sister, who hates when I am away so much, but loves when I spend time with her, you constantly remind me of the things in life that are important. You are truly one of the strongest people I have ever met. You have been able to cope with a progressive handicap better than I have ever imagined that I could. Thank you for encouraging me, despite all of the troubles you have been faced with. I love that you can still put on a smile, laugh, and cry for other people. You are truly an inspiration to many, including a huge inspiration to me, and I love you a ton. To my brother, whom I have always looked up to and admired, you are fun and funny and have one of the biggest hearts of anyone I have met. Thank you for your curiosity in what I have been studying

and researching and your interest in what I do. It is inspiring to me that you take interest in what I do. I appreciate your support and love you a lot. To the rest of my family and friends that have taken a profound interest in my many decisions and have been supportive, I graciously thank you.

Chapter 1

Introduction

1.1. Barcoded Nanowires

Metal nanowires have been prepared with segments of different materials along their lengths. These particles can be synthesized in a large number of optically distinguishable striping patterns, and thus have been referred to as barcoded nanowires. These barcoded wires can be used for encoding information such as the type of biological assay being performed on the surface of the particle. Thus, they have application in multiplexed bioanalysis. Striped metal nanowires, synthesized by templated electrodeposition, are tens to hundreds of nanometers in diameter and several microns in length. The length of each segment can be as small as tens of nanometers or as long as the entire wire.

Optically encoded (barcoded) particles also have potential applications analogous to barcodes in the retail industry, where the products are tracked by the barcode pattern. Typically, the barcode labels used on retail products are readily identifiable to the human eye. In addition to these overt tags, there is also interest in microscopic barcodes invisible to the naked eye. Striped nanowires can serve as such microscopic identifiers and have enormous potential for use in biological sensing applications where many different bioassays must be followed simultaneously. In this last application, the barcoded nanowires perform a function analogous to the individual spots of a DNA microarray, encoding the identity of biomolecules attached to their surface.

1.2. Synthesis of Striped Metal Nanowires

Striped metal nanowires are typically prepared by electrochemically reducing metal ions into the pores of a template. Porous aluminum oxide or track-etch membranes are commonly used.[1-6] Alumina membranes are prepared by anodizing Al at constant potential to give a nanoporous membrane.[4,6] Pore diameters can be varied (from tens to several hundred nanometers) by controlling the anodization potential.[5] Track-etch membranes are prepared by using nuclear fission fragments to attack a nonporous sheet of desired material (e.g. polycarbonate, or polyester), to yield indentations in the material that are further chemically etched into pores.[6]

To produce barcoded nanowires electrochemically, one side of a template membrane (e.g. Al_2O_3) is coated with a silver film to serve as a cathode for reducing metal ions from solution into the pores of the membrane template. This can be accomplished by vapor deposition or sputtering. The opposite side of the template is then immersed in a plating solution of a desired metal for electrochemical deposition. The length of the metal stripe created is dictated by the amount of current passed and the amount of time the metal is allowed to deposit. Once a stripe of a desired length has been created, the plating solution is simply changed such that the next metal segment can be added. The thickness of each individual stripe can in principle be controlled with great accuracy during the electrodeposition process.[7-8] Indeed, repeating Cu and Co segments only 8 nm thick have been prepared from a solution containing both metal ions.[9] Selective electrodeposition of each metal from this solution is accomplished by careful control over plating solution composition (i.e. relative concentrations of the two metal

ions) and the electrode potential, which is switched between values favoring Cu deposition to those favoring Co deposition during synthesis.[10-12]

The aspect ratio (l/d, where l is the length and d is the diameter of the nanowires) of the wires is controlled by the membrane pore diameter (which dictates the wire's width), and the amount of deposition time (which determines the length). The maximum wire length is limited by the thickness of the template (which is roughly 50-60 μm for commercial alumina membranes) and to breakage for wires with high aspect ratios (~25:1 aspect ratio). Once the electrochemical deposition is complete, the silver backing and membrane are dissolved away, leaving behind a suspension of striped metal nanowires.

To date, barcoded nanowires have been prepared with Au, Ag, Pt, Pd, Ni, Co, and Cu metal segments.[13] Figure 1.1a shows a reflectance image of a 320 nm diameter AuAgPd striped nanowire imaged at a wavelength of 430 nm. At this wavelength, Au has the lowest reflectivity, followed by Pd, then Ag. Figure 1.1 shows that these metals can be optically distinguished based on reflectivity differences. The number of possible distinctive patterns or permutations available to the barcoded metal wires is m^s, where m is the number of metal types and s is the number of stripes in each wire. For example, wires consisting of 4 metals (ie, Au, Pt, Co, and Ag) with 6 stripes leads to 4,096 possible striping patterns ($4^6 = 4{,}096$). Ag/Au striped wires having 13 distinguishable stripes have been reported; $2^{13} = 8{,}192$ possible patterns.[14] Addition of a third metal leads to over 1.5 million possible patterns. To account for patterns that repeat in the forward and reverse direction, the following equation should be used: $possibilities = \frac{m^s + m^{ceil(\frac{s}{2})}}{2}$, where m is the number of metals in the nanowires, s is the number of stripes, and ceil stands for ceiling

function, which rounds the exponent of *n* to the next highest integer (i.e. 3/2 rounds up to 2). Using this equation, the actual number of different patterns that could be obtained from a 4-metal, 6-stripe wire is 2,080, and for a 3-metal, 13-segment particle is 7.98 x 10^5.

1.3. Nanowire Characterization

Once nanowires are fabricated, they are characterized via many methods to determine their actual compositions, sizes, shapes, optical, and magnetic properties. Transmission electron microscopy (TEM) is used to determine the size and shape of nanowires. Scanning electron microscopy (SEM) is used to examine the stripes and the metal-metal interfaces between segments. With SEM, striping patterns of heterostructured nanowires and surface defects can be identified that cannot be detected using TEM. Figure 1.2 is an example of a field emission (FE) SEM image of a 5-μm-long, 320-nm-diameter AuAuAgAu striped nanowire. Energy dispersive X-ray spectroscopy is used to determine the average chemical composition of nanowires, including the microstructure of single metal and multilayered wires.[15-17]

In identifying the striping pattern in barcoded nanowires, optical reflectance microscopy is used. The striping pattern is deciphered based on reflectance differences of adjacent metal stripes. For optical resolution using reflectance detection, the different metal segments have to be separated by a distance greater than $\lambda/2NA$, were NA is the numerical aperture of the objective lens (a typical oil immersion lens has NA = 1.4). The optical properties of 320-nm-diameter nanowire segments resemble those of their bulk counterparts.[5,18-22] Reflectance values for various bulk metals, plotted over a range of

wavelengths, are shown in Figure 1.3.[23] The differences in reflectivity of the various metal types allows for the detection of multiple metal stripes in a single barcoded nanowire. Figure 1.1b shows a line scan of the AuAgPd striped nanowire pictured in Figure 1.1a. This scan illustrates the changes in reflectance intensity across the length of the wire. Walton *et al.*[24] have demonstrated a 100-particle library of barcoded nanowires in which more than 70 of the patterns could be identified with greater than 90% accuracy. These authors developed software (called NBSee) for rapid readout of barcode striping patterns.

1.4. Biological Multiplexing

Performing many simultaneous experiments (i.e. multiplexing), has become an important theme in bioanalysis. For example, functional genomics experiments often follow mRNA expression levels for many or even all genes in an organism's genome simultaneously. These experiments employ fluorescence on planar microarrays in which spots of DNA corresponding to the different genes of an organism's genome are positioned on a planar glass slide.[25,26] The x,y coordinates of each spot correlate to its identity. Microarrays permit the detection of thousands to tens of thousands of species at once, saving both time and reagents. However, there are some drawbacks of using microarrays, which include limitations in the dynamic range of analyte detection, long diffusion times for analyte binding, and variations in fluorescence signals between arrays.[27] Encoded particles have been introduced to address issues of diffusion and increase flexibility in microarray design.[28,29] Polystyrene microbeads incorporating red and infrared fluorescent dyes in different intensity ratios are one type of encoded particle

introduced for use in multiplexing applications.[30-32] Although microbeads offer improved diffusion as compared to two-dimensional arrays, the use of fluorescence limits the number of species that can be simultaneously detected, as the spectral bandwidths of the fluorescent peaks are large and oftentimes overlap. Semiconductor quantum dots, which have reduced spectral bandwidths compared to molecular dyes, have been used in place of organic fluorophores in encoded beads as well as other applications.[33-38] These particles are very promising for multiplexing, and are resistant to photobleaching; however, the detection still relies on fluorescence, which ultimately limits the number of species that are possible to detect simultaneously (i.e. only one color of fluorophore can typically be used in detection, as other channels are occupied with encoding the particle identity).

Barcoded nanowires are a promising alternative to fluorescent tags in some applications. The barcode striping pattern will not photobleach, reflective read-out is simple and does not require expensive excitation sources or detectors, and many patterns can be synthesized and are optically detectable. These particles can be employed as encoded substrates for biosensing, analogous to DNA chips, or as tags for simultaneous detection and identification, analogous to fluorescent molecules or nanocrystals. Figure 1.4 illustrates the second approach, where barcoded nanowires may potentially be used as tags to detect and to identify specific DNA hybridization events. In this example, a glass slide is spotted with several different capture sequences of DNA selective to the 5' (or 3') region of the target sequence. Target sequences, labeled double prime (") in the figure, bind to the surface via hybridization to these capture strands. They are then detected by hybridization-driven assembly of barcoded nanowires that carry a third strand of DNA,

complementary to the 3' (or 5') region of the target sequence. Optical reflectance microscopy can then be used to count and identify the wires bound to each spot on the surface, giving the amount and identity of target molecules present in the initial solution. This approach is conceptually simple and does not require fluorescence for detection. Improvements in the selectivity of nanoparticle attachment will be important for the ultimate use of this approach in multiplexed analyses.[39]

Barcoded nanowires not only serve as identifying markers, but also can serve as easily detectable substrates on which binding events take place.[40] Figure 1.5 illustrates how barcoded nanowires can serve as encoded substrates for antigen and DNA detection.[41] Figure 1.5 (left) illustrates a standard sandwich immunoassay performed on the nanowire surface. The striped particles are first derivatized with a capture antibody (*a*) that is specific for an analyte, which in this case is also an antibody. Following incubation of the capture antibody with the analyte (*b*), a fluorescently labeled detection antibody (*c*) is added. Figure 1.5 (right) shows the analogous experiment for DNA detection. Here the barcoded nanowire serves as the substrate on which a DNA probe sequence (*a*) is attached. Probe sequences are designed to be complementary to one half of the target sequence, as in the previous example (Figure 1.4). The target DNA sequence (*b*) binds to the probe from solution via hybridization, and is subsequently detected by hybridization to a fluorescently tagged third DNA strand (*c*). In either of these two types of bioassay, target detection and quantification is made possible by the fluorescence intensity of the labeled probe molecules, while target identification (i.e. DNA sequence) is determined by the nanowire barcode pattern as observed in reflectivity optical microscopy.[40,41]

Both immunoassays and DNA hybridization assays have been performed on barcoded nanowires.[40,41] Nicewarner-Pena et al. demonstrated two simultaneous immunoassays in which two different fluorescent dyes were employed.[40] Keating and coworkers have reported three simultaneous DNA assays using a single fluorescent probe for all three assays.[41] Under some conditions, it proved possible to observe the barcode striping pattern in the fluorescence image,[41] such that acquisition of a single image enabled both identification and detection. Barcoded nanowire libraries of 100 particles have already been reported[24] and could be combined with these types of biological assays for increased multiplexing. Ultimately, it should be possible to perform thousands or tens of thousands of different DNA hybridizations simultaneously on different particles in the same suspension, similar to the level of multiplexing now possible only with planar DNA microarrays.

1.5. Objectives

The main objective of this thesis work is to develop multiplexed DNA hybridization assays using barcoded metal nanowires. Many factors important to bioassay design have been explored and are presented in this work. Chapter 2 illustrates a method for preventing the oxidation of silver segments in striped metal wires once biomolecules are attached. This research is important for the storage of biomolecule derivatized nanowires, particularly when there is interest in reanalysis of a pre-reacted sample. Also, for assays aimed at detecting DNA targets, it is ideal to provide nanowire surfaces pre-derivatized with DNA probe sequences for convenience of assay performance. Once biomolecules are attached to Au and Ag nanowires, it is ideal to store

them in a buffer solution to preserve the integrity of the biomolecule. Buffer solutions, however, prove to oxidize silver segments of the wires. This chapter offers a solution to this problem by using sodium citrate reducing agent in the buffer to prevent deterioration of silver segments.

Chapter 3 details the investigation of optimal fluorophore proximities from the metal nanowire surfaces for achieving both quenching and unquenching of fluorescence. This work was performed primarily to develop guidelines for designing DNA molecular beacon assays that rely on the metal surfaces for fluorescence quenching. Molecular beacons are hairpin-structured, single-stranded DNA probes that typically have a fluorophore molecule appended to one end and a quencher molecule at the other. In the assay presented here, the metal surface serves in place of the quencher and acts as an identifying tag for increased multiplexing abilities. In the presence of complementary DNA, the beacon changes conformation and moves the fluorophore further from the metal surface, allowing it to fluoresce. If no complementary DNA is present, the beacon fluorophore remains close to the metal surface of the wire and will be quenched. This chapter also illustrates the importance of hybridization efficiency when performing DNA assays on metal surfaces, as the fluorescence trends as a function of distance change depending upon the hybridization efficiency of the assay. Because nanowires that contained both silver and gold segments were used, we were able to directly compare differences in intensity for fluorescent probes attached to two different metals.

Chapter 4 utilizes the discovered phenomena described in Chapter 3 to develop nanowire bound molecular beacon assays further. The main advantage of creating such assays stems from the numerous identifying tags that can be produced as barcoded metal

nanowires, such that multiplexing capabilities become impressive. Further studies presented here include; effects of beacon design, different methods of adsorbing the beacons to the nanowires, analysis of beacon assays after long term storage in a citrate buffer, and performance of closed tube assays. Also described here were effects of different salt concentrations on beacon quenching efficiency.

The focus of Chapter 5 was to develop an array-based sensor, similar in design to a DNA microarray, which relies on barcoded metal nanowires as tags for DNA binding events. This array sensor has the capabilities of being highly multiplexed and does not rely on fluorescence for the detection of binding interactions. In this chapter, data are presented where discrimination between two different patterned wires, one with and one without complementary DNA, allowed only ~5 % nonspecific binding of the wires with noncomplementary DNA. These data suggest the possibility of creating a multiplexed array using barcoded metal nanowires as tags for DNA binding interactions.

Because metal surfaces greatly affect fluorescence signal in terms of quenching and enhancement, and different metals exhibit different properties on fluorophores, there was interest in exploring the use of glass-coated metal nanowires in multiplexed bioapplications. The glass coating was expected to provide a barrier for the fluorophores and reduce the effects of the metal on fluorescence signal. Chapter 6 describes methods to glass coat wires to achieve different glass thicknesses and tests the stability of these wires by continual sonication in nitric acid, which is known to dissolve silver segments. Here, it is shown that the glass coating allowed for uniform fluorescence along wires and prevented longer wires from breaking when derivatized with biomolecules. Also

presented are 2-plex assays conducted on both glass- and non-glass-coated wires towards the detection of DNA sequences differing by only a one base mismatch.

1.6. References

1. Brumlik, C. J.; Menon, V. P.; Martin, C. R. J. *J. Mater. Res. 1994*, *9*, 1174-1183.
2. Yi, G.; Schwarzacher, W. *Appl. Phys. Lett*. **2000**, *74*, 1746-1748.
3. Dubois, S.; Michel, A.; Eymery, J. P.; Duvail, J. L.; Piraux, L. J. *J. Mater. Res.* **1999**, *14*, 665-671.
4. Masuda, H.; Nishio, K.; Baba, N. *Thin Solid Films* **1993**, *223*, 1-3.
5. Hornyak, G. L.; Patrissi, C. J.; Martin, C. R. *J. Phys. Chem. B* **1997**, *101*, 1548-1555.
6. Martin, C. R. *Science* **1994**, *266*, 1961-1966.
7. Paunovic, M.; Schlesinger, M. *Fundamentals of Electrochemical Deposition*; John Wiley & Sons, Inc.: New York, 1998.
8. Schlesinger, M.; Paunovic, M. *Modern Electroplating*; John Wiley & Sons, Inc.: New York, 2000.
9. Wu, Y.; Fan, R.; Yang, R. P. *Nano Lett.* **2002**, *2*, 83-86.
10. Liu, K.; Nagodawithana, K.; Searson, P. C.; Chien, C. L. *Phys. Rev. B* **1995**, *51*, 7381-7384.
11. Fert, A.; Piraux, L. *Magn. Magn. Mater*. **1999**, *200*, 338-358.
12. Hong, K.; Yang, F. Y.; Liu, K.; Reich, D. H.; Searson, P. C.; Chein, C. L. *J. Appl. Phys.* **1999**, *85*, 6184-6186.
13. Keating, C. D.; Natan, M. J. *Adv. Mat.* **2003**, *15*, 451-454.
14. Reiss, B. D.; Freeman, R. G.; Walton, I. D.; Norton, S. M.; Smith, P. C.; Stonas, W. G.; Keating, C. D.; Natan, M. J. *J. Electroanal. Chem.* **2002**, *522*, 95-103.
15. Hu, J.; Odom, T. W.; Lieber, C. M. *Acc. Chem. Res.* **1999**, *32*, 435-445.

16. Lui, B.; Zeng, H. C. *J. Am. Chem. Soc.* **2003**, *125*, 4430-4431.

17. Piraux, L.; Dubois, S.; Duvail, J. L.; Ounadjela, K.; Fert, A. *J. Magn. Magn. Mater.* **1997**, *175*, 127-136.

18. Link, S.; El-Sayed, M. A. *J. Phys. Chem. B* **1999**, *103*, 8410-8426.

19. Foss, C. A.; Hornyak, G. L.; Stockert, J. A.; Martin, C. R. *J. Phys. Chem.* **1994**, *98*, 2963-2971.

20. Preston, C. K.; Moskovits, M. *J. Phys. Chem.* **1993**, *97*, 8495-8503.

21. Hulteen, J. C.; Patrissi, C. J.; Miner, D. L.; Crosthwait, E. R.; Oberhauser, E. B.; Martin, C. R. *J. Phys. Chem. B* **1997**, *101*, 7727-7731.

22. Link, S.; Mohamed, M. B.; El-Sayed, M. A. *J. Phys. Chem. B* **1999**, *103*, 3073-3077.

23. *CRC Handbook of Chemistry and Physics*; 71st ed.; CRC Press: Cleveland, OH, 1990.

24. Walton, I. D.; Norton, S. M.; Balasingham, A.; He, L.; Oviso, D. F.; Gupta, D.; Raju, P. A.; Natan, M. J.; Freeman, R. G. *Anal. Chem.* **2002**, *74*, 2240-2247.

25. Schena, M. *DNA Arrays: A Practical Approach*. University Press: Oxford, 1999.

26. McBeath, G.; Schreiber, S. L. *Science* **2000**, *289*, 1760-1762.

27. Shena, M. *Microarray Biochip Technology*; TelChem International, Inc.: Sunnydale, California, 2000.

28. Nolan, J. P.; Sklar, L. A. *Trends Biotechnol*. **2002**, *20*, 9-12.

29. Braeckmans, K.; De Smedt, S. C.; Leblans, M.; Pauwels, R.; Demeester, J. *Nat. Rev. Drug Dis.* **2002**, *1*, 447-456.

30. Walt, D. R. *Science* **2000**, *287*, 451-452.

31. McBride, M. T.; Gammon, S.; Pitesky, M.; O'Brien, T. W.; Smith, T.; Aldrich, J. L.; Anglois, R. G.; Colston, B.; Venkateswaran, K. S. *Anal. Chem.* **2003**, *75*, 1924-1930.

32. Stitzel, S. E.; Sein, D. R.; Walt, D. *J. Am. Chem. Soc.* **2003**, *125,* 3684-3685.

33. Bruchez, M.; Moronne, M.; Gin, P.; Weiss, S.; Alivisatos, A. P. *Science* **1998**, *281*, 2013-2018.

34. Han, M.; Gao, X.; Su, J. Z.; Nie, S. *Nat. Biotech.* **2001**, *19*, 631-635.

35. Alivisatos, A. P. *J. Phys. Chem.* **1996**, *100*, 13226-13239.

36. Colvin, V. L.; Schlamp, M. C.; Alivisatos, A. P. *Nature* **1994**, *370*, 354-357.

37. Alivisatos, A. P. *Science* **1996**, *271*, 933-937.

38. Gerion, D.; Pinaud, F.; Williams, S. C.; Parak, W. J.; Zanchet, D.; Weiss, S.; Alivisatos, A. P. *J. Phys. Chem. B* **2001**, *105*, 8861-8871.

39. Mbindyo, J. K. N.; Reiss, B. D.; Martin, B. R.; Keating, C. D.; Natan, M. J.; Mallouk, T. E. *Adv. Mater.* **2001**, *13*, 249-254.

40. Nicewarner-Pena, S. R.; Freeman, G.; Reiss, B. D.; He, L. Pena, D. J.; Walton, I. D.; Cromer, R.; Keating, C. D.; Natan, M. J. *Science* **2001**, *294*, 137-141.

41. Nicewarner-Pena, S. R.; Carado, A. J.; Shale, K. E.; Keating, C. D. *J. Phys. Chem. B* **2003**, *107*, 7360-7367.

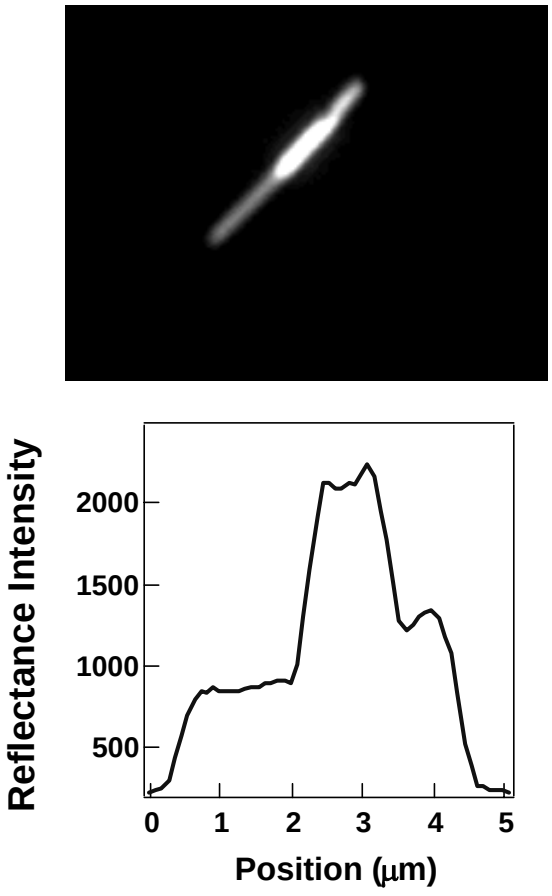

Figure 1.1. (A) Reflectance image of a AuAgPd nanowire taken at 430 nm wavelength. (B) Line scan profile of intensity versus distance along the nanowire length.

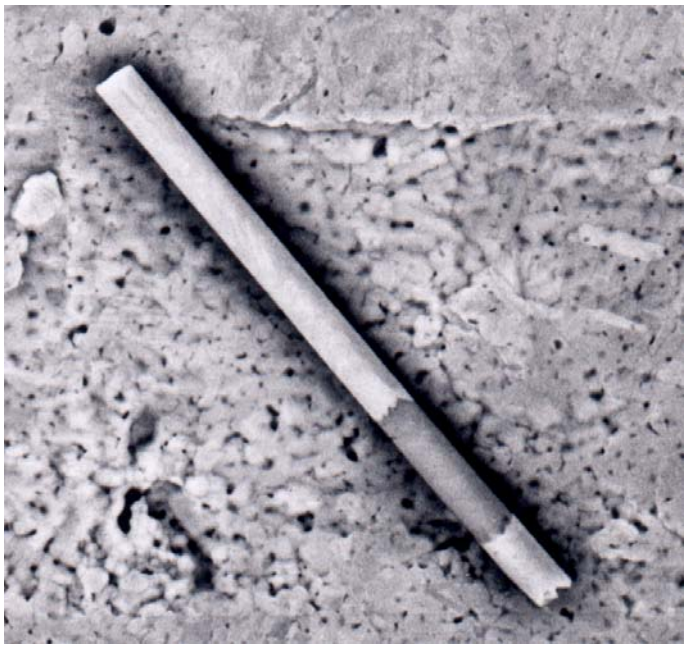

Figure 1.2. Field emission SEM image of a AuAuAgAu nanowire, acquired with backscattered electron detection. The Ag segment appears darker as compared to the Au.

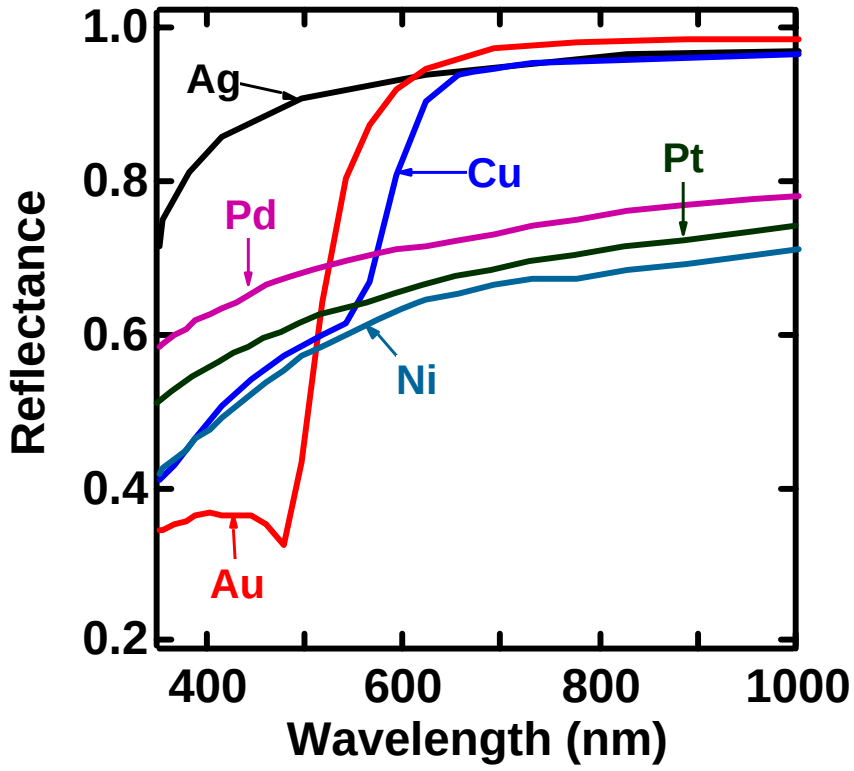

Figure 1.3. Reflectance values for various bulk metals.[41]

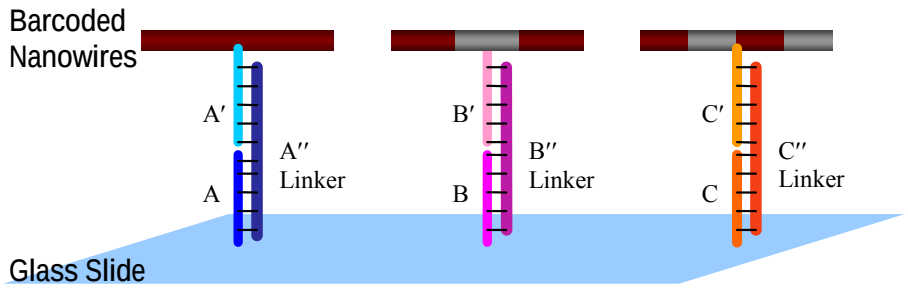

Figure 1.4. Overview of non-fluorescent bioassay using barcoded nanowires. DNA strands labeled A-C are not complementary to their primed counterparts (A′-C′), however, the strands labeled as double prime (″) link the respective sequences to their primed counterparts via complementary DNA hybridization. (Not drawn to scale).

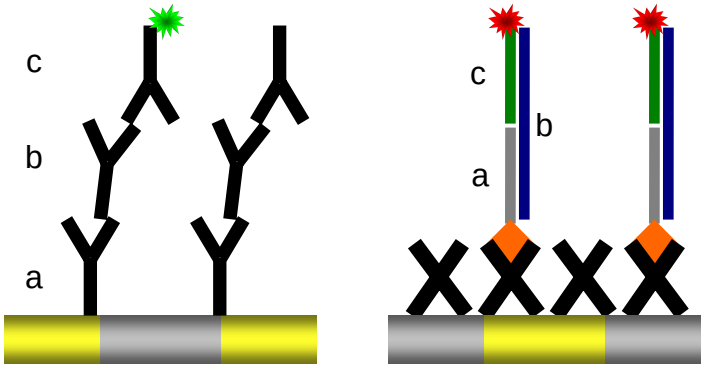

Figure 1.5. Schematic of assays using barcoded nanowires as substrates. **(Left)** For immunoassays, the striped particles are first derivatized with a capture antibody (**a**) that is specific for the analyte (**b**), which is also an antibody. Following incubation of the capture antibody with the analyte, the fluorescently labeled detection antibody (**c**) is added. **(Right)** For DNA hybridization assays, particles are derivatized with NeutrAvidin (NA) followed by reaction with a biotinylated capture sequence (**a**) that is specific for a solution phase analyte (**b**). Fluorescently labeled oligonucleotides (**c**) were then added for detection.[40]

Chapter 2

Preservation of Bioconjugated Barcoded Metal Nanowires Using Citrate Buffer

2.1. Introduction

Nanobarcodes™ (NBC) are striped metal nanowires generally several microns in length and ~300 nm in diameter, prepared by sequential electrodeposition of metals such as Au, Ag, Pd, Ni, or Pt in alumina template membranes.[1] These particles are attractive as identification tags for applications ranging from brand protection in the retail market to multiplexed bioanalysis.[2] They can be fabricated in a multitude of striping patterns and are identifiable by simple optical reflectance microscopy.[2,3] Of the metals used as segments in these particles, Au and Ag are particularly attractive due to the large difference in reflectivity between these metals under blue illumination, which provides excellent contrast for readout of the striping pattern, or barcode.[3] Ag metal is less noble than Au and prone to oxidation. Indeed, we had previously noted some degradation of Ag nanowire segments when stored in air or H_2O and have found that storage in EtOH protects against oxidation.[3] It is, however, of interest to preserve protein and DNA conjugated NBCs, which require storage in aqueous buffer.

Ag metal surfaces and particles are important in a wide variety of biosensing applications.[4] Ag is attractive due to its favorable optical properties in surface plasmon resonance (SPR),[5,6] localized surface plasmon resonance (LSPR),[7,8] and surface-enhanced spectroscopies including fluorescence,[9-11] absorbance,[11] and Raman scattering.[12] In addition, Ag films have been used on quartz crystal microbalance[13,14] and electrochemical

sensors.[15] Biosensor construction generally requires attachment of DNA, proteins, or other biomolecules to the Ag substrates.[1-3,16-21] Unfortunately, the coupling of biomolecules onto Ag surfaces has often proven difficult, due to the instability of Ag surfaces and nanoparticles.[22,23] While many of the optical investigations of Ag have been carried out under vacuum, biosensing is generally done in (oxygenated) aqueous buffers.[3,21,22]

Dry Ag films in oxygen-rich environments undergo an alteration in interference color and appear rough within a few days.[24] During oxidation, cracking and flaking of the oxide takes place, a process which facilitates diffusion of the oxygen to the surface beneath, thus causing continual oxidation damage to the film.[24-26] It has been proposed that the silver oxide formation on the surface during oxidation acts as a catalyst for further oxidation of underlying silver.[24] Although this oxidation process has not been characterized to the same degree in oxygenated aqueous solutions, it is known to occur. The instability of Ag films has caused difficulties for biosensing applications due to oxidation.[13,27]

When Ag-containing NBCs oxidize in air, water, or salt buffer, the initial deterioration appears as pits in the surface of the Ag segments. Eventually, larger portions of the surface disintegrate, leaving behind large voids in the Ag segments. When agitated, the wires degrade faster, presumably due to increased O_2 diffusion and improved access to underlying Ag.[24] The degradation of NBCs and their bioconjugates is of interest because it may impact the long-term storage of these materials for use in biological analyses. Potential consequences of Ag oxidation in NBCs include (1) the loss of attached biomolecules as the surface deteriorates, (2) alteration of particle optical

properties as the surface pits and becomes less uniform, which could lead to difficulties in barcode pattern identification, and (3) wire breakage as Ag segments disappear, which could also lead to misidentification of barcode patterns.

Silver metal surfaces can be protected from oxidation by coating with alkanethiol monolayers or polymeric or inorganic thin films.[13,23,27-32] For example, Su and coworkers have demonstrated that polystyrene or carboxy-poly(vinyl chloride) films protected Ag-coated quartz crystal microbalance biosensors from Ag oxidation and the associated degradation in sensor response.[13,27] Ag nanospheres have been coated with Au or SiO_2 shells for added stability and biofunctionalization.[22,29] Takenouti and coworkers have used hexadecanethiol self-assembled monolayers to prevent Ag tarnishing and corrosion.[31,32] These methods have been successful in protecting Ag; however, they all require surface modification and may not be readily adopted by the molecular biology community. We were interested in preventing Ag oxidation in barcoded nanowires *without* introducing surface coatings.

Herein we describe an experimental study conducted in an effort to characterize and prevent the deterioration of Ag in bare and bioconjugated NBCs stored in aqueous buffer. We have found that buffer solutions containing sodium citrate as a reducing agent greatly reduce the rate of nanowire degradation. Our results indicate that bare, unfunctionalized NBCs survive in hybridization buffer ~2 weeks before extensive deterioration. This is comparable to the length of time that the wires survived in both air and water (14 days before extensive pitting).[3] When sodium citrate is added to the buffer, NBCs last on average three times longer than those in hybridization buffer alone. Agitation of NBC suspensions in any buffer greatly increases the rate of Ag deterioration.

However, addition of citrate still offers significant preservation. We also compared hybridization buffer with and without citrate as a storage solution to prevent the oxidation of silver in fluorescent DNA:NBC bioconjugates. After 12 days of storage in hybridization buffer, fluorescent DNA detached from the DNA-conjugated NBCs as they deteriorated, while the NBCs stored in citrate-containing hybridization buffer did not show significant deterioration at nine weeks.

2.2. Materials and Methods

2.2.1. Materials

Monobasic and dibasic sodium phosphate, trisodium citrate, PBS buffer (0.01 M phosphate buffered saline; 0.138 M NaCl; 0.0027 M KCl; pH 7.4), and sodium chloride were purchased from Sigma. All water used was distilled and purified to 18.2 MΩ through a Barnstead Nanopure system. NeutrAvidin™ was obtained from Pierce and reconstituted to appropriate concentrations in nanopure water. DNA sequences used are as follows: A) 5'-biotin-AAA AAA ACG TTG TCT GAT GCG TCA, B) 5'-ACA CAG ACG TAC TAT CAT TGA CGC ATC AGA CAA CGT, and C) 5'-ATG ATA GTA CGT CTG TGT-ROX (where ROX is a rhodamine fluorophore). Two of the DNA sequences (A and B) were synthesized on an Expedite 8909 DNA synthesizer using reagents purchased from Glen Research, and the third sequence (C) was purchased from IDT, Inc.

Striped metal nanowires with striping patterns encoded 011110, 000111 and 001100, where 0 and 1 represent 0.75 μm length segments of Au and Ag, respectively, were purchased from Nanoplex Technologies (Menlo Park, CA). These particles were

"bare" (i.e. no molecules had been intentionally added post-synthesis) unless otherwise noted. NBCs were rinsed three times in water before use, as they were previously stored in ethanol. Typically, a 1000 μl batch of NBC's contains $1x10^9$ nanowires. NBSee Analysis Software (version 1.0.26, from Nanoplex Technologies) was used for NBC identification of nanowire patterns and to investigate the degree of degradation that caused the software to no longer recognize the wire patterns.

2.2.2. Buffer Preparation

Buffers were made using a standard high-salt hybridization buffer (HB), consisting of 0.3 M NaCl and 10 mM sodium phosphate at pH 7.2. The citrate-containing buffers (CB) were prepared to concentrations of 40, 100, or 300 mM of sodium citrate in HB.

2.2.3. Oxidation of Silver NBCs Segments

To a 25 μl aliquot of rinsed nanowires (000111), 200 μl of 40 mM citrate buffer was added. To a separate aliquot, hybridization buffer was added in the same quantities. The nanowire samples were allowed to sit undisturbed on the benchtop over the course of the experiment, except when an aliquot was removed every third day for imaging. When imaged, both reflectance optical microscopy and FE-SEM data were obtained.

2.2.4. NBSee Software Analysis

Nanowire samples consisting of 80 μl wires, rinsed in water with the supernatant removed, were resuspended in 80 μl of either hybridization buffer, 40 mM citrate buffer, or in ethanol. Two samples were made containing each solution such that one sample could be left to rest on the benchtop and the other continuously agitated on a vortex genie. The samples were sonicated briefly before imaging to reduce clumping of wires, as the NBSee program cannot identify wires that are touching or clumped. These samples were more concentrated with nanowires than previous experiments, which allowed for a greater number of nanowires per image and more statistical data when analyzed by NBSee.

2.2.5. Optical Microscopy

Brightfield reflectance images were acquired using a Nikon TE-300 inverted microscope equipped with a 12 bit high resolution Coolsnap HQ camera (Photometrics). A CFI plan fluor 100x oil immersion lens (N.A. = 1.3) was used in conjunction with Image-Pro Plus software (version 4.5) to image the samples. The light source was a 175 W ozone-free Xe lamp, and a Sutter Instruments filter wheel (Lambda 10-2) allowed for wavelength selection. Samples were prepared by either drying 10 μl aliquots of nanowires onto glass coverslips (Fisher 12-542-C) and then adding a 10 μl drop of water to the sample to adhere the coverslip to a glass slide or by sandwiching an 8 μl sample between two coverslips. All reflectance images were taken at 430 nm, which is the wavelength that gives the highest reflectance contrast between Au and Ag.[3]

2.2.6. Electron Microscopy

Field emission-scanning electron microscopy images were obtained using a JEOL 6700F FE-SEM located at the PSU Materials Characterization Lab. Secondary electron imaging (SEI) mode was used with an accelerating voltage of 15 kV. To prepare the samples, an Al stud covered in copper tape (EM Sciences) was used to support 8 μl of nanowires, which were dried in a vacuum dessicator for 2 hours prior to imaging.

2.2.7. Fluorescent DNA-Coated Nanowires

A 40 μl sample of NBCs (patterned 011110) was washed three times in water prior to addition of 200 μl of 0.25 mg/ml NeutrAvidin. The wires were then vortexed for 2 hours and rinsed three times in water. They were then resuspended in 10 μM DNA (*A*) in PBS buffer (0.01 M phosphate, 0.138 M NaCl, 0.0027 M KCl, pH = 7.4), and vortexed for 4 hours at room temperature. The NBCs were then rinsed three times in PBS buffer and resuspended to a final concentration of 10 μM DNA (*B*) in HB and were vortexed for 4 hours at room temperature. Following three rinsings in HB, the final fluorescent DNA strand (*C*) was hybridized at a concentration of 10 μM in HB for 4 hours at room temperature. The excess DNA was rinsed from the system in three washings using HB. The DNA conjugated wires were divided equally into 2 tubes of which 100 μl of HB was added to one tube and 100 μl CB was added to the other. Tubes were then allowed to sit on the benchtop at room temperature, undisturbed with the exception of the occasional removal of an aliquot for imaging.

2.3. Results and Discussion

NBCs are routinely stored for long periods in ethanol after synthesis, and Ag segments stored in this way retain their integrity indefinitely.[3] However, once biomolecules such as antibodies or DNA are attached to NBCs, it is necessary to store the bioconjugates in an aqueous buffer solution. Although oxidation could be prevented by substitution of Pd or Pt in place of Ag segments, Ag provides the greatest contrast with Au, and therefore is generally preferred.[3] In an effort to slow the oxidation of Ag segments, addition of the reducing agents citrate and dithiothreitol (DTT), to buffer solutions was investigated. These were selected because they are frequent additives in buffers for biological molecules. We found that DTT-containing buffers hastened the rate of silver degradation in nanowires over those stored in HB alone, perhaps because this molecule can serve as a good ligand for Ag(I). We have observed similar effects from other short-chain thiols such as mercaptoethanol and mercaptopropanol. Therefore, we focused on citrate, and DTT was eliminated from the study.

2.3.1. Silver Survival Versus Time

To determine the length of time Ag-containing nanowires would survive in citrate buffer solution as compared to those stored in a non-citrate buffer solution, two separate aliquots of NBCs patterned 000111 (half Au and half Ag) were stored in either hybridization buffer (HB) or in HB containing 40 mM citrate buffer (CB) on the benchtop for up to 53 days. Reflectance optical microscopy and FE-SEM data were obtained daily over the length of this study. The optical microscopy provides information

on changes in reflectance, which are important for barcode pattern identification and would impact the homogeneity of a fluorescence assay carried out on the NBC surface. FE-SEM enables visualization of the nanostructure as Ag oxidation proceeds. Figure 2.1 shows representative reflectance and FE-SEM images of wires imaged after zero, seven, and seventeen days. The first signs of degradation were observed in the form of Ag segment pitting in FE-SEM and darker spots in the reflectivity images for the nanowires stored in HB as early as 2 days after addition of buffer. Samples stored in CB did not show this initial degradation until day 7 in both FE-SEM and reflectivity images. By day 17, the wires in HB displayed substantial degradation, while the corresponding wires in CB showed very little damage. It was not until day 53 that the NBCs stored in CB had similar degradation to those stored in HB for 17 days (Figure 2.2). In general, NBCs stored in CB extended the life of the silver nanowires by nearly three times over those stored in HB.

2.3.2. Effects of Solution Mixing on Oxidation of Silver

During a typical bioassay experiment, NBCs are agitated on a rotary shaker, tumbler, or vortexer both during derivatization with capture probes and reaction with target biomolecules. Since agitation will help oxygenate the solution, it was of interest to determine to what extent it accelerated the rate of damage to Ag segments. We selected the most vigorous of the mixing methods, vortexing. To determine whether vortexing the samples increased the rate of degradation, NBCs (pattern 001100) were prepared in HB, 40 mM CB, or 95 % ethanol. Ethanol is our standard NBC storage solvent when no biomolecules are attached, and is very effective at preventing Ag oxidation; unstirred

samples are undamaged after one year.[3] Each sample was divided in half; one half was vortexed continuously and the other half was stored in the respective solutions on the benchtop. The wires were imaged daily over a twelve-day period. Optical reflectance images for these samples after 7 and 12 days are shown in Figures 2.3 and 2.4, respectively.

At day 7, the wire samples vortexed in HB showed clear signs of Ag degradation, with dark regions visible in the reflectance images (Figure 2.3E). All other samples, including wires vortexed in CB, showed essentially no signs of damage. After 12 days, the HB sample showed dark regions in the reflectance from Ag segments, much like what was observed after 7 days of vortexing. The HB sample that had been continuously vortexed for 12 days showed mainly broken wires (i.e. the Ag segments had failed entirely). In contrast, the ethanol and CB samples showed no change. It should be noted that vortexing continually for 7 days goes far beyond the demands of any potential bioassay application. Nonetheless, this study showed that the degradation of agitated wires stored in HB was accelerated greatly over those allowed to rest undisturbed on the benchtop, and that protection by addition of 40 mM citrate to the HB of a sample continuously vortexed for 12 days was as effective as storage undisturbed in ethanol.

2.3.3. Ability to Identify Wire Patterns Correctly After Silver Oxidation

Use of NBCs in multiplexed bioanalysis requires accurate pattern recognition. Since Ag degradation leads to areas of reduced reflectance, it could hinder NBC identification. To investigate this possibility, we tested the impact of NBCs silver segment degradation on the ability of the NBSee software to identify the nanowires

correctly. This software was designed by Nanoplex Technologies for the purpose of identification and analysis of NBCs.[21] Image sets were analyzed using NBSee software programmed to discard wires not at least 4.3 μm in length; unbroken wires should be 4.5 μm long. This range was used to identify only wires that were not broken. Typically during bioanalysis, it is desirable to identify which biomolecules are attached to which NBCs. Therefore, it is important to identify only the NBCs that are not broken and are fully identifiable.

Using NBSee, all samples were identified with greater than 80 % accuracy through day 12, with the exception of the vortexed HB sample (Figure 2.5). Less than 100 % identification accuracy indicates that some of the wires were identified as having patterns other than 001100. Misidentification can arise from polydispersity in the initial NBC sample or post-synthesis degradation; decreases over time indicate that pitting of the Ag segments and/or wire breakage caused incorrect wire assignment. Nanowires in ethanol were imaged as a control, as no Ag oxidation is observed for these samples over an entire year.[3] NBCs left undisturbed in ethanol remained relatively constant at 94 % for day 5 and 92 % for day 12 (Figure 2.6). The percentage of correctly identified wires stored in CB decreased from 92 % to 89 % (Figure 2.5). Those stored in HB decreased from 90 % to 85 %. These very small changes reflect the fact that the wires do not undergo much degradation in either CB or HB after only 12 days when sitting undisturbed. However, the percent correctly identified dropped precipitously to just 12 % for the vortexed HB sample by day 12. This substantial decrease tracks the increase in Ag segment degradation and wire breakage observed in the reflectance images of these samples. In contrast, NBCs vortexed for 12 days in CB showed no significant decrease

in pattern identification accuracy, underscoring the protective effect of the citrate. The fact that nanowire identification by NBSee did not decline significantly for the 12 day undisturbed HB and 7 day vortexed HB samples, despite noticeable changes in their reflectance images (Figures 2.3E and 2.4B), indicates the robustness of the pattern identification by the NBSee software. The program anticipates that each segment will be 750 nm in length, which reduces the impact of small dark regions within a Ag stripe, and the user interface enables selection of identification criteria to discard broken wires from analysis by dictating the expected length. From the standpoint of multiplexed analysis, this means that small amounts of Ag degradation will not impact particle identification.

2.3.4. Testing Different Concentrations of Citrate for Silver Preservation

We initially selected citrate based on its use in Ag(I) reduction for preparation of colloidal Ag sols.[33] These recipes call for a 1 % (38.8 mM) citrate solution.[33] To determine whether additional reducing agent would provide further increases in Ag stability, we compared hybridization buffer with 40 mM, 100 mM, and 300 mM citrate. NBCs (pattern 000111) were left undisturbed on the benchtop in each of these buffers. Reflectance images of these wires after 7, 12 and 19 weeks show no additional improvement for the higher citrate concentrations (Figure 2.7). Whole, slightly pitted, and broken wires can be found in all three samples after 19 weeks. These data suggest that 40 mM citrate is sufficient for preserving the wires over several months.

2.3.5. Bioconjugated Metal Nanowires in the Presence of Citrate

NBC-based multiplexing is generally performed using fluorescence to report the presence and amount of target biomolecules. Fluorescence intensity for NBC-based assays is sensitive to both the underlying metal identity (i.e. Au vs. Ag) and to inhomogeneities such as can result from Ag degradation. We performed a DNA sandwich hybridization assay on nanowires composed almost entirely of Ag, with short Au caps on each end. Capture probes biotinylated on the 5' end were attached to the wire surface via adsorption to a NeutrAvidin™ protein, after which the particles were exposed to the target strand, followed by a fluorescently tagged detection strand with a 3' rhodamine dye. After assembling this DNA sandwich on the nanowire surface, the sample was divided into two aliquots; half of the wires were stored in HB, with the other half in CB. Both nanowire bioconjugate samples showed greater longevity as compared with bare Ag segments, due to the protective effect of the protein and DNA layer. Eventually, however, the wires in HB began to show signs of Ag oxidation. By day 18 pitting is evident in the wires stored in HB. After 63 days of storage in their respective buffers, the optical reflectance and fluorescence images of the wires showed that the samples stored in HB had degraded substantially, while those in CB showed little evidence of oxidation (Figure 2.8). The sample stored in HB contained many broken wires, and very low fluorescence intensity remained on the wires, while those stored in CB showed minimal degradation and fluorescent DNA still present even after 63 days, the longest time evaluated (Figure 2.8). Thus, we recommend that when Ag-containing nanowire bioconjugates are stored prior to use, citrate or another mild reducing agent be added to maintain sample integrity.

2.4. Conclusions

Barcoded nanowires offer a promising route for multiplexed bioanalysis.[2] Silver and Au segmented Nanobarcodes™ are of particular interest, as these metals provide the greatest contrast with blue illumination, and can provide uniform intensity for fluorescent assays performed in the red.[3] Unfortunately, Ag is less stable than other possible NBC metals (Au, Pd, Pt) and will degrade over a time scale of weeks in aqueous buffers. Although this does not present any problems for uses in which the NBCs are conjugated and used within a few days, slow air oxidation of stored bioconjugated wires could lead to degradation of Ag segments and eventual wire breakage. We have shown that adding 40 mM citrate to the buffer markedly slows silver oxidation. No surface modification was necessary. Bioconjugated NBCs were stable for more than two months in citrate-containing 0.3 M NaCl, 50 mM phosphate buffer (pH 7). Presumably similar results would be achieved by storing in deoxygenated buffers, under Ar(g); however, addition of citrate is much more convenient. Addition of citrate will enable longer storage of biolabeled nanobarcodes prior to use and may aid in the prevention of silver surface degradation of biotagged Ag thin films such as those used in surface plasmon resonance and surface enhanced Raman scattering studies.

2.5. References

1. Nicewarner-Pena, S. R.; Freeman, R. G.; Reiss, B. D.; He, L.; Pena, D. J.; Walton, I. D.; Cromer, R.; Keating, C. D.; Natan, M. J. *Science* **2001**, *294,* 137-141.

2. Keating, C. D.; Natan, M. J. *Adv. Mater.* **2003**, *15,* 451-454.

3. Nicewarner-Pena, S. R.; Carado, A.J.; Shale, K. E. Keating C.D. *J. Phys. Chem. B* **2003**, *107,* 7360-7367.

4. Rosi, N. L.; Mirkin, C. A. *Chem. Rev.* **2005**, *105,* 1547-1562.

5. Raether, H. Surface Plasmons on Smooth and Rough Surfaces and on Gratings. Springer-Verlag, Berlin, **1988**.

6. Neumann, T.; Johansson, M.-L.; Kambhampati, D.; Knoll, W. *Adv. Funct. Mater.* **2002**, *12*, 575-586.

7. Haes, A. J.; Van Duyne, R. P. *Expert Rev. Mol. Diagn.* **2004**, *4*, 527.

8. Haes, A. J., Van Duyne, R. P. *J. Am. Chem. Soc.* **2002**, *124,* 10596-10604.

9. Lakowicz, J. R.; Geddes, C. D.; Gryczynski, I.; Malicka, J.; Gryczynski, Z.; Aslan, K.; Lukomska, J.; Matveeva, E.; Zhang, J.; Budugu, R.; Huang, J. *J. Fluor.* **2004**, *14*, 425-441.

10. Lakowicz, J. R. *Anal. Biochem.* **2001**, *298*, 1-24.

11. Moskovits, M. *Rev. Mod. Phys.* **1985**, *57*, 783-826.

12. Vo-Dinh, T. *Sensors and Actuators B* **1995**, *29*, 183-189.

13. Su, X. *Biochem. Biophy. Res. Commun.* **2002**, *290*, 962-966.

14. Baily, L.E.; Kambhampanti, D.; Kananzawa, K. K.; Knoll, W.; Frank, C. W. *Langmuir* **2002,** *18*, 479-489.

15. Matsuura, H.; Sato, Y.; Sawaguchi, T.; Mizutani, F. *Sensors and Actuators B* **2003**, *91*, 148-151.

16. Sokolov, K.; Chumanov, G.; Cotton, T. M. *Anal. Chem.* **1998**, *70,* 3898-3905.

17. Malicka, J.; Gryczynski, I.; Lakowicz, J. R. *Anal. Chem.* **2003**, *75,* 4408-4414.

18. Wang, J.; Song, F.; Zhou, F. *Langmuir* **2002**, *18,* 6653-6658.

19. Yokota, H.; Saito, K.; and Yanagida, T. *Phys. Rev. Lett.* **1997**, *80,* 4606-4609.

20. Malicka, J.; Gryczynski, I.; Gryczynski, Z.; Lakowicz, J. R. *Anal. Biochem.* **2003**, *315,* 57-66.

21. Walton, I. D.; Norton, S. M.; Balasingham, A.; He, L.; Oviso, D. F.; Gupta, D.; Raju, P. A.; Natan, M. J.; Freeman, R. G. *Anal. Chem.* **2002**, *74,* 2240-2247.

22. Charles, S. A.; Endericks, T.; Evans, A. G.; Garnham, S. E.; Irlam, J. C.; Pollard-Knight, D.; Downes, M.; Heaney, P. J.; Finlan, M. F.; Garland, P. B. A Biosensor Based on Surface Plasmon Resonance-Principles, Performance and Applications. *UCLA Symposia on Molecular and Cellular Biology.* Volume 126: *Biotechnology and Human Genetic Predeposition to Disease* (Cantor, C.R.,

Caskey, C.T., Hood, L. E., Kamely, D., and Omenn, G. S., Eds.) **1990**, pp 291-298, John Wiley & Sons, Inc., New York.

23. Cao, Y. W.; Jin, R.; Mirkin, C. *J. Am. Chem. Soc.* **2001**, *123*, 7961-7962.

24. Pettersson, L. A. A.; Snyder, P. G. *Thin Solid Films* **1995**, *270*, 69-72.

25. Zheludkevich, M. L.; Gusakov, A. G.; Voropaev, A. G.; Vecher, A. A.; Kozyrski, E. N.; Raspopov, S. A. *Oxid. Met.* **2004**, *61*, 39-48.

26. Czanderna, A. W. *J. Phys. Chem.* **1964**, *68,* 2765-2772.

27. Su, X.; Ng, H. T.; Dai, C.-C.; O'Shea, S. J.; Li, S. F. Y. *Analyst* **2000**, *125*, 2268-2273.

28. Li, W.; Virtanen, J. A.; Penner, R. M. *Langmuir* **1995**, *11*, 4361-4365.

29. Morales, A.; Duran, A. *J. Sol-gel Sci. Technol.* **1997**, *8*, 451-457.

30. Liu, S.; Zhang, Z.; Han, M. *Anal. Chem*. **2005**, *77*, 2595-2600.

31. Bernard, M. C.; Dauvergne, E.; Evesque, M.; Keddam, M.; Takenouti, H. *Corrosion Science* **2005**, *47*, 663-679.

32. Evesque, M.; Keddam, M.; Takenouti, H. *Electrochim. Acta* **2002**, *49*, 2937-2943.

33. Lee, P. C.; Meisel, D. *J. Phys. Chem. B* **1982**, *86*, 3391-3395.

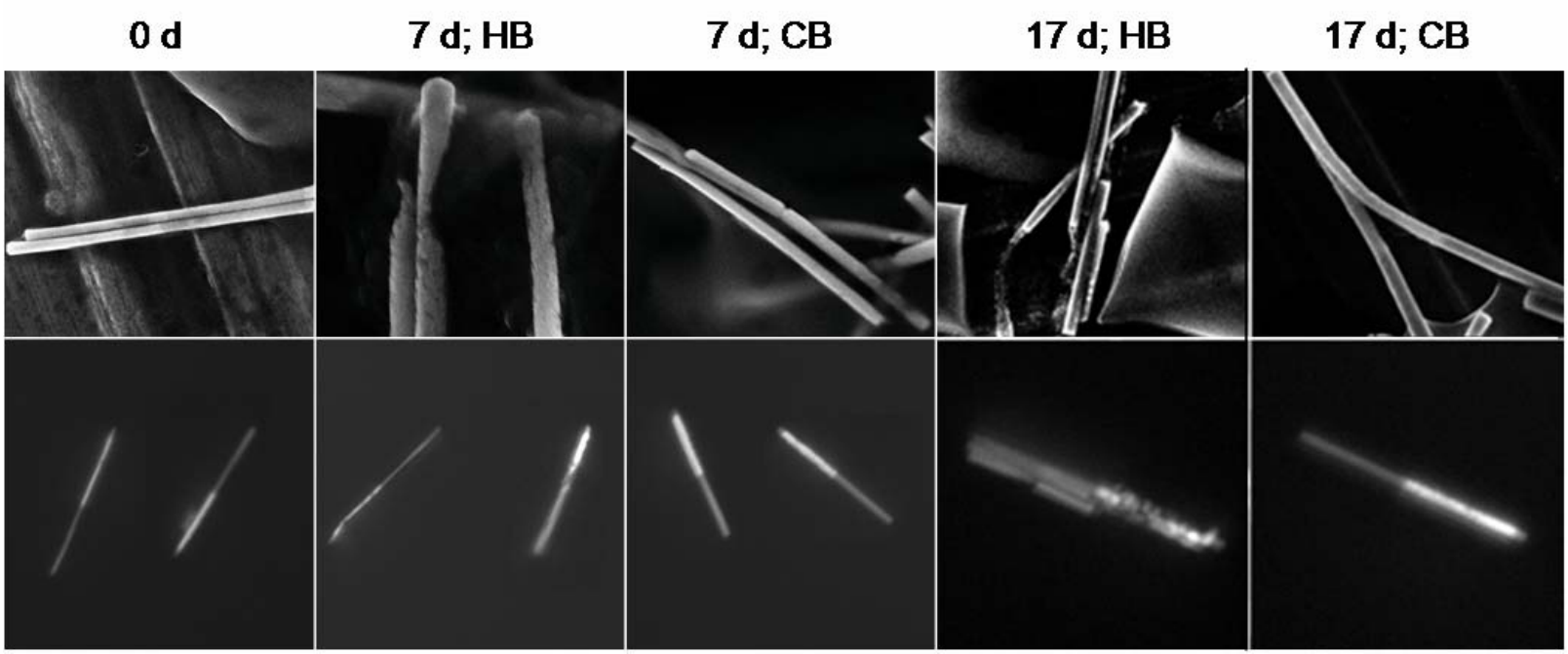

Figure 2.1. Nanowires (pattern 000111) after storage in hybridization buffer (HB) or citrate buffer (CB) for the number of days indicated. Top images are FE-SEM and bottom images are optical reflectance.

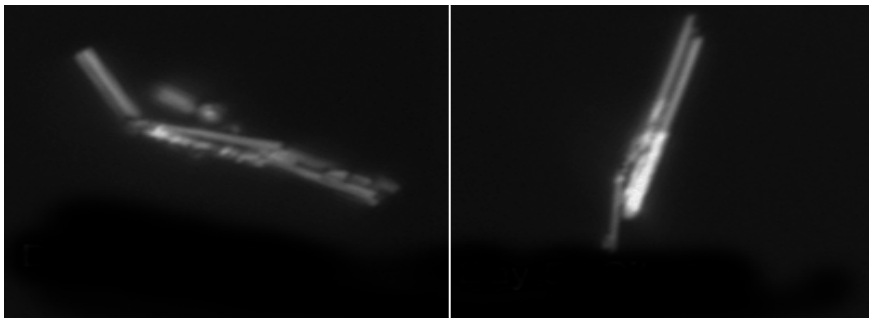

Figure 2.2. Reflectivity images of underivatized 000111 nanowires in citrate buffer after 53 days. Wires are at a similar stage of degradation compared to day 17 in hybridization buffer.

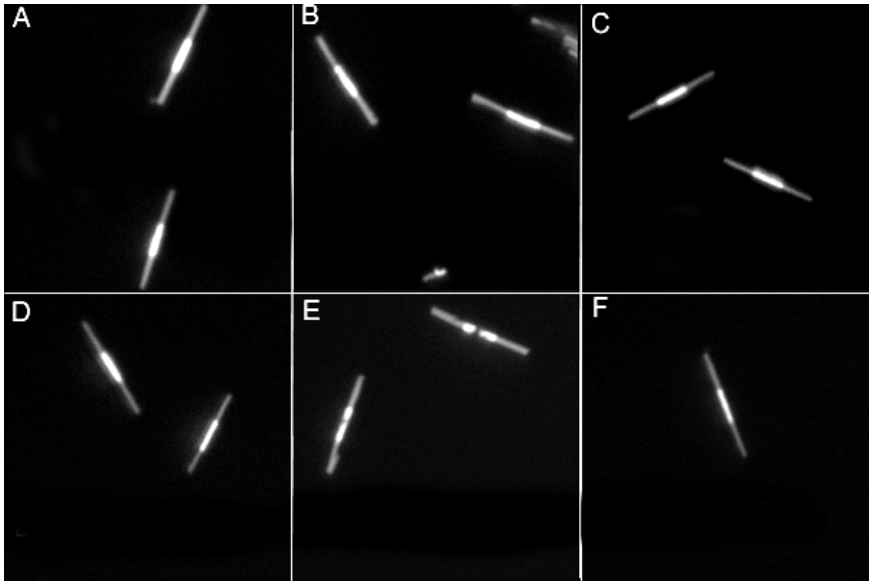

Figure 2.3. Reflectivity images at 430 nm illumination after 7 days of benchtop storage in: ethanol (A), hybridization buffer (B), and citrate buffer (C). (D-F) images represent wires vortexed in: ethanol (D), hybridization buffer (E), and citrate buffer (F).

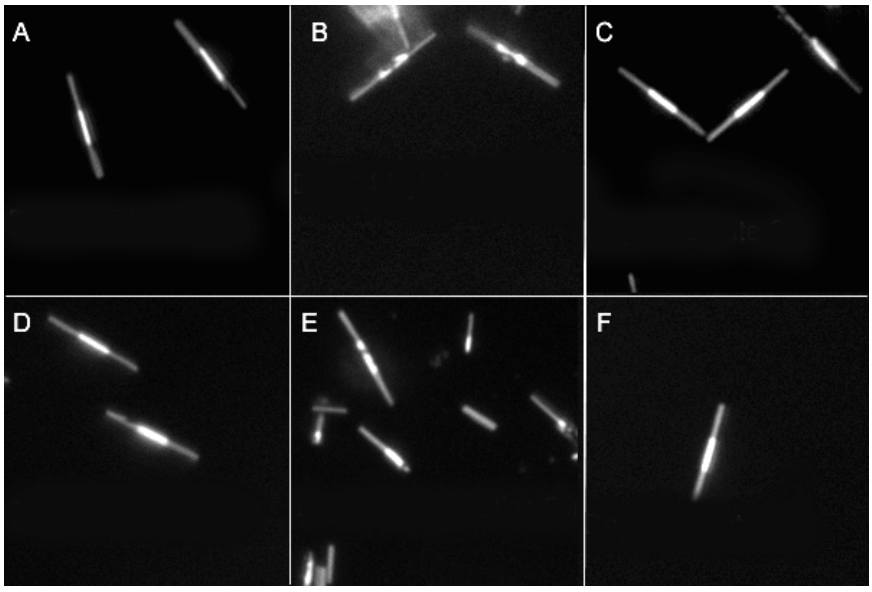

Figure 2.4. Reflectivity images of 001100 nanowires at 430 nm illumination. Top: images taken after 12 days undisturbed benchtop of storage in: ethanol (A), hybridization buffer (B), and citrate buffer (C). Bottom: images taken after 14 days continuous vortexing in: ethanol (D), hybridization buffer (E), and citrate buffer (F).

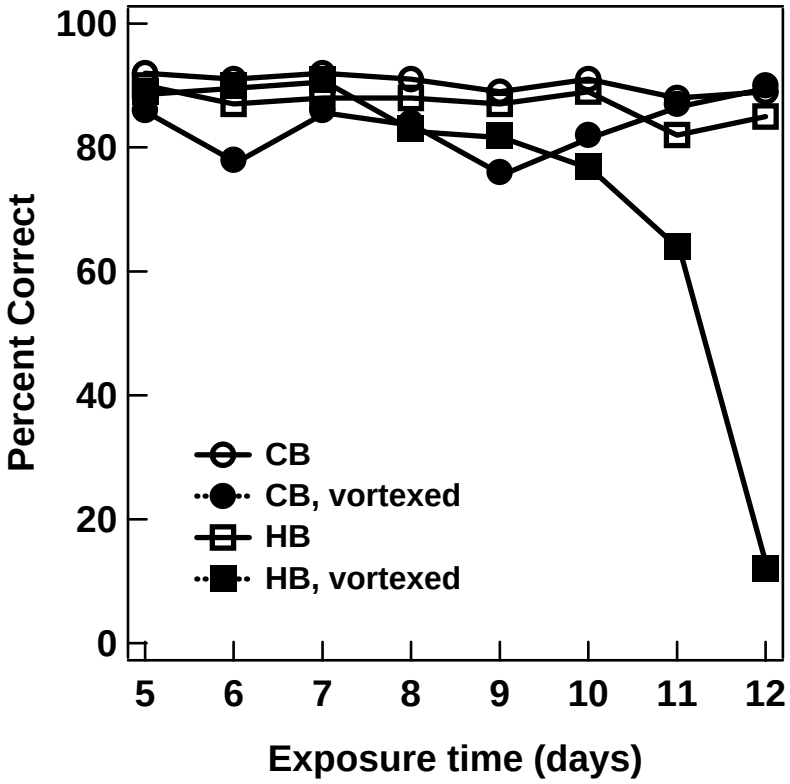

Figure 2.5. Graph showing percentage of nanowires correctly identified by NBSee software from days 5-12, after storage in citrate buffer and hybridization buffer, vortexed and non-vortexed.

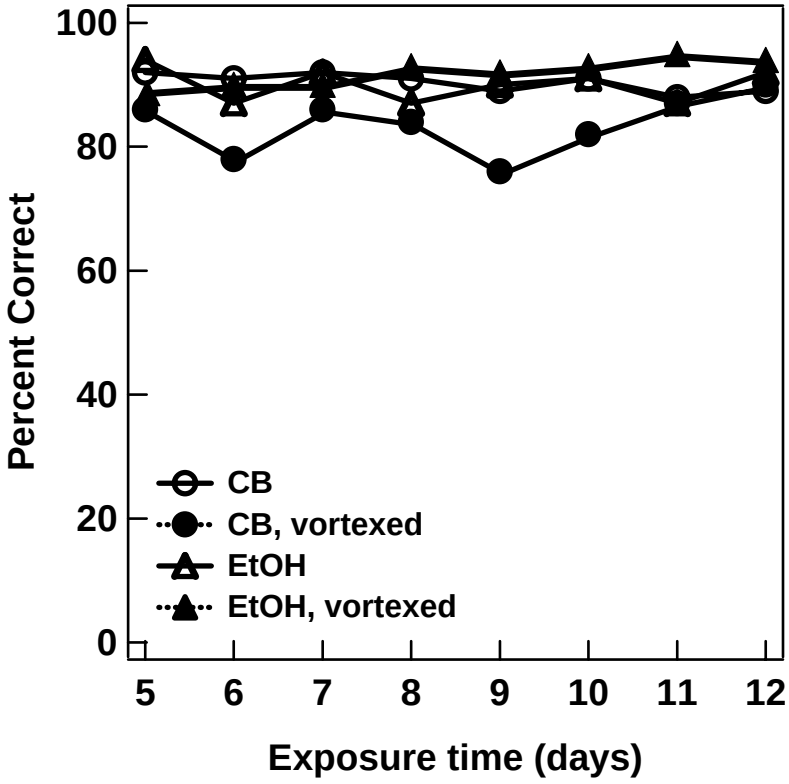

Figure 2.6. Graph of percentage of nanowires correctly identified by NBSee software from days 5-12, when stored in citrate buffer or ethanol, vortexed and non-vortexed.

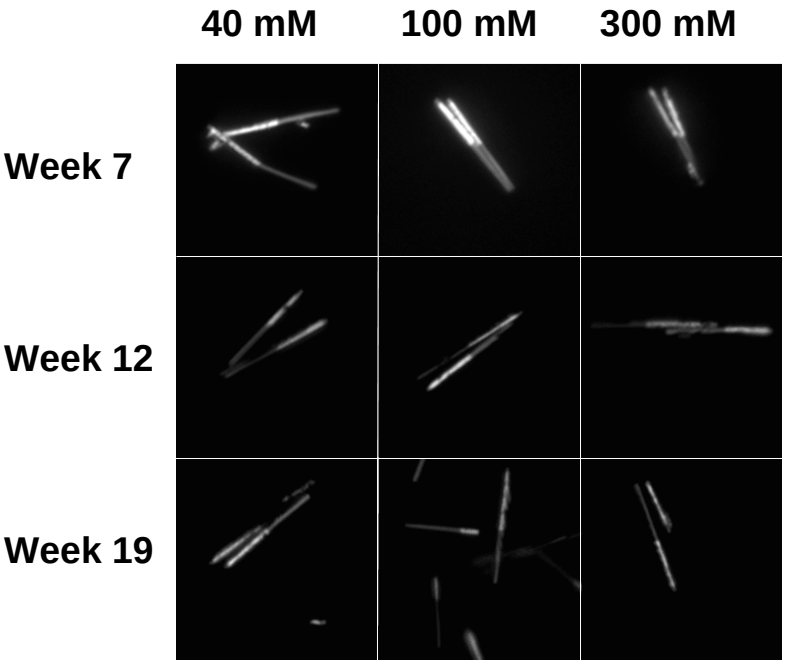

Figure 2.7. Reflectance microscopy images of 000111 nanowires stored in different concentrations of citrate buffer (40, 100, or 300 mM) for varying lengths of time.

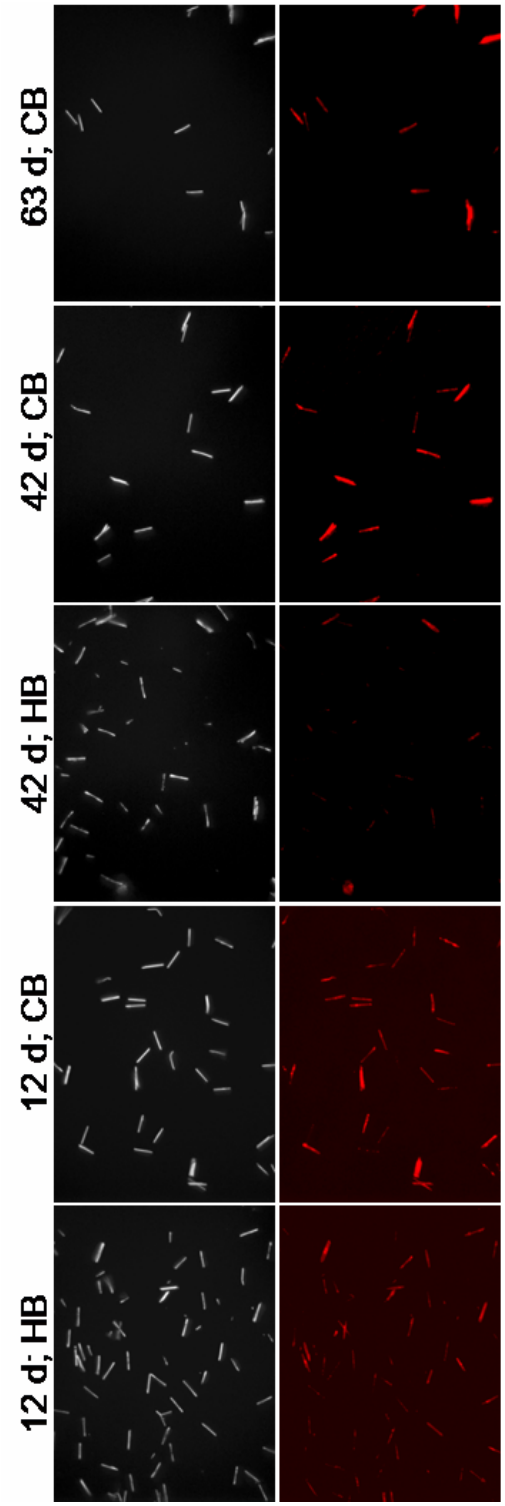

Figure 2.8. Nanowires (pattern 000111) after storage in hybridization buffer (HB) or citrate buffer (CB) for the number of days indicated. Top images are FE-SEM and bottom images are optical reflectance.

Chapter 3

Distance-dependent Emission from Dye-labeled Oligonucleotides on Striped Au/Ag Nanowires: Effect of Secondary Structure and Hybridization Efficiency

3.1. Introduction

When chromophores are placed close to a metal surface, their fluorescence emission intensity can be altered due to quenching or electromagnetic enhancement.[1-5] Quenching occurs at distances very close to planar metal surfaces, usually ≤5-10 nm, while surface-enhanced fluorescence (SEF) generally occurs at tens of nanometers from the surface and is sensitive to the nanoscale roughness of the metal. [1-16] Although much smaller in magnitude than the related phenomenon of surface-enhanced Raman scattering (SERS), SEF has been shown to provide up to ~10-fold increases in emission, which could be analytically important in detection strategies.[1-5,17-20] Predicting the optimal separation for a given experiment with precision can be difficult, as it varies with the identity and curvature of the metallic surface.[1-20] The behavior of fluorescent dyes on or near metal surfaces is becoming increasingly important for biosensing applications, where fluorescence is used to indicate the occurrence of specific binding events. [3,5]

Bioassays can take advantage of fluorescence enhancement, quenching, or both. Incorporation of a metal film can provide additional discrimination between surface-bound and free chromophores by increasing emission under evanescent wave excitation.[5,21] For example, Hong and Kang recently reported detection of cardiac

markers via metal-particle-enhanced fluorescence in a surface immunoassay on optical fibers.[18] Fluorescence quenching was employed by Perez-Luna *et al.* in a displacement immunoassay, where target binding led to release of labeled receptors from an Au film and a concomitant ~tenfold increase in intensity.[22] In some cases, probe conformational changes alter the metal–chromophore separation upon target binding. Maxwell *et al.* bound 3'-thiolated, 5'-dye-labeled oligonucleotides to 2.5 nm diameter Au particles as probes for complementary target DNAs.[23] In the absence of target, the 5' dye moiety was able to approach the metal surface and fluorescence was quenched; hybridization removed the fluorophore from the particle whereupon emission increased substantially. This approach is conceptually similar to that of solution-phase molecular beacon probes, which are oligonucleotides having regions of partial complementarity at their 3' and 5' ends, such that they form hairpin loop structures. Traditionally, a fluorescent dye is appended to one end of the DNA sequence and a quencher molecule to the opposite end. When in solution, they exist in "dark" hairpin loop structures with the dye and quencher in close proximity. Upon addition of a complementary target sequence, the hairpin unfolds to bind target, allowing fluorescence to occur.[24-29] Libchaber and coworkers have demonstrated that 1.4 nm gold particles can be used in place of molecular quenchers, providing quenching efficiencies >99 %.[30]

An important advantage of molecular beacon-style assays is that no washing or target labeling is required. A disadvantage is the limited degree to which solution-phase beacons can be multiplexed, due to the requirement for spectrally distinguishable dyes and efficient quenching. One solution is to immobilize the beacon probes on a surface, where they could be used in array format. Towards this end, beacon probes have been

immobilized on glass,[31,32] polystyrene,[33] agarose,[34] and metal[35-37] surfaces. On metals, the surface itself can serve as the quencher. Krauss and coworkers introduced beacon-style probes on macroscopic, planar Au surfaces for target DNA sequence detection, and demonstrated excellent discrimination between fully complementary and single nucleotide mismatched targets.[35,36] We recently reported a surface-bound beacon assay where Au/Ag striped nanowires (marketed as Nanobarcodes™) were used for simultaneous detection of five human pathogenic target sequences.[37] These particles are cylindrical, several microns in length, ~300 nm in diameter, and contain multiple segments of Au and Ag in patterns readily differentiated by reflectance optical microscopy.[38-40]

Here we report the effect of dye-metal separation on fluorescence emission from cylindrical nanowires composed of Ag and Au segments. Emission from dye-labeled oligonucleotides at metal surfaces has been investigated previously. Lakowicz and coworkers have reported a number of surface effects on fluorescence, including enhanced intrinsic fluorescence from unlabeled DNA,[41] improved photostability,[42] and increased resonant energy transfer between DNA-bound molecular donors and acceptors.[43] This group has also reported increased apparent quantum yields and decreased lifetimes for Cy3 and Cy5-labeled dsDNA adsorbed nonspecifically onto Ag particles.[44] The kinetics of labeled complementary strands to surface-bound probe DNAs have been followed in real time by both surface plasmon field enhanced[21] and epi-illumination[45,46] fluorescence spectroscopy. Despite this prior work, guidance on optimum length or base position for fluorescently tagging surface-bound probe strands is lacking. The effect of dye–Ag island film separation has been investigated by preparation of protein multilayers to

which cyanine dye labeled oligonucleotides were attached.[47] The maximum enhancement was about 12-fold, at ~9 nm from the metal surface (i.e., one layer of streptavidin and biotinylated BSA between the metal and the DNA).[47] For labeled DNA bound to the surface without intervening protein layers, the conformation of the DNA can dramatically alter the dye-surface separation, and with it the emission intensity. Rant, Tornow and coworkers used this effect to probe conformational changes in 5'-thiolated, 3'-dye-labeled 12- and 24-base single-stranded oligonucleotides.[48] Fluorescence increased with increasing DNA surface density, due to steric interactions forcing the strands to "stand up" to a greater extent on the surface.

We present data which build on these results to elucidate the effect of chromophores incorporated after the 8^{th}, 12^{th}, 24^{th}, 36^{th}, and 48^{th} position along a 52-base 5'-thiolated probe strand extended from the surface by hybridization to a nonfluorescent complementary oligonucleotide. By performing the fluorescence measurements for each length simultaneously in a multiplexed format, we were able to compare directly and quantitatively the effect of dye incorporation at each position as a function of probe surface coverage and hybridization buffer. We found that the observed metal-dye separation dependence was highly sensitive to hybridization efficiency, due to increased DNA extension from the surface upon hybridization. This effect was more important than the number of dye molecules present on the surface, with ten-fold lower probe coverages leading to higher emission intensities due to improved hybridization.

To explore the effect of probe secondary structure, we also tested molecular-beacon-style probe sequences having 5'-thiols and 3'-chromophores. The beacon probes were less sensitive to hybridization efficiency than their unstructured counterparts;

among 24, 34, and 48 base beacon probes, the 34-mer gave the highest fluorescence intensities in the presence of DNA target regardless of the hybridization buffer used. We interpret this as a result of differences in conformational flexibility for unquenched states of unstructured single-stranded probes (which are quite flexible at these lengths) and the beacon probes, which should unfold into unquenched states only upon binding to complementary target strands. Thus, while fluorescence from traditional single-stranded DNA probes lacking secondary structure occurs from molecules sampling a range of metal-dye separations, any emission observed from beacon probes should be from the double-stranded state (i.e. maximum metal-dye separation).

Because the striped nanowires contained segments of both Au and Ag, the effects of each metal could be directly compared within each experiment. Differences in fluorescence patterning on Au and Ag were observed as a function of chromophore identity and metal–dye separation. For example, emission intensity for TAMRA-labeled oligonucleotides changed from brighter on Ag for 24-base probes to brighter on Au for 48-base probes. We also observed regions of brighter fluorescence at the ends of nanowires and at surface defects where heightened electromagnetic fields affect the fluorescence. It is hoped that our results on fluorescence emission for different metal-dye separations, probe conformations, dye identities, and metal substrates will prove useful in the design of bioassays in which these effects are important.

3.2. Materials and Methods

3.2.1. Materials

Nanobarcodes™ patterned 000010, 001100, 010100, 011110, 100001, 001010, 010010, and 011000, where 0 represents a 0.75 μm segment of Au and 1 represents a 0.75 μm segment of Ag, were purchased from Nanoplex, Inc. (now Oxonica). Each batch of nanowires consisted of ~1x10^9 wires per 1 ml ethanol. Nanowires were rinsed three times in water (by centrifugation) to remove the ethanol prior to use. Hybridization buffer (0.3 M PBS) was made in house and was prepared using 0.3 M NaCl and 10 mM sodium phosphate at pH 7.0, and 0.01 M PBS buffer (0.01 M phosphate buffered saline; 0.138 M NaCl; 0.0027 M KCl; pH 7.4) was purchased from Sigma. Commercial hybridization buffer (HS114) was obtained from Molecular Research Centers, Inc. EDTA buffer was prepared according to Krauss and coworkers, using 0.5 M NaCl, 20 mM cacodylic acid, and 0.5 mM EDTA, pH=7.[35] All water used in these experiments and in preparation of the buffers was purified through a Barnstead Nanopure System to 18 MΩ resistivity.

3.2.2. Surface–Dye Separation Experiments with Unstructured DNA Probes

Probes for dye-surface separation experiments were designed by inserting a nonhybridizing, internal rhodamine red-X NHS ester labeled thymine base after the 8^{th}, 12^{th}, 24^{th}, 36^{th}, or 48^{th} base position of a 51-base oligonucleotide. We anticipate that this labeled thymine forms a single base bulge loop,[49] minimizing interference of the dye molecule with hybridization. This insertion does not appreciably decrease the stability of duplex formation at any of the positions used here (predicted melting temperatures for

these sequences in 0.3 M salt are all ~82 ^{o}C). Because the bulge does not increase the overall length of the duplex formed, we refer throughout this chapter to the separation in terms of the base just prior to the labeled thymine. All sequences are listed in Table 3.1 and were purchased from Integrated DNA Technologies, Inc. DNA sequences were received as disulfides, which were cleaved before use, resulting in a single thiol moiety terminating the sequence. To cleave the disulfide, the DNA was first dissolved in a 100 mM solution of DTT (dithiothreitol) in 1 ml 0.1 M Na_3PO_4 buffer (pH 8.3) for a half hour, and then the small thiol fragments were removed using Centri-Spin Separation Columns (Princeton Separations). The resulting DNA sequences (terminated with a single –SH group) were diluted in water to a concentration of 10 μM and were stored in the freezer at –80 °C.

3.2.3. Preparation of Distance Dependence Assays

Aliquots of 25 μl of each type of NBC were rinsed three times in water and resuspended in 100 μl 0.01 M PBS buffer. Each internally labeled DNA sequence was added at a final concentration ranging between 1-2 μM to different patterned NBCs (concentrations were held constant within a single experiment, but varied slightly from experiment to experiment). Nanowire patterns allowed for identification of the corresponding attached DNA sequence. Thiolated DNA (*8D*, *12D*, *24D*, *36D*, or *48D*) was allowed to self-assemble to the wires for at least 4 hours while tumbling at room temperature, then were rinsed three times in 0.01 M PBS buffer. The samples were resuspended in 100 μl of either HS114 hybridization buffer or 0.3 M PBS for

hybridization. Complementary DNA (*CD*) was added at a final concentration of 5 μM, and was allowed to hybridize overnight at room temperature while tumbling. Samples were then rinsed 3 times (by centrifugation) in 0.3 M PBS and resuspended in 250 μl of the same buffer. The samples were then imaged using optical microscopy (see below).

3.2.4. Hybridization Efficiency

Two separate aliquots of NBCs patterned 000010, one containing 150 μl of wires, and the other containing 300 μl, were rinsed in water and resuspended in 0.01 M PBS buffer to their original volumes. To the 150 μl sample, *48D* DNA was added, and to the 300 μl sample, *NFD* DNA was added for surface attachment, at a final concentration of 5 μM. The DNA was allowed to attach for 4 hrs at room temperature while tumbling. The samples were then rinsed four times in 0.01 M PBS buffer and were resuspended in 0.01 M PBS buffer to original volumes. The 150 μl sample was then divided into a total of three tubes each containing 50 μl of wires, such that three samples were available to collect surface coverage data from (see below). The 300 μl sample was divided into two tubes (150 μl each). The buffer from one of the tubes was removed and replaced with HS114 hybridization buffer. A total of 10 μM 5'-TAMRA-labeled *CD* DNA was added to each tube and was allowed to hybridize overnight at room temperature. Both samples were then rinsed in 0.3 M PBS buffer and were further divided into three separate samples each containing 50 μl of nanowires. Mercaptoethanol was then added to these six samples for determination of surface coverage (see below).

3.2.5. Beacon Performance as a Function of Buffer and Beacon Length

Beacon probes were each attached to a different patterned NBC by first washing 50 μl of each type of NBC two times in 0.01 M PBS, and resuspending them in 50 μl of 0.01 M PBS. Beacon probes (either 24B, 34B, or 48B) were then added to the wires (500 μl of 5 μM probe in water) and were allowed to attach overnight at room temperature while rotating. Next, 300 μl of 0.3 M PBS was added for 2 hours at room temperature while rotating, and the samples were then washed three times in 0.3 M PBS buffer. From these beacon coated wire samples, 3 μl aliquots were each added to separate 42 μl volumes of either 0.3 M PBS, EDTA, or HS114 buffer and the DNA targets were hybridized at a final concentration of 5 μM while rotating at 37 °C for one hour. The samples were then rinsed two times in 0.3 M PBS buffer before imaging.

3.2.6. Sensitivity of Nanowire Beacon Assay

Beacon probe (48B) was attached to NBCs patterned 00001 in the same manner as described in the previous section. A range of target DNA concentrations was prepared such that the final concentrations of target when added to 50 μl 0.3 M PBS buffer ranged from 0 M to $1x10^{-6}$ M. To the separate 50 μl aliquots of target in buffer, 3 μl of beacon-coated wires were added. Beacon targets were allowed to hybridize at 50 °C for 3 hrs while tumbling. Samples were rinsed three times in 0.3 M PBS before being imaged.

3.2.7. Fluorescence Patterning

For each set of experiments, 50 μl of NBCs patterned 000111 were rinsed three times in water by centrifugation, and were resuspended in 5 μM DNA beacon in 0.3 M PBS buffer at a final volume of 150 μl. Beacons used for the different dye study were sequenced the same as *34B* except terminated with different fluorophores (Cy3, Cy5, or 6-FAM). For the study using different length DNA, either *24B*, *34B*, or *48B* DNA was used which was labeled with TAMRA fluorophores. Beacons were added to each tube at a final concentration of 5 μM in 150 μl 0.3 M PBS buffer and were allowed to hybridize with gentle agitation at room temperature for 4 hrs. The samples were then rinsed three times in 0.3 M PBS and were resuspended in 50 μl 0.3 M PBS buffer for imaging.

3.2.8. Imaging and Emission Intensity Quantification

Brightfield reflectance images were acquired using a Nikon TE-300 inverted microscope equipped with a 12 bit high resolution Coolsnap HQ camera (Photometrics). A CFI plan fluor 60x oil immersion lens (N.A. = 1.4) was used in conjunction with Image-Pro Plus software (version 4.5) to image the samples. The light source was a 175 W ozone free Xe lamp, and a Sutter Instruments filter wheel (Lambda 10-2) allowed for wavelength selection. Sample preparation for analysis by optical microscopy involved dropping a 10 μl aliquot of sample onto a glass coverslip (Fisher 12-542-C), allowing the wires to settle to the surface of the cover slip, then sandwiching the sample between the coverslip and a glass slide. All reflectance images were taken at 430 nm, due to high reflectance contrast between Au and Ag at this wavelength.[38,39]

Fluorescence intensity values for samples were obtained quantitatively using NBSee Software designed by Nanoplex Technologies, Inc., for identification of patterned wires and quantification of corresponding fluorescence.[50] Over thirty (and typically several hundred) of each nanowire striping pattern were analyzed and averaged to generate the log normal mean fluorescence intensities (Cox's method of normalization).[51] The error bars reported are the 95% confidence interval.

3.2.9. DNA Surface Coverage

Surface coverage determination methods used were similar to those described by Demers *et al*.[52] To obtain coverages of fluorescent DNA bound to nanowires, 5 μl of mercaptoethanol was added to the nanowire solutions that remained after imaging, and the samples were allowed to tumble on a rotator at room temperature overnight. The DNA was displaced into solution, which was collected above the wires, and the fluorescence intensity was determined using a Fluorolog-3 fluorimeter. This fluorimeter was equipped with a 450 W Xe lamp, and double grating excitation spectrometer and a single grating emission spectrometer. Calibration standards were used to determine the concentration of DNA in each sample.

3.3. Results and Discussion

Characterization of fluorescence behavior on nanowires of different metals can provide insight for future design and optimization of fluorophore-based bioassays on metal substrates and guidance for other metal-fluorophore investigations. Using barcoded metal nanowires for this work enabled us to directly compare results from the

two adjacent metals on each wire (Au and Ag in this case), as well as from multiple experiments performed simultaneously on particles having different patterns. This avoids irregularities from variability in lamp intensity, focus, etc., and makes direct, quantitative comparison of fluorescence on different wires and/or adjacent metals possible.

3.3.1. Dye-Surface Separation Dependence for Unstructured Probe DNAs: Effect of Hybridization Efficiency

True distance dependence data for quenching and SEF on metal nanowires could be acquired by coating the wires with inorganic or organic films of known thickness and attaching the chromophore to the film.[8,11,14-16] However, the relevant variable for optimization of surface-based nucleic acid assays is not the absolute distance dependence of the response, but rather the optimal number of nucleobases between the metal and the fluorophore. Thus, variables such as surface coverage and whether the DNA is single- or double-stranded may be as important as oligonucleotide length. To avoid potentially substantial differences in surface coverage or hybridization efficiency between different DNA probe lengths, we used a single length of DNA for all distance dependence experiments and varied the position of dye-labeled thymine bases along this length. Figure 3.1 illustrates the experimental design. Dye-labeled DNA was attached to the barcoded nanowires via 5'-thiol moieties and hybridized to unlabeled complementary strands to both increase the rigidity and extension of the DNA and approximate DNA hybridization assay conditions. We chose to incorporate the labeled thymine bases in the thiolated strand that would be attached to the surface rather than the complementary strand, as this more closely mimics surface-bound molecular beacon probes. Rhodamine

red dye was chosen based on availability for internally labeling DNA sequences and for spectral similarity to TAMRA, which we have used in molecular beacon assays.

In this experiment, five different sequences with fluorophores positioned after the 8^{th}, 12^{th}, 24^{th}, 36^{th}, and 48^{th} base of separate 52 base long sequences were investigated. Each of these five sequences was bound to nanowires having different barcode patterns, as illustrated in Figure 3.1. DNA 52 bases long was used to assure extention of a few bases beyond the furthest positioned internal fluorophore (49^{th} base) such that similar DNA-fluorophore interactions were experienced by all of the fluorophores. Estimated fluorophore-metal separations (for the base immediately 5' to the labeled thymine, calculated as 3.4 Å/base plus the C_6 spacer)[29] for the fully extended nanowire bound DNA sequences are as follows: 8^{th} base ~3.6 nm, 12^{th} base ~4.8 nm, 24^{th} base ~8.6 nm, 36^{th} base ~12.3 nm, and 48^{th} base ~16.0 nm. The five DNA:nanowire conjugates were mixed together prior to imaging, enabling simultaneous data collection for all five labeled positions, and eliminating factors such as variations in lamp intensity between samples with time and the need for internal reference standards.[53] Figure 3.2 shows a representative reflectance and corresponding fluorescence image from this experiment. The reflectance image enables identification of the nanowire patterns (Ag segments are brighter than Au with blue illumination), while the corresponding fluorescence images provide emission intensity. These data, hybridized in 0.3 M PBS buffer, suggest that base positions 8 and 12 are very efficiently quenched, while positions 24, 36, and 48 give much higher fluorescence intensities.

Quantification of fluorescence response was obtained from multiple reflectance and fluorescence images of using NBSee data analysis software.[50] This software first identified isolated nanowires (i.e. clumped wires are omitted from analysis) and identified their barcode patterns based on linescans through each wire in the reflectance images. It then referred to the corresponding fluorescence images to determine the fluorescence intensity for each wire. The fluorescence values were averaged across each wire, then compiled to give an overall mean fluorescence intensity for each wire pattern (i.e., each labeled base position). Figure 3.3 gives the relative averaged fluorescence intensities of samples hybridized in two different buffers (0.3 M PBS and commercially available HS114). Two distinct trends were observed, depending on the hybridization buffer used. In the HS114 samples, as the position of the fluorophore was moved further from the surface of the wire, the fluorescence intensity increased. The HS114 hybridization buffer, although its composition is not revealed by the manufacturer, presumably contains surfactant (noted by the foamy nature of the buffer) and other reagents to reduce nonspecific binding. The same experiment hybridized in 0.3 M PBS buffer resulted in a different fluorescence trend (Figure 3.3). The fluorescence intensities in these samples were highest with a metal-fluorophore separation of 24 bases (~8.6 nm if fully extended) from the metal surface, then remained relatively constant, and/or decreased slightly beyond that distance.

We suspected that the difference in the two buffers was due to higher stringency for the HS114 buffer, leading to lower hybridization efficiency and consequently changing the dye-surface separation. Figure 3.4 illustrates this concept. Sample A, which has a lower percentage of double stranded DNA, has a smaller average dye–

surface separation than sample B, which has higher hybridization efficiency. The 0.3 M NaCl buffer is used to overcome electrostatic repulsion due to the high density of oligonucleotides on surfaces,[54] while the commercial HS114 buffer was presumably designed for use in solution-phase hybridization reactions. We therefore compared the hybridization efficiencies of the two buffers under otherwise identical conditions. Separate samples, one with fluorescently labeled DNA (*48D*) attached to nanowires and the other with non-fluorescent DNA of the same sequence (*NFD*), were prepared to determine the surface coverage of probe and amounts of hybridization, respectively. From the surface-bound fluorescent DNA sample, the surface coverage of probe was determined to be $7x10^{12}$ oligos/cm^2. The hybridization efficiency in 0.3 M PBS was 43 %, while that in HS114 buffer was just 19 % (note that hybridization efficiencies near 100 % for surface-bound oligonucleotides, particularly for the lengths used here, generally require special attention to steric factors[55-57]). These hybridization results explain the existence of the two trends identified in the distance dependence data: in PBS buffer, more than twice as much of the labeled DNA was double stranded as compared to when HS114 buffer was used, causing more DNA to be rigid and extended further from the surface. Single-stranded DNA is flexible, allowing the fluorophore to reside closer to the surface. Thus, the average metal–dye separation is much greater for the 0.3 M PBS samples than for the HS114 samples. We expect that neither set of samples provides metal–dye separations as high as are calculated based on label position and assuming fully-extended DNA (i.e. 16 nm for the 48^{th} base). Bearing this in mind, our observations for optimal base position are not inconsistent with decreased quenching after approximately 5 nm from the surface, and no SEF. A small SEF effect cannot be ruled

out; however, if SEF was substantial in this system, we would not expect the "leveling off" of emission intensity after 24 bases that is observed for the 0.3 M PBS samples, but rather a maximum followed by a decrease prior to leveling off.[1-5]

Because of the large difference in persistence length for single-stranded versus double-stranded DNA, and the distance-dependence of quenching by metals, differences in fluorescence intensity due to the extent of hybridization can be quite large. Indeed, Nie and coworkers have used this to their advantage to develop a molecular-beacon-style DNA detection assay in which fluorescent DNA probe strands that lacked secondary structure (i.e. no hairpin was designed into the sequence) were attached via thiols to Au nanoparticles.[23] When no target was present, the DNA looped around the particles where the fluorophore was quenched, but in the presence of target, the double-stranded DNA was extended from the particle surface, greatly increasing the emission.[23] To investigate the importance of having the DNA double stranded in our experiments, we attached 5'-thiolated, 3'-TAMRA-labeled, 24-base single-stranded DNA (*24S*) to nanowires, and either the complementary strand was added, or no target was added. The samples with complementary DNA were 2.5 times more fluorescent than those that were single stranded, despite the facts that (i) the same number of dye molecules were present on the wires in each case, and (ii) this probe sequence was designed to avoid secondary structure.

In our distance dependence experiments, hybridization efficiency of surface bound DNA was more important in determining the overall emission intensity than the number of dye molecules present. Figure 3.5 shows fluorescence intensity as a function of dye position, DNA surface coverage, and hybridization buffer. Solid lines correspond

to 0.3 M PBS buffer, while dashed lines indicate HS114 buffer. Data sets are shown for each buffer at two different surface coverages of dye-labeled DNA: 7-8 x 10^{11}/cm^2 and 6-8 x 10^{12}/cm^2. As in Figure 3.3, samples hybridized in HS114 buffer show an increase in mean fluorescence, while those in 0.3 M PBS buffer reached a maximum then leveled off as a function of labeled base position. The two experiments with the lower dye-labeled DNA coverages had more than five-fold *higher* average fluorescence than samples with an order of magnitude greater number of dye molecules on the surface. These data underscore the critical importance of steric hindrance in determining hybridization efficiency in surface-based nucleic acid experiments. Decreased hybridization efficiencies for the higher surface coverage samples result in more flexible, less fully extended strands and consequently greater quenching, as described above. Additionally, at higher coverages, the fluorophores may be experiencing collisional quenching with neighboring fluorophores, thus further decreasing the intensities.

3.3.2. Dye-Surface Separation Dependence for Molecular Beacon-Style Probe DNAs: Effect of Secondary Structure

The principal difference between the DNA sequences used in the experiments described above and those used in molecular beacon-style experiments is the presence of secondary structure in the beacon probe sequences. To determine how well our predictions from the fluorophore-distance study translated to the design of DNA beacon assays, we studied three different length hairpin probe sequences (24, 34, and 48 bases in length, each with an identical 5 base pair "stem" region, and different "loop" lengths) attached to barcoded nanowires. To determine the separation dependence of fluorescence

intensity, each sequence was hybridized to a complementary target sequence (*C24B*, *C34B*, or *C48B*) so that the fluorescence emission would not be quenched by the metal surface (as it should be for the beacon probes in the absence of target). Hybridization was performed in both the 0.3 M PBS and HS114 buffers used for distance dependence experiments, and also in a third buffer ("EDTA") introduced by Krauss and coworkers for beacon probes on planar Au surfaces.[35] Figure 3.6 shows the relative fluorescence intensities after hybridization for each beacon probe length in each of the three buffers; fluorescence intensities have been normalized to a scale of 0 to 100 for each of the three different buffers, in order to highlight length-dependent differences between the probes. Irrespective of buffer used, the intensity trends as a function of distance are similar. The 34-base beacon probe gave the highest fluorescence intensity, with both longer and shorter probes giving lower intensities.

The surface–dye separation dependence of the beacon probes in all three buffers is more similar to the 0.3 M PBS distance dependence data (Figures 3.3 and 3.5) than to the HS114 data. This is consistent with the effects of probe secondary structure. For molecular beacon probes, unlike traditional single-stranded DNA probes (i.e. without secondary structure), fluorescence emission is quenched in the absence of target DNA, because the hairpin structure holds the fluorophore very close to the metal surface (Figure 3.7). Thus, decreased hybridization efficiencies should not result in the same magnitude of change in fluorophore–metal separation. Differences in intensity as a function of probe length are smallest in HS114 buffer, which gave lower hybridization efficiencies for traditional DNA binding experiments as described above. Formation of secondary structure, like hybridization to target strands, requires overcoming electrostatic

repulsions. Thus, a more stringent buffer such as HS114 favors both less target binding (i.e. less fluorescence) and also less hairpin folding (i.e. more fluorescence). The fraction of fluorescence arising from unfolded probes should be lowest for the higher ionic strength buffers (0.3 M PBS and EDTA); thus, we can expect these buffers to best approximate a fully double-stranded response. Clearly, differences in intensity due to the effects of the hybridization buffer are more complicated for beacons than for non-hairpin sequences. Stringency conditions for optimizing hybridization of unstructured probes are not directly applicable to beacon probe assays, as the stem interactions must also be considered. Additionally, changing the probe length may also impact steric hindrance at the surface, which could alter the hybridization efficiency. For the data shown in Figure 3.6, probe surface coverage was held approximately constant ($1.2 - 2.5 \times 10^{11}$ probes/cm^2) for all probe lengths to minimize differences in steric effects between the samples.

The data in Figure 3.6 suggest that the separation-dependence of molecular beacon probes, unlike unstructured probes such as those in Figures 3.3 and 3.5, will be relatively insensitive to hybridization efficiency. This is because while the conformational flexibility of unstructured single stranded DNA complicates the observed separation-dependence of emission, beacon probes have limited conformational possibilities (quenched hairpins or fully extended duplexes).[29] This is critically important for bioassay applications, since the major factor responsible for the degree of hybridization on the surface in a bioassay will be solution target concentration, i.e., the quantity to be measured, rather than choice of buffer, which would be held constant under assay conditions.

We investigated the effect of target concentration (i.e., hybridization efficiency) for a 48-base beacon probe on the nanowire surface. If distance dependence effects complicated the response to target concentration, one might expect to see a trend different than an increase in fluorescence intensity with increasing target concentration. Figure 3.8 shows the log mean fluorescence intensity of each assay containing different concentrations of DNA target. As the concentration of target DNA was decreased, the fluorescence intensity also decreased. This suggests that the distance dependence effects did not complicate the fluorescence response although the percent hybridization was changed. A common figure of merit for molecular beacon assays is the quenching efficiency, QE, defined as the ratio of fluorescence present when quenched versus unquenched, is calculated as [1-(signal in absence of target/signal with target)] %. In this assay, the quenching efficiency calculated at 1 μM target was 88 %. Since our focus here was on the separation dependence, we did not optimize assay conditions before acquiring the data in Figure 3.8. Nonetheless, there was a substantial change in the fluorescence between the target and no target samples, such that the presence or absence of target was apparent. The sensitivity of this assay is in the 100 pM to 10 nM range in its current form (<1 nM limit of detection based on average intensity for the no target control plus twice the standard deviation),[58] and is limited by inefficient quenching. This is comparable to sensitivities reported by other groups for surface-bound molecular beacon assays.[32,33,35] Typical quenching efficiencies for surface bound beacons are in the 80 to 95 % range,[32,42,53,54] with the highest reported values >99 % from Krauss and coworkers for beacons bound to planar Au.[35] Libchaber and coworkers reported quenching efficiencies

of 99.97 % for solution-based beacon structures where organic quenchers were replaced by 1.4 nm Au clusters.[30]

3.3.3. Fluorescence Patterning Phenomena

Some patterning of fluorescence intensity on the Au/Ag striped nanowires is observable in Figure 3.2. Indeed, we often observe patterned fluorescence intensities on the nanowires. We have previously reported fluorescence patterning in sandwich immunoassays, where the dye molecules were bound to the secondary antibodies (i.e. relatively far from the metal surface). In those earlier experiments, the fluorescence patterning we observed correlated with the reflectivities of the underlying metals.[38] Thus, although the dyes were located in the near field of the metal nanowires, useful predictions of patterning could be made simply by treating the wire as a variably reflective mirror (i.e., shorter wavelengths of excitation and emission were more efficiently reflected from Ag as compared with Au, in accordance with the wavelength-dependent bulk reflectivities of these metals). A key difference between those experiments and the experiments described here is the magnitude and variability of the dye-surface separation. Here, rather than holding the separation constant at ~15 nm, we are varying it between ~3.6 nm and ~16 nm, depending on the labeled probe position (0.34 nm per base plus the six carbon spacer). Additionally, while the surface attachment chemistry was insensitive to metal identity in the immunoassay data, thiols can be expected to give higher coverages on Ag as compared to Au,[59,60] which may influence patterning (either making Ag brighter due to a greater number of dye molecules, or darker due to lower hybridization efficiency and therefore less extension from the surface).

While studying different length DNA beacon probes on striped metal nanowires, we noticed that fluorescence patterning varied with dye–metal separation (Figure 3.2). Figure 3.9 explores this effect further: reflectance and corresponding fluorescence images are shown for half Au/half Ag nanowires coated with internally-rhodamine labeled, thiolated sequences *8D* through *48D* and hybridized to complementary DNA in 0.3 M PBS buffer. Reflectance and fluorescence linescans for a representative wire from those samples with appreciable fluorescence intensity are shown. Strong fluorescence patterning is observed for rhodamine after the 12^{th} and 24^{th} base positions, with intensities on average ~3-fold brighter on the silver segments than the gold. At a distance of 36 bases, the rhodamine dye shows less distinct patterning, barely discernable on some wires in this sample. Rhodamine positioned 48 bases from the surface also shows very little patterning.

More striking changes in fluorescence patterning were observed for greater changes in dye-metal separation. Figure 3.10 shows reflectance and corresponding fluorescence images and linescans for half gold-half silver nanowires coated with TAMRA labeled DNA sequences of various lengths after hybridization to complementary strands. All experiments in this figure were conducted under identical conditions (0.3 M PBS buffer). The shortest length DNA (24 bases) shows fluorescence patterning that matches the reflectance patterning of the nanowires, where silver is brighter and gold is darker. This result is qualitatively similar to what was seen in Figure 3.9 for the internal rhodamine labels after the 24^{th} base position, despite the change to TAMRA dye. To achieve greater metal-dye separations, we compared this result with intensities for 34- and 48-base molecular beacon probes with 5'-thiols and 3'-TAMRA.

Probes with secondary structure were used in order to maximize the extension from the surface upon hybridization. For beacon probes 34 bases in length, approximately uniform fluorescence is observed on Au and Ag segments. Beacon probes 48 bases long exhibited a *reversal* in fluorescence patterning, such that fluorescence intensities from TAMRA on the Au segments were brighter than on Ag segments of the wires. The observed changes in surface patterning arose primarily from changes in the emission intensity for TAMRA on the Ag segments, while emission on the Au segments was relatively insensitive to metal–dye separation.

The observation of fluorescence reversal in the TAMRA-labeled beacon probe experiments, as compared with just a reduction in the degree to which fluorescence was brighter on Ag vs. Au in the rhodamine-labeled unstructured probe experiments could be due to differences in the dye and/or to the greater metal-dye separations probed in the beacon experiment. Unfortunately, we were unable to purchase rhodamine-labeled beacon probes to test directly which of these effects was dominant. However, the excitation and emission wavelengths for rhodamine (588 and 608 nm, respectively) are at longer wavelengths than for TAMRA (559 and 583 nm). Based on reflectivity arguments,[38] TAMRA is expected to give *lower* intensities on Au segments as compared to rhodamine. Thus, while dye-specific properties cannot be ruled out as the cause of these differences, we favor interpretation of the stronger apparent distance-dependence of the TAMRA-labeled beacon probes (Figure 3.10) as arising from the greater surface-dye separation for these probes as compared to those lacking secondary structure (Figure 3.9).

The nature of the metal–fluorophore interaction depends not only on the separation between them, and the identity of the metal, but also on the identity of the dye.

For example, low quantum yield dyes have been reported to exhibit particularly impressive surface enhanced fluorescence on colloidal silver surfaces.[6,61] In the case of molecular beacon probes, additional properties may become important. For example, efficient quenching of the dye may benefit from weak adhesion between the dye and the metal surface. The size of the dye, and electrostatic considerations may also come into play, potentially impacting the ability of the hairpin structures to fold and/or unfold. We compared four different fluorescent dyes with a range of excitation/emission frequencies, extinction coefficients, and quantum yields (Table 3.2). In these experiments, 5'-thiolated beacon probes with the dyes at their 3' end were attached to nanowires composed of half Ag and half Au. The chemical structures of these dyes are also different, with greater positive charge and less condensed structures for the two cyanine dyes as compared with the FAM and TAMRA.

We compared 34-base molecular beacon-style probes with TAMRA, Cy3, Cy5, and 6-FAM fluorophores, after exposure to unlabeled complementary DNA to extend the probe stands. Figures 3.10 (middle panel) and 3.11 show results for each of these dyes, on half Au/half Ag nanowires. Several differences between the dyes can be observed. Cy3 gave the highest peak intensity, with a sharp spike of fluorescence near the Au/Ag interface at the center of the wire, and smaller spikes at both ends. Cy5 also showed sharp spikes of intense emission corresponding to the Au/Ag interface, the edges of the wire, and a defect in the Ag segment that appears dark in the reflectance image. In contrast, TAMRA and 6-FAM appear to be less sensitive to edges and surface defects in the wires. These regions of intense fluorescence response most likely arise from SEF at regions of heightened electromagnetic fields.[1-5] This interpretation is consistent not only

with the positions of these regions, but also with the low quantum yields for the two cyanine dyes as compared with 6-FAM and TAMRA.[62]

In addition to fluorescence patterns caused by SEF, emission intensities for dyes on Ag and Au portions of the wires can be compared. TAMRA and Cy3 exhibited roughly equal intensity on Au and Ag segments of the nanowires, such that one segment could not be readily distinguished from the other in the fluorescence images. On the other hand, 6-FAM dye was much brighter on Ag than Au, and Cy5 was somewhat brighter on Au than Ag. These differences correlate with differences in excitation and emission wavelengths of the dyes. 6-FAM is the shortest wavelength dye, while TAMRA and Cy3 are similar in color, and Cy5 was the longest wavelength dye investigated here. However, since the data in Figures 3.9 and 3.10 show metal-dye separation can alter the relative intensities on Au and Ag segments, it is clear that more than excitation and emission wavelengths for the dyes are involved in the patterning. Other factors may include differences in the distance dependence of electromagnetic field distribution above the two metals.

Finally, we note that in related experiments reported by Sha *et al*., the effect of dye selection on quenching efficiency for nanowire beacon bioassays was investigated. Of the dyes tested (Cy5, FITC, Rhodamine 6G, Texas Red, and TAMRA), Texas Red gave the best performance, with 94 % Q.E. TAMRA gave 89 % Q.E., and was chosen over Texas Red for further studies due to its commercial availability.[37] Dye performance in our experiments gave comparable results, with Cy3 giving the highest, 6-FAM the lowest overall intensity, and TAMRA giving the best Q.E.

3.4. Conclusions

The promise of metallic surfaces and nanostructures, including barcoded metal nanowires, for fluorescence-based bioanalysis led us to investigate factors that influence emission from surface-bound dyes. Emission from internal rhodamine dye in 52-base DNA on striped metal nanowires revealed that after base position 8 and 12, quenching remained significant. Positions after the tagged 24 to 48 bases lead to much brighter fluorescence intensities. The shape of the intensity–separation response was sensitive to the hybridization efficiency of the surface-bound probes for complementary DNA (i.e., percent double-stranded), dictated by the hybridization buffer used. Samples with ~20 % hybridization efficiency showed increased emission with increased separation from the metal surface, while samples with ~40 % hybridization efficiency showing an increase up to 24 bases, and a leveling off or slight decrease in intensity at greater separations. These differences result from the greater metal–dye separation for double-stranded as compared to single stranded DNA (i.e. the average separation was greater for the samples with twice as much double stranded DNA). Increasing the surface coverage of fluorescently tagged DNA *decreased* the fluorescence intensity, due to steric inhibition of hybridization, which led to increased quenching because less of the DNA was in its fully extended double-stranded form.

In contrast, the separation-dependent response of dye-labeled oligonucleotides designed to form hairpin secondary structures analogous to solution-phase molecular beacons were relatively insensitive to the hybridization buffer. The formation of secondary structure in the absence of complementary DNA leads to efficient quenching of emission. This means that any fluorescence observed should arise from probes which

have bound complementary strands, and results in less complicated target response curves for probes having secondary structure than might be expected for metal-bound, chromophore-labeled probes otherwise.

Selection of striped metal nanowires, composed of identifiable patterns of Ag and Au segments, enabled us to perform many of these experiments in a multiplexed fashion for direct, quantitative comparisons, e.g., between different dye labeling positions. In addition, differences in emission intensity from chromophores on the Ag vs. Au segments of the nanowires could be readily compared. We observed differences in fluorescence patterning as a function of metal-chromophore separation, with emission from TAMRA-labeled DNA changing from brighter on Ag for 24-base probes to brighter on Au for 48-base probes. While our results do not suggest substantial surface enhancement of fluorescence under the conditions of our experiments, anomalously bright emission noted from the ends, metal-metal interfaces, and surface defects does suggest some SEF at these sites of greater nanoscale roughness.

This research provides insight into the importance of DNA conformation and hybridization efficiency on performance in fluorescence-based experiments on metal surfaces and points to the benefits of encoded nanowires for multiplexed surface characterization. Our findings are relevant to the design of bioassays at metal surfaces, particularly those based on hybridization to surface-bound probe DNA strands. Differences between the fluorescence response of probe sequences designed to avoid versus encourage the formation of secondary structure should be taken into account in assay design and interpretation.

3.5. References

1. Moskovits, M. *Rev. Mod. Phys*. **1985**, *57*, 783-826.

2. Chance, R. R.; Prock, A.; Silbey, R. *Adv. Chem. Phys*. **1978**, *37*, 1-65.

3. (a) Lakowicz, J. R. *Anal. Biochem.* **2001**, *298*, 1-24. (b) Lakowicz, J .R. *Anal. Biochem*. **2005**, *337*, 171-194.

4. Meitiu, H. *Prog. Surf. Sci.* **1984**, *17*, 153-320.

5. Neumann, T.; Johansson, M.-L.; Kambhampati, D.; Knoll, W. *Adv. Funct. Mater*. **2002**, *12*, 575-586.

6. Weitz, D. A.; Garoff, S.; Gersten, J. I.; Nitzan, A. *J. Chem. Phys.* **1983**, *78*, 5324-5338.

7. Corni, S.; Tomasi, J. *J. Chem. Phys.* **2003**, *118*, 6481-6494.

8. (a) Sokolov, K.; Chumanov, G.; Cotton, T. M. *Anal. Chem.* **1998**, *70*, 3898-3905. (b) Chumanov, G.; Sokolov, K.; Gregory, B. W.; Cotton, T. M. J. *J. Phys. Chem.* **1995**, *99*, 9466-9471.

9. Whitmore, P. M.; Robata, H. J.; Harris, C. B. *J. Phys. Chem.* **1982**, *77*, 1560-1568.

10. Yokota, H.; Saito, K.; Yanagida, T. *Phys. Rev. Lett.* **1998**, *80*, 4606-4609.

11. Knobloch, H.; Brunner, H.; Leitner, A.; Aussenegg, F.; Knoll, W. *J. Phys. Chem.* **1993**, *98*, 10093-10095.

12. (a) Huang, X.; Lee, K. T.; George, T. F. *J. Phys. Chem.* **1986**, *85*, 567-572. (b) Glass, A. M.; Liao, P. F.; Bergman, J. G.; Olson, D. H. *Optics Letters* **1980**, *5,* 368-370. (c) Wokaun, A.; Lutz, H. P.; King, A. P.; Wild, U. P.; Ernst, R. R. *J. Phys. Chem.* **1983**, *79*, 509-514. (a) Amos, R. M.; Barnes, W. L. *Phys. Rev. B.* **1999**, *59*, 7708-7714. (d) Alivisatos, A. P.; Waldeck, D. H.; Harris, C. B. *J. Chem. Phys.* **1985***, 82*, 541-547. (e) Zhang, J.; Malicka, J.; Gryczynski, I.; Lakowicz, J. R. *J. Chem. Phys. B* **2005**, *109*, 7643-7648.

13. Aslan, K.; Lakowicz, J. R.; Geddes, C. D. *Anal. Bioanal. Chem.* **2005**, *382*, 926-933.

14. Kummerlen, J.; Leitner, A.; Brunner, H.; Aussenegg, F. R.; Wokaun, A. *Molec. Phys.* **1993**, *80,* 1031-1046.

15. Tarcha, P. J.; DeSaja-Gonzalez, J.; Rodriguez-Llorente, S.; Aroca, R. *Appl. Spec.* **1999**, *53*, 43-48.

16. Schneider, G.; Decher, G.; Nerambourg, N.; Praho, R.; Werts, M. H. V.; Blanchard-Desce, M. *Nano Lett*. **2006**, *6*, 530-536.

17. Tovmachenko, O. G.; Graf, C.; van den Heuvel, D. J.; van Blaaderen, A.; Gerritsen, H. C. *Adv. Mater*. **2006**, *18*, 91-95.

18. Hong, B.; Kang, K. A. *Biosens. Bioelectron*. **2006**, *21*, 1333-1338.

19. Stranik, O.; McEvoy, H. M.; McDonagh, C.; MacCraith, B. D. *Sens. Actuat. B* **2005**, *107*, 148-153.

20. Zhang, J.; Lakowicz, J. R. *J. Phys. Chem.* B **2006**, *110*, 2387-2392.

21. Liebermann, T.; Knoll, W.; Sluka, P.; Herrmann, R. *Coll. Surf. A* **2000**, *169*, 337-350.

22. Perez-Luna, V. H.; Yang, S.; Rabinovich, E. M.; Buranda, T.; Sklar, L. A.; Hampton, P. D.; Lopez, G. P. *Biosens. Bioelectron.* **2002**, *17*, 71-78.

23. Maxwell, D. J.; Taylor, J. R.; Nie, S. *J. Am. Chem. Soc.* **2002**, *124*, 9606-9612.

24. Tyagi, S.; Kramer, F. R. *Nat. Biotechnol.* **1996**, *14*, 303-308.

25. Heyduk, T.; Heyduk E. *Nat. Biotechnol.* **2002**, *20*, 171-175.

26. Fang, X.; Li, J. J.; Tan, W. *Anal. Chem.* **2002**, *72*, 3280-3285.

27. Alberts, D. P.; Parman, J. M.; Goddard, N. L. *Biophys. J.* **2003**, *84*, 3212-3217.

28. Antony, T.; Thomas, T.; Sigal, L. H.; Shirahata, A.; Thomas, T. J. *Biochem.* **2001**, *40*, 9387-9395.

29. Bonnet, G.; Tyagi, S.; Libchaber, A.; Kramer, F. R. *Proc. Nat. Acad. Sci. USA* **1999**, *96*, 6171-6176.

30. Dubertret, B.; Calame, M.; Libchaber, A. J. *Nat. Biotechnol.* **2001**, *19*, 365-370.

31. (a) Fang, X.; Liu, X.; Schuster, S.; Tan, W. *J. Am. Chem. Soc*. **1999**, *121*, 2921-2922. (b) Brown, L.; Cummins, J.; Hamilton, A.; Brown, T. *Chem. Commun*. **2000**, 621-622.

32. Liu, X.; Tan, W. *Anal. Chem*. **1999**, *71*, 5054-5059. (b) Liu, X.; Farmerie, W.; Schuster, S.; Tan, W. *Anal. Biochem*. **2000**, *283*, 56-63. (c) Yao, G.; Tan, W. *Anal. Biochem*. **2004**, *331*, 216-223.

33. Steemers, F.; Ferguson, J. A.; Walt, D. R. *Nat. Biotechnol*. **2000**, *18*, 91-94. (b) Epstein, J. R.; Leung, A. P. K.; Lee, K.-H.; Walt, D. R. *Biosens. Bioelectron*. **2003**, *18*, 541-546.

34. Rang, H.; Li, J.; Liu, H.; Liu, Q.; Mei, Q.; Wang, Y.; Zhu, J.; He, N.; Lu, Z. *Nucl. Acids Res*. **2002**, *30*, e61.

35. Du, H.; Strohsahl, C. M.; Camera, J.; Miller, B. L.; Krauss, T. D. *J. Am. Chem. Soc.* **2005**, *127*, 7932-7940.

36. Du, H.; Disney, M. D.; Miller, B. L.; Krauss, T. D. *J. Am. Chem. Soc.* **2003**, *125*, 4012-4013.

37. Sha, M. Y.; Yamanaka, M.; Walton, I. D.; Norton, S. M.; Stoermer, R. L.; Keating, C. D.; Natan, M. J.; Penn, S. G. *Nanobiotechnology* **2005**, *1*, 327-335.

38. Nicewarner-Pena, S. R.; Carado, A. J.; Shale, K. E.; Keating C. D. *J. Phys. Chem. B* **2003**, *107,* 7360.

39. Nicewarner-Pena, S. R.; Freeman, R. G.; Reiss, B. D.; He, L.; Pena D. J.; Walton, I. D.; Cromer, R.; Keating, C. D.; Natan, M. J. *Science* **2001**, *294,* 137-141.

40. Keating, C. D.; Natan, M. J. *Adv. Mater.* **2003**, *15,* 451-454.

41. Lakowicz, J. R.; Shen, B.; Gryczynski, Z.; D'Auria, S.; Gryczynski, I. *Biochem. Biophys. Res. Commun.* **2001**, *286*, 875-879.

42. Malicka, J.; Gryczynski, I.; Fang, J.; Kusba, J.; Lakowicz, J. R. *J. Fluor.* **2002**, *12*, 439-447.

43. Malicka, J.; Gryczynski, I.; Fang, J.; Kusba, J.; Lakowicz, J. R. *Anal. Biochem.* **2003**, *315*, 160-169.

44. Malicka, J.; Gryczynski, I.; Maliwal, B. P.; Fang, J.; Lakowicz, J. R. *Biopolymers (Biospectroscopy)*, **2003**, *72*, 96-104.

45. Malicka, J.; Gryczynski, I.; Lakowicz, J. R. *Biochem. Biophys. Res. Commun.* **2003**, *306*, 213-218.

46. Malicka, J.; Gryczynski, I.; Gryczynski, Z.; Lakowicz, J. R. *Anal. Chem*. **2003**, *75*, 6629-6633.

47. Malicka, J.; Gryczynski, Z.; Lakowicz, J. R. *Anal. Biochem*. **2003**, *315*, 57-66.

48. Rant, U.; Arinaga, K.; Fujita, S.; Yokoyama, N.; Abstreiter, G.; Tornow, M. *Langmuir* **2004**, *20*, 10086-10092.

49. Nucleic Acids: Structures, Properties, and Functions, Bloomfield, V. A.; Crothers, D. M.; Tinoco Jr., I. University Science Books: Sausalito, CA, 2000.

50. Walton, I. D., Norton, S. M., Balasingham, A., He, L., Oviso, D. F., Jr.; Gupta, D., Raju, P. A., Natan, M. J., and Freeman, R. G. *Anal. Chem.* **2002**, *74*, 2240-2247.

51. Zhou, X.-H.; Gao, S. *Stat. Med*. **1997**, *16*, 783-790.

52. Demers, L. M.; Mirkin, C. A.; Mucic, R. C.; Reynolds, R. A., III; Letsinger, R. L.; Elghanian, R.; Viswanadham, G. *Anal. Chem.* **2000**, *72*, 5535-5541.

53. Wehry, E. L. Molecular Fluorescence and Phosphorescence Spectrometry. In *Instrumental Techniques for Analytical Chemistry*; Settle, F. A., Ed.; Prentice Hall: Upper Saddle River, New Jersey, 1997; pp 507-539.

54. (a) Mirkin, C. A.; Letsinger, R. L.; Mucic, R. C.; Storhoff, J. J. *Science* **1996**, *382*, 607-609. (b) Jin, R.; Wu, G.; Li, Z.; Mirkin, C. A.; Schatz, G. C. *J. Am. Chem. Soc*. **2003**, *125*, 1653-1654.

55. (a) Herne, T. M.; Tarlov, M. J. *J. Am. Chem. Soc.* **1997**, *119*, 8916-8920. (b) Steel, A. B.; Levicky, T. M.; Herne, T. M.; Tarlov, M. J. *Biophys. J.* **2000**, *79*, 975-981.

56. (a) Shchepinov, M. S.; Case-Green, S. C.; Southern, E. M. *Nucleic Acids Res.* **1997**, *25*, 1155-1161. (b) Southern, E.; Mir, K.; Shchepinov, M. *Nature Genetics Supplement* **1999**, *21*, 5-9.

57. Nicewarner-Peña, S. R.; Raina, S.; Goodrich, G. P.; Fedoroff, N. V.; Keating, C.D. *J. Am. Chem. Soc.* **2002**, *124*, 7314-7323.

58. Harris, D. C.; Quantitative Chemical Analysis, 4th ed.; W. H. Freeman and Company: New York; 1995.

59. Herrwerth, S.; Eck, W.; Reinhardt, S.; Grunze, M. *J. Am. Chem. Soc*. **2003**, *125*, 9359-9366.

60. Ulman, A. *Chem. Rev*. **1996,** *96*, 1533-1554.

61. Maliwal, B. P.; Malicka, J.; Gryczynski, I.; Gryczynski, Z.; Lakowicz, J. R. *Biopolymers (Biospectroscopy)* **2003**, *70*, 585-594.

62. www.idtdna.com, accessed May 27, 2006.

Table 3.1. DNA sequences used in this work.

Sequence Name	Sequence (5′-3′)	Description
8D	Thiol C_6-TTT CAT GG*_T_ TAG CGT ATG CTA GAT CGC GTA AAT GAA TGC CTA GAT CAG CGA T	5'-thiol, internal dye after the 8th of 52 bases
12D	Thiol C_6-TTT CAT GGT AGC *_T_GT ATG CTA GAT CGC GTA AAT GAA TGC CTA GAT CAG CGA T	5'-thiol, internal dye after the 12th of 52 bases
24D	Thiol C_6-TTT CAT GGT AGC GTA TGC TAG ATC *_T_GC GTA AAT GAA TGC CTA GAT CAG CGA T	5'-thiol, internal dye after the 24th of 52 bases
36D	Thiol C_6-TTT CAT GGT AGC GTA TGC TAG ATC GCG TAA ATG AAT *_T_GC CTA GAT CAG CGA T	5'-thiol, internal dye after the 36th of 52 bases
48D	Thiol C_6-TTT CAT GGT AGC GTA TGC TAG ATC GCG TAA ATG AAT GCC TAG ATC AGC G*_T_A T	5'-thiol, internal dye after the 48th of 52 bases
NFD	Thiol C_6-TTT CAT GGT AGC GTA TGC TAG ATC GCG TAA ATG AAT GCC TAG ATC AGC GAT	5'-thiol, 51 bases (no dye)
CD	ATC GCT GAT CTA GGC ATT CAT TTA CGC GAT CTA GCA TAC GCT ACC ATG	48 base complement to *8D*, *12D*, *24D*, *36D*, *48D*, and *NFD*
48B	Thiol C_6-GCG AGT AAA AGA GAC CAT CAA TGA GGA AGC TGC AGA ATG GGA TAC TCG-TAMRA	5'-thiol, 3'-TAMRA 48 base beacon probe with 6 base "stem"
34B	Thiol C_6-GCG AGG AGA CCA TCA ATG AGG AAG CTG CAC TCG C-TAMRA	5'-thiol, 3'-TAMRA 34 base beacon probe with 5 base "stem"
24B	Thiol C_6-GCG AGA TCA ATG AGG AAG CCT CGC-TAMRA	5'-thiol, 3'-TAMRA 24 base beacon probe with 5 base "stem"
24S	Thiol C_6-GAG ACC ATC AAT GAG GAA GCT GCA -TAMRA	5'-thiol, 3'-TAMRA 34 base unstructured probe (no "stem")
C24B	GGC TTC CTC ATT GAT	15-base complement to *24B*
C34B	TGC AGC TTC CTC ATT GAT GGT CTC	24-base complement to *34B* and *24S*
C48B	GTA TCC CAT TCT GCA GCT TCC TCA TTG ATG GTC TCT TTT A	40-base complement to *48B*

* marks the location of an internal rhodamine red-X NHS ester fluorophore. Underlined portions of sequences show stem regions of beacon sequences.

Table 3.2. Properties of fluorescent dyes studied.

Dye	λ_{ex} (nm)	λ_{em} (nm)	$\varepsilon_{\lambda max}$ (M^{-1} cm^{-1})	Quantum Yield
6-FAM	495	520	75,000	0.9
Cy 3	550	564	150,000	0.1
TAMRA	559	583	89,000	0.7
Cy 5	648	668	250,000	0.2

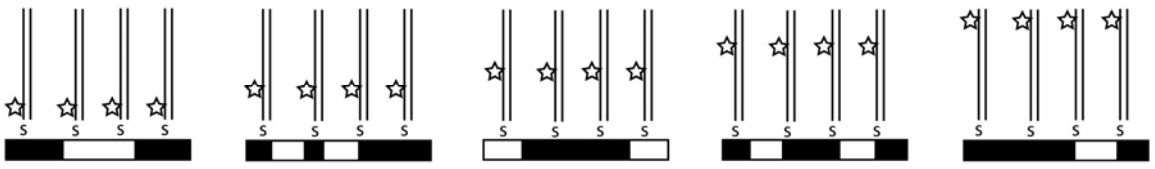

Figure 3.1. Illustration of distance-dependent fluorescence study.

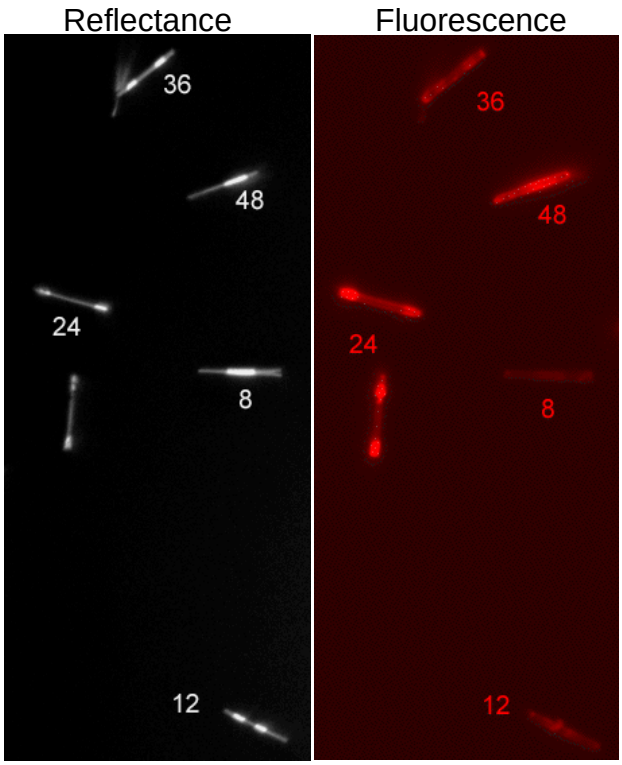

Figure 3.2. Reflectance and corresponding fluorescence images of internal rhodamine labels at five different positions within thiolated 52-base oligonucleotides attached to Au/Ag encoded metal nanowires. Unlabeled complementary strands were hybridized in 0.3 M PBS buffer. The numbers in the images indicate which DNA base is labeled for each nanowire pattern (e.g., wires with bright Ag ends and a dark Au middle in the reflectance image are coated with DNA labeled at the 24th base). Five separate samples were mixed after DNA attachment to obtain this image.

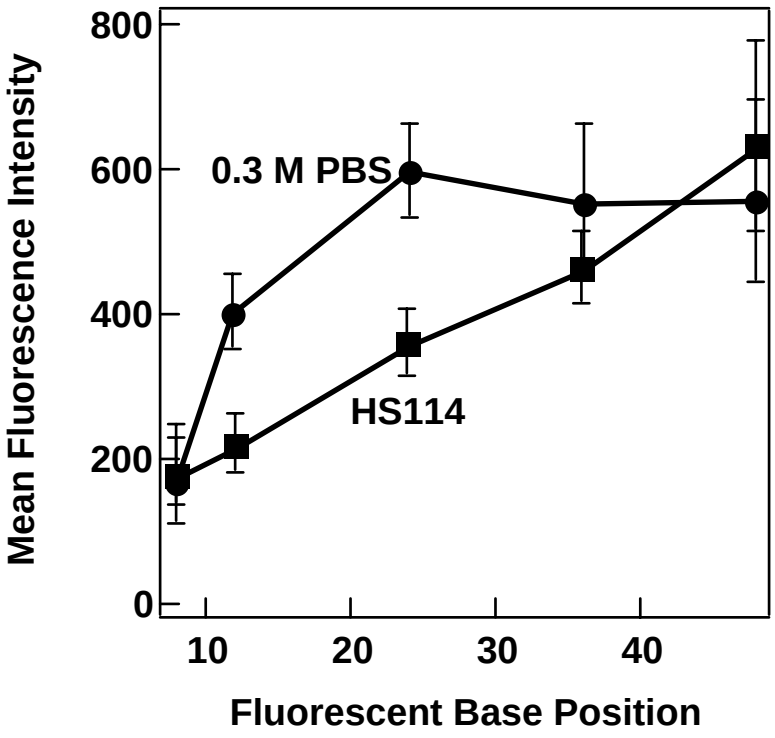

Figure 3.3. Quantification of the effect of dye label position on fluorescence intensity for the multiplexed experiment shown in Figure 3.2, which was hybridized in 0.3 M PBS, and another hybridized in HS114 buffer. Error bars represent the 95 % confidence intervals.

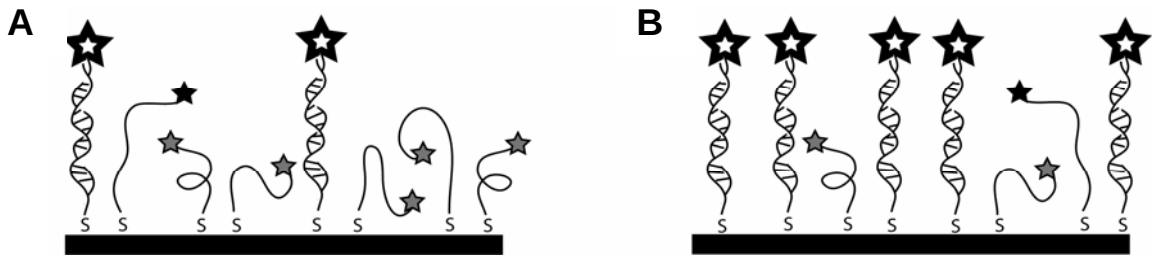

Figure 3.4. Illustration of hybridization efficiency impacting average dye–metal separation where (A) shows lower hybridization efficiency than (B).

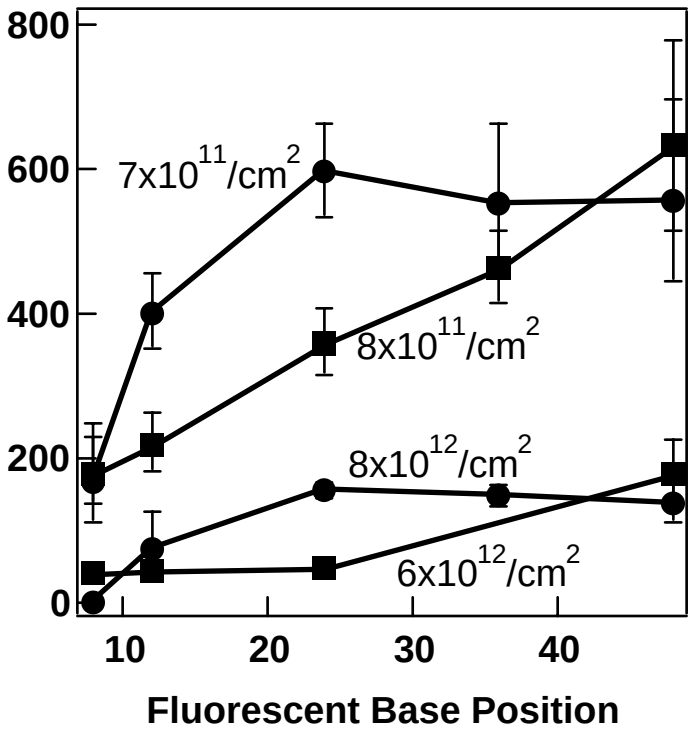

Figure 3.5. Quantification of the effect of dye label position on fluorescence intensity as a function of surface coverage of DNA. Hybridization was performed in two different buffers; 0.3 M PBS (●) and HS114 (■). The surface coverages of fluorescent DNA attached to the nanowires are reported in the figure for each experiment. Errors reported are the 95 % confidence intervals.

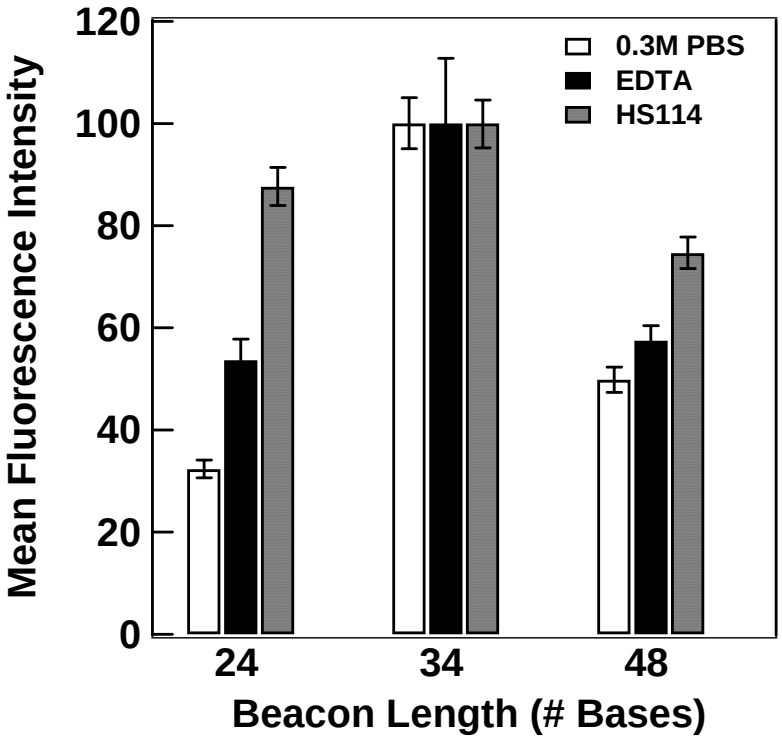

Figure 3.6. Effect of molecular beacon probe length and hybridization buffer on fluorescence intensity after exposure to complementary DNA. Errors reported are the 95 % confidence intervals.

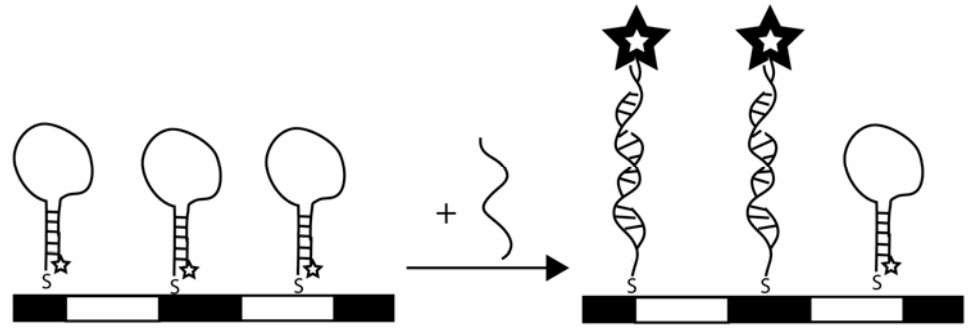

Figure 3.7. Illustration of nanowire-bound molecular beacon probes and hybridization.

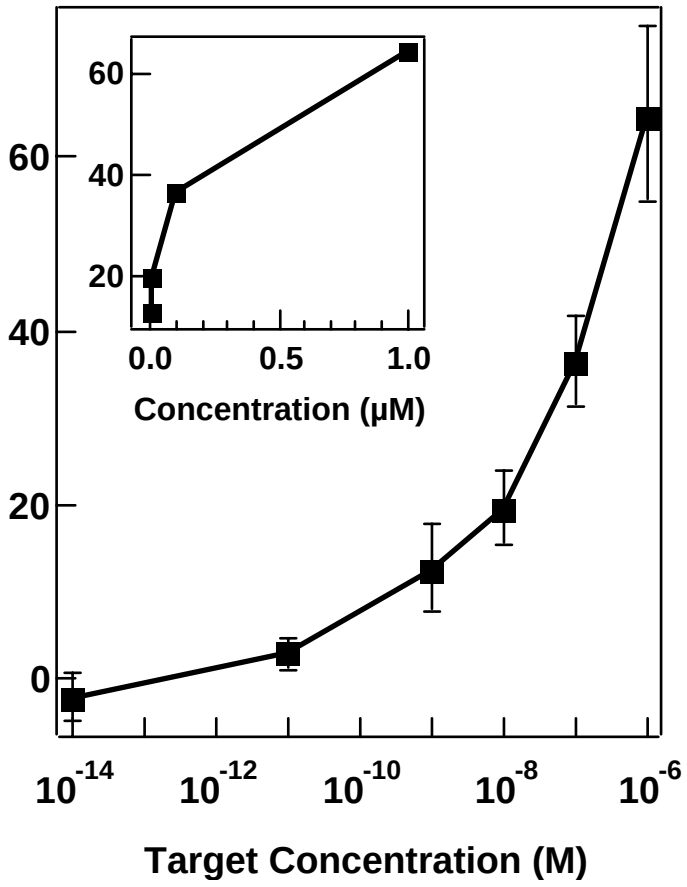

Figure 3.8. Mean fluorescence response of a nanowire-based molecular beacon assay as a function of DNA target concentration. Inset shows same data plotted on a linear scale. Error bars represent the 95 % confidence intervals.

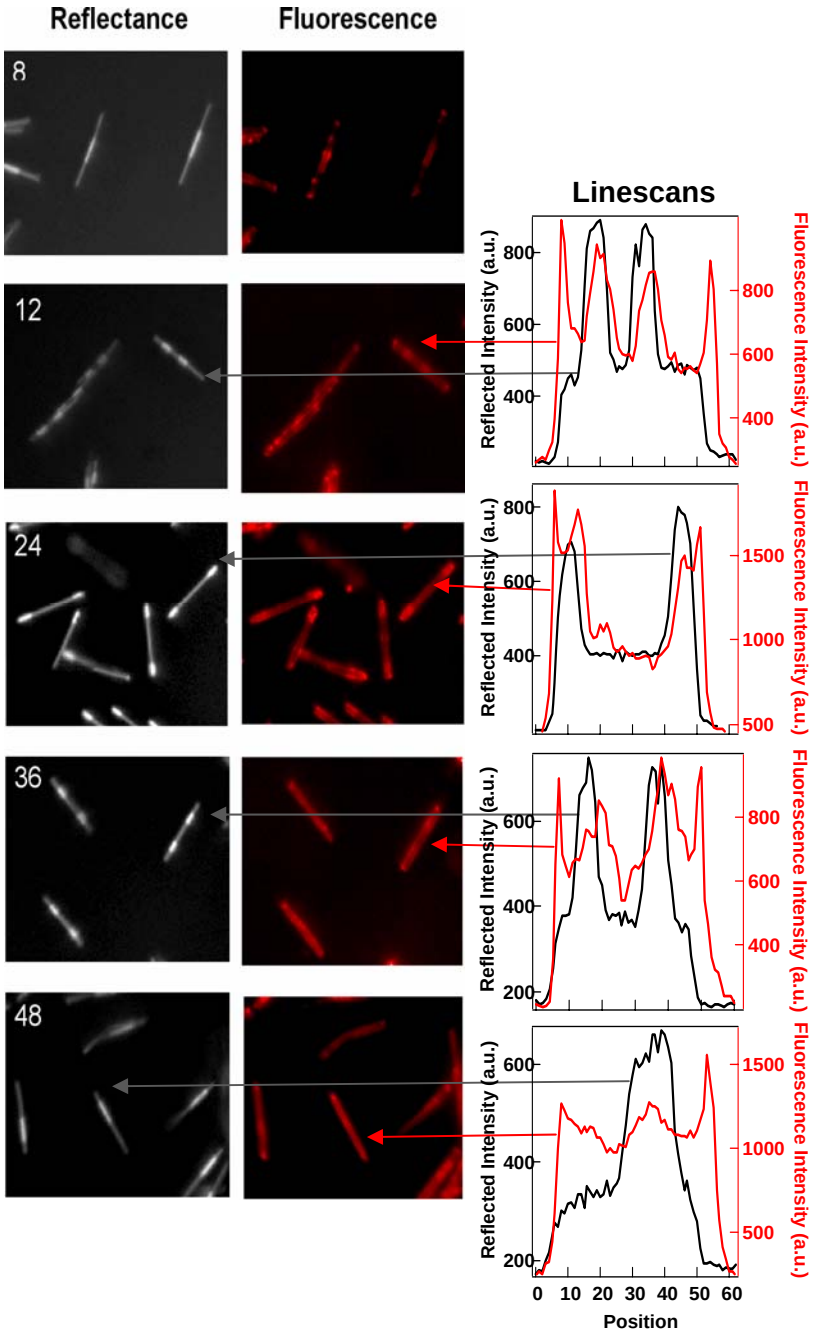

Figure 3.9. Reflectance and corresponding fluorescence images of nanowires coated with 5‘-thiolated oligonucleotides internally labeled with rhodamine red-X dye at different base positions. Line scans correspond to the wires indicated by arrows. The left axis corresponds to the black trace (reflectance) and the red trace corresponds to the right axis (fluorescence).

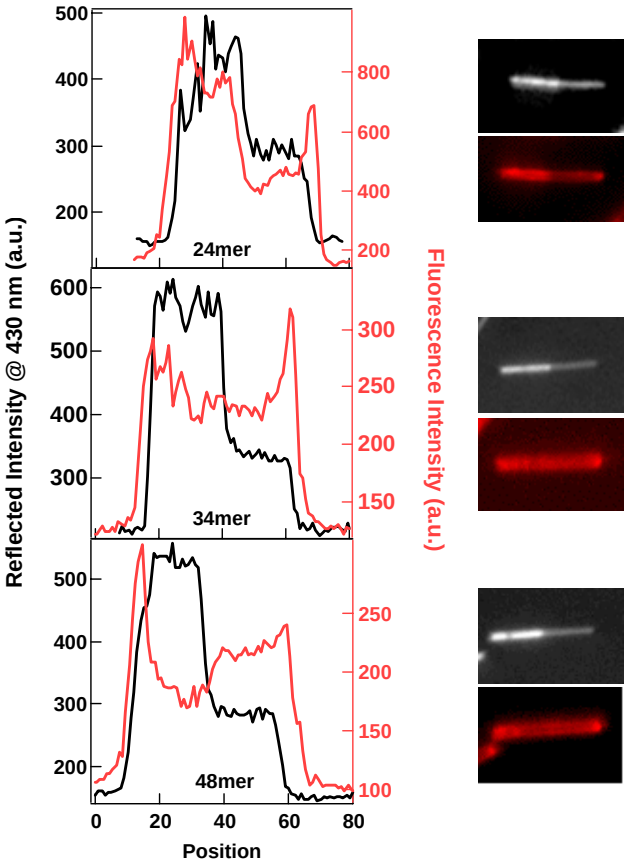

Figure 3.10. Line scans and corresponding reflectance (top) and fluorescence (bottom) images of half Ag/half Au nanowires coated with 5'-thiol, 3'-TAMRA probe oligonucleotides of different lengths. The 24-base probe did not have secondary structure; however, the 34- and 48-base probes were molecular beacons with self-complementarity at the 5' and 3' ends. Unlabeled complementary DNA was present in all cases to extend the probes from the surface. The black trace (reflectance) corresponds to the axis on the left and the red trace (fluorescence) to the axis on the right.

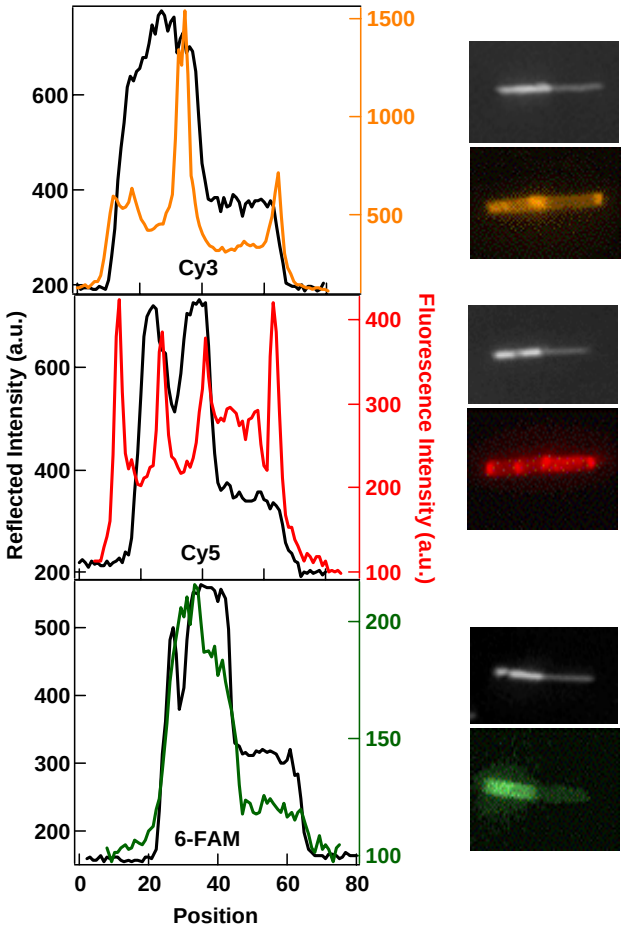

Figure 3.11. Line scans with corresponding reflectance (top) and fluorescence (bottom) images of nanowires coated with 5'-thiol, 3'-fluorophore, 34-base molecular beacon probes, for three fluorophores. The black traces (reflectance) correspond to the left axis and the colored traces (fluorescence) correspond to the right axis.

Chapter 4

Coupling Molecular Beacons to Barcoded Metal Nanowires for Multiplexed, Sealed Chamber DNA Bioassays

4.1. Introduction

Many approaches to nucleic acid detection have appeared, some of which provide exceptional sensitivity[1-3] or selectivity[3-6]. In addition to these important parameters, ease of use, the ability to simultaneously test for multiple target sequences, and contamination risk can dominate the selection of a particular assay type for a given application. Molecular beacon probes can provide nucleic acid detection under "closed tube" conditions, which simplifies assay performance and greatly reduces contamination risk. Molecular beacons (MBs)[7-9] are nucleic acid probe molecules designed with complementarity at their 3' and 5' ends such that they fold into a stem-and-loop (hairpin) structure. Traditionally, a fluorophore and a quencher moiety are attached to the opposing ends. When in the hairpin conformation, the quencher is held close to the fluorophore, quenching emission.[7,10,11] Binding to target separates the donor and acceptor dyes and results in a fluorescence signal.

Advantages to using MBs for DNA detection include: no target labeling, no need to wash after hybridization, and a single hybridization step (as compared with sandwich DNA assays, which require two hybridization steps, with a wash after each one).[7] Challenges in multiplexing MB experiments include the requirement for spectrally distinct dyes, each with an efficient quencher.[12-13] MB bioassays incorporating four

different dyes have been used to enable simultaneous detection of several targets in homogeneous solution.[14] Larger numbers of dyes are difficult to spectrally differentiate.

A promising approach to greater levels of multiplexing (i.e., > 4) for MB probes is to attach the probe molecules to a surface in an array format.[15-18] Tan and coworkers attached biotinylated MBs to fiber optic probes via a layer of streptavidin.[19,20] The resulting biosensors provided real-time detection of nucleic acids with ~1 nM sensitivity and could differentiate single base mismatches from fully complementary targets.[19,20] MBs have also been attached to fluorescently-encoded microspheres for simultaneous detection of four different sequences.[21] Assay performance is influenced by the chemistry at the interface. Lu and coworkers improved quenching in surface-bound MB probes by attaching them to an agarose film on top of glass slides, in an effort to more closely mimic solution conditions. [16] Yao and Tan varied the length of a linker between the MB and the surface, and reduced unfavorable electrostatic interactions with the streptavidin layer to optimize assay performance; the increase in emission intensity after target binding rose from 2x the initial (control) value to 5.5x.[15] For comparison, the increase in fluorescence for solution phase MBs can be on the order of 100x.[22,20] Indeed, the effect of surface immobilization on MB probes can dominate sensor performance, largely due to high backgrounds caused by inefficient quenching. Recently, Lu, Tan and coworkers demonstrated a TaqMan probe array, where Taq polymerase nuclease activity results in cleavage of a 5' quencher to turn on fluorescence at the surface during PCR amplification.[23] This approach does not require probe secondary structure on the surface, and thus avoids the problems of ineffective quenching typically observed for immobilized MB probes.

Several groups, including ourselves, have reported MB assays in which the quencher is a metal nanoparticle or metal surface.[17,24-27] In this case, the probe strand is attached to the metal particle or surface via one end, and a fluorophore on the other end is quenched by close proximity to the metal surface while the probe maintains its hairpin conformation. Metals can provide extremely efficient quenching; Dubertret *et al*. showed that 1.4 nm Au clusters gave better performance in molecular beacons than the common molecular quencher, DABCYL.[25] Krauss and coworkers bound MB-style probes to planar Au films via 5' thiol groups. Despite the surface immobilization, quenching efficiencies were improved as compared to MBs immobilized on glass.[17,24] This could be due to differences in surface chemistry and more efficient quenching by metal surfaces as compared to molecules. For molecular quenchers, two mechanisms of quenching are observed: resonant energy transfer, which can occur over several nanometers, and contact quenching, which requires closer approach.[28] Fluorescence quenching by metal surfaces is effective out to ~5 nm, and the large size of the surface means that multiple conformations of the probe molecules can approach to within this separation. Consequently, even linear probes can be quenched in the absence of –and fluorescent in the presence of– target due to the greater conformational flexibility of single stranded DNA as compared to double stranded DNA.[27] This effect is greatest when probe surface densities are low, such that the probes can "lie down" on the metal, interacting not only via the 5' thiol, but also –transiently– through the 3' dye and/or the bases; Nie and coworkers demonstrated a homogeneous solution assay based on this effect for 2.5 nm Au nanoparticles.[29]

We recently reported an assay in which 5' thiolated MB probes were assembled onto striped metal nanowires (Nanobarcodes® Particles, NBCs). Five different nanowire striping patterns were used to identify specific beacon sequences in a five-plex assay for simultaneous detection of nucleic acid signatures for human pathogens.[26] The encoded nanowires are several microns in length, and ~300 nm in diameter, and have up to six different stripes of Au or Ag. Many distinguishable "barcode" or metal striping patterns can be encoded into the nanowires during synthesis via templated electrodeposition.[30-32] Here we discuss beacon assembly onto the nanowire surface, as well as the effect of hybridization buffer and of changing the length of the "loop" and "stem" regions of the beacon probes on assay performance. Sensitivity and selectivity of the beacon probe-based nanowire assays is presented. Finally, we demonstrate simultaneous detection of three pathogen-specific DNA oligonucleotides in a sealed chamber, no wash multiplexed assay (Figure 4.1), and show that storage of probe-coated wires before use does not negatively impact assay performance. Beyond demonstrating proof-of-principle for a sealed chamber, multiplexed assay of possible future clinical interest, this work provides insight into the effect of surface confinement on molecular beacons. The latter should prove valuable not only for multiplexed MB-based assays such as are described here, but also in the design of experiments in which other structured probes are bound to solid supports, e.g., aptamers[33] designed to detect small molecules, ions, and proteins.

4.2. Materials and Methods

4.2.1. Materials

The striped nanowires used in this work were commercially available Nanobarcodes® Particles (NBCs, Oxonica Inc.) patterned 000111, 00001, 00010, 00100, and 100100, where 0 and 1 represent ~0.75 μm segments of Au and Ag, respectively. These particles were synthesized by electrodeposition into aluminum oxide membranes as described previously.[30,32,34] Nanowires were stored in ethanol (~$1x10^9$ wires per 1 ml ethanol) and were rinsed three times in water (by centrifugation) to remove the ethanol prior to use. Buffers used in the experiments were: 1) 0.3 M PBS (0.3 M NaCl and 10 mM sodium phosphate, pH 7.0) 2) 40 mM Citrate (40 mM citrate in 0.3 M PBS) 3) 0.01 M PBS buffer (0.138 M NaCl; 0.0027 M KCl; 10 mM sodium phosphate, pH 7.4), purchased from Sigma, 4) commercial hybridization buffer (HS114), obtained from Molecular Research Centers, Inc., 5) Tris (100 mM $MgCl_2$, 20 mM Tris-HCl, pH 8.0), and 6) CAC buffer (0.5 M NaCl, 20 mM Cacodylic acid, and 0.5 mM EDTA, pH 7.0). *Note: Cacodylic acid is dimethyl arsenate, a toxin and carcinogen; use gloves and a fume hood.* All water used in these experiments was purified through a Barnstead Nanopure System to 18 MΩ resistivity. All rinses and washes of samples were done by centrifugation and removal of resulting supernatant. DNA beacons were designed using mfold DNA folding program[35] and were purchased from Integrated DNA Technologies, Inc. The sequences used are listed in Table 4.1. Probes *HIV*, *HCV*, *SARS*, and *DENV-2* were designed to detect human immunodeficiency virus, hepatitis C virus, severe acute respiratory syndrome, and strains of Dengue virus subtype 2 (DENV-2), respectively.[26,36,37]

4.2.2. Disulfide Bond Cleavage

DNA sequences were received as disulfides, which in some experiments were cleaved before use, resulting in a single thiol moiety terminating the sequence. To cleave the disulfide, the DNA was first dissolved in a 100 mM solution of DTT (dithiothreitol) in 1 ml 0.1 M phosphate buffer (pH 8.3) for 30 min, and then the small thiol fragments were removed using Centri-Spin Separation Columns (Princeton Separations) following the manufacturer protocol. The resulting DNA sequences (terminated with a single –SH group) were diluted in water to a concentration of 10 μM and were stored in the freezer at –80 °C.

4.2.3. Attaching Beacons to Nanowires

(Used for all experiments unless otherwise noted). Aliquots of 100 μl of wires were washed and resuspended in 100 μl 0.01 M PBS. Beacons were attached by adding 500 μl of 5 μM probe in water overnight at room temperature while tumbling. Next, 600 μl 0.3 M PBS was added and allowed to react for 2 hours to assemble a greater number of probes on the surface. The wires were then washed three times with 0.3 M PBS by centrifugation and were resuspended in 100 μl 0.3 M PBS buffer for further use.

4.2.4. Pre-cleaved vs. Uncleaved Beacons

For this study, HCV beacon was used. Half of the original batch of the DNA beacon was cleaved by disulfide reduction prior to use (following protocol above), and the other half was not cleaved. Both cleaved and uncleaved beacons were attached to

wires patterned 010000 using the attachment protocol previously described (above). For hybridization, 3 μl of beacon derivatized wires were added to 42 μl CAC buffer and 2 μl 100 μM DNA target (no target samples simply had the target excluded) and were allowed to hybridize at room temperature for 2 hours. Samples were not rinsed prior to imaging.

4.2.5. Effect of Loop Length

Attached to three separate aliquots of wires patterned 000111 were beacon sequences *L14*, *L24*, and *L28* following the protocol described above. Samples with and without complementary target were prepared by adding 3 μl of probe coated wires to each of six tubes (six tubes because target and no target sample for each beacon) in 42 μl CAC buffer , and 2 μl 100 μM DNA target (which was omitted for no target samples). Hybridization was performed at room temperature for two hours while tumbling. Samples were rinsed two times by centrifugation in 0.3 M PBS buffer prior to imaging. (It is important to note, however, that rinsing is not necessary prior to imaging as discovered in later experiments).

4.2.6. Effect of Stem Length

Four aliquots of 30 ul of wires patterned 00100 were used as substrates for beacon probes *DENV-2(4)*, *DENV-2(5)*, *DENV-2(6)*, and *DENV-2(7)*. Probe attachment was performed here slightly differently than described above by suspending the wires in 98 μl of 0.01 M PBS buffer, adding 2 μl of respective 100 μM DNA, and allowing the samples to rotate overnight at room temperature. To each sample, 100 μl 0.3 M PBS buffer was

added and rotated for an additional 2 hours at room temperature. Excess DNA was then rinsed out 3 times with 100 μl aliquots of the 0.3 M PBS buffer. Wires were resuspended in 60 μl of this same buffer and stored at 4 °C until use. Hybridization was performed at room temperature, 40 ^{o}C or 60 ^{o}C using 10 μl of probe-coated nanowires added to each target at a final concentration of 5 μM in 30 μl CAC buffer. Control target samples had the same amount of target added; however, the sequence was non complementary to the beacon probe (*HCV* target was used for the noncomplementary samples). Samples were not rinsed prior to imaging.

4.2.7. Testing Different Hybridization Buffers in Triplex Assays

Triplex assays were performed in four different hybridization buffers in the presence and absence of target. Wires patterned 00100, 00001, and 00010 were coated with beacons *HIV*, *SARS*, and *HCV*, respectively. One μl of each of the three batches of beacon-coated wires was mixed together in each of the sample tubes such that 3 μl of wires total resided in each tube. Samples were prepared such that all 3 targets could be added to the triplexed wires in each of four hybridization buffers (PBS, CAC, TRIS, and HS114) and the experiment was duplicated such that no targets were added to separate batches of triplexed wires in each hybridization buffer. Therefore, a total of eight triplexed samples existed (one for each buffer with target and one for each buffer without target). Added to each sample were 47 μl of the specified hybridization buffer and 1 μl of 10 μM of each type of target. (No target samples did not have target added). This entire protocol was repeated such that hybridization at both room temperature and 50 °C

could be studied. All samples were hybridized 1 hr at either temperature. The samples were not rinsed before imaging.

4.2.8. Effect of Salt Concentration

Wires patterned 100100 were derivatized with *DENV-2(5)* beacon following the protocol originally outlined for probe attachment. Hybridization was performed in 20 mM cacodylate buffer to which different amounts of NaCl had been added. Five μl of the functionalized wires were added to 35 μL each buffer formulation, along with 1 μl of 100 μM DNA target and were then hybridized for 1 hour either at room temperature or 50 °C. Samples were then imaged at room temperature using optical microscopy.

4.2.9. Sensitivity of Nanowire Beacon Assay

Beacon probes (*HCV*) were attached to nanowires patterned 00010. Final target DNA concentrations 0 to $1x10^{-6}$ M were prepared in 50 μl 0.3 M PBS buffer. To 47 μl aliquots of target in 0.3 M PBS buffer, 3 μl of beacon-coated wires in 0.3 M PBS were added (yielding a final volume of 50 μl). Beacon targets were allowed to hybridize at 50 °C for 2 hrs while tumbling. Samples were rinsed three times in 0.3 M PBS before imaging.

4.2.10. Single Base Mismatch Detection

Wires patterned 000010 were derivatized with DNA beacon sequence *SBM*. Aliquots of 34 μl of 2x TMAC (tetramethyl-ammonium chloride buffer, Sigma), 3 μl of 2

μM oligo target (complementary or containing one of the possible mismatched nucleotides at the location labeled in Table 4.1 (no target sample simply had target DNA omitted)), and 3 μl of beacon coated nanowires were mixed, sonicated, and allowed to hybridize at 55 °C for 30 min. The samples were centrifuged and resuspended in 500 μl of 1xSSPE-0.1 % SDS buffer (purchased from Promega and added SDS (dodecyl sulfate, sodium salt from Aldrich)) and allowed to mix in this buffer at room temperature for 10 min before removing the buffer by centrifugation. The wires were then suspended in 0.1xSSPE-0.05 % SDS for 7 min while rotating at 55 °C, for an additional rinse. The wires were then rinsed 3 times in 0.5 M CAC buffer and resuspended in 50 μl CAC buffer before imaging.

4.2.11. Multiplexed Sealed Chamber Assays

To perform sealed chamber assays, single well silicon spacers measuring 20 mm in diameter and 0.5 mm deep were used (Press-to-Seal™silicon isolators, Molecular Probes, Eugene, OR). To attach the silicon spacers to coverslips, tape was first applied to the spacer and removed to pull off any lint or particles that would prevent a tight seal; then, they were applied to the coverslip. The tape regimen was then redone on the top-side of the spacer before adding reagents. Hybridization buffer was then added (145 μl of 0.3 M PBS), 3 μl total beacon coated wires (in experiments where three types of wires were mixed for multiplexing, 1 μl of each type was used), and 2 μl of 100 μM of each target was added. Beacon sequences *HIV*, *SARS*, and *HCV* were coated onto wires patterned 00100, 00001, and 00010, respectively, using methods previously described. A

glass slide was then attached to the top of each sample before placement in an incubator at 50 °C for 10 min. The samples were allowed to cool for 30 min before imaging. Silicon spacers were reused in subsequent experiments by thorough washing in detergent, rinsing in water, air drying, and repeating the tape process to remove any dust prior to use.

4.2.12. Storage in Citrate Buffer

HIV, *SARS*, and *HCV* beacons were coated onto wires patterned 00100, 00001, and 00010, respectively, following the attachment protocol outlined above. Once the beacons were attached, the wires were rinsed as described, but instead of storage in 0.3 M PBS buffer, 100 μl 40 mM citrate buffer was added for storage. After the specified number of days (0, 22, 65, or 110), 1 μl aliquots were removed from each of the three batches, rinsed once in 0.3 M PBS, and mixed in one tube for hybridization. This was done for multiple tubes such that in one tube, all three targets were added, another tube had no targets added, and other tubes contained combinations of certain targets to test multiplexing capabilities. Hybridization was performed with 2 μl of 10 μM target in 47 μl CAC buffer at 50 °C while tumbling. The samples were not rinsed to remove excess target before imaging.

4.2.13. Optical Microscopy

Brightfield reflectance images were acquired using a Nikon TE-300 inverted microscope equipped with a 12 bit high resolution Coolsnap HQ camera (Photometrics).

A CFI plan fluor 60x oil immersion lens (N.A. = 1.4) was used in conjunction with Image-Pro Plus software (version 4.5) to image the samples. The light source was a 175 W ozone free Xe lamp, and a Sutter Instruments filter wheel (Lambda 10-2) allowed for wavelength selection. Samples were prepared by first sonicating the tubes of sample to reduce wire clumping and sandwiching a 10 μl aliquot between two coverslips. Wires were allowed to settle onto the bottom slide for 30 seconds before imaging. All reflectance images were taken at 430 nm, which provides good reflectance contrast between Au and Ag.[30,38] Fluorescence images were taken using a filter cube selective for TAMRA fluorophore excitation. All imaging was performed at room temperature.

4.2.14. Probe Surface Coverage Determination

Surface coverage was obtained by adding 5 μl mercaptoethanol to 200 μl buffer containing 5 μl beacon-coated nanowires. The samples were allowed to tumble on a rotator at room temperature overnight. The DNA was displaced into solution and was collected in the supernatant. The fluorescence intensity was determined using a fluorolog-3 fluorimeter, equipped with a 450 W Xe lamp, and double grating excitation spectrometer and a single grating emission spectrometer in a 180 μl volume cuvette. Calibration standards were used to determine the beacon concentrations in each sample.

4.3. Results and Discussion

4.3.1. Beacon Attachment Methods

We compared two methods for beacon probe attachment onto the nanowire surface based on 5′ terminal thiol groups. Thiol terminated DNA sequences are purchased as disulfides ($DNA^{5'}$-S-S-$C_6H_{12}OH$), and generally this disulfide is cleaved using dithiothreitol as a reducing agent, then run down a desalting column to collect the thiolated DNA prior to use. Integrated DNA Technologies recommends cleaving the disulfide bond immediately prior to use to avoid regeneration of the disulfides. This method is routinely used by ourselves and others for preparation of DNA conjugates with colloidal Au nanospheres, which are sensitive to aggregation in the presence of salts and uncharged, short-chain thiols.[39-41] However, since adsorption to metal surfaces is known to cleave disulfides[42,43] pre-assembly reduction and separation may be unnecessary for nanowire derivatization. Advantages to allowing the surface to perform the disulfide cleavage reaction include reduced time and effort, and avoiding loss of thiolated DNA during the separation step. To determine whether pre-assembly disulfide cleavage was necessary, we compared mean fluorescence intensities for a 5' thiolated, 3' TAMRA molecular beacon probe (*HCV*) pre-cleaved using DTT before attachment to the nanowires and the same beacon sequence not cleaved prior to adsorption (Figure 4.2). Beacon probe attachments were performed using identical protocols. In the absence of target, minimal fluorescence intensity is desired and in the presence of target a great increase in signal is favorable. The "no target" samples should exhibit minimal fluorescence, as beacons should be folded and quenched. Our measured quenching efficiencies (calculated as [1-(signal in absence of target/signal with target)], %)

improved from 90 % for the DTT cleaved to 96 % for the uncleaved samples. However, the overall fluorescence intensity for the uncleaved sample was only about one-third that for the DTT cleaved sample. This corresponded to a substantial difference in beacon probe surface coverage for the two attachment strategies, with 4 x 10^{12} molecules/cm^2 (25 nm^2/molecule) for the DTT cleaved probes, and only 7 x 10^{11} probes/cm^2 (140 nm^2/molecule) for the uncleaved probes. The large areas occupied by oligonucleotides on surfaces underscore the fact that these molecules are negatively charged and adopt a number of conformations, including dynamic transitions between the hairpin loop and unfolded random coil. We rationalize the difference in surface coverage between the two samples as resulting from more efficient attachment for the cleaved probes, for which the sulfur atoms are less hindered, coupled with the effect of coadsorbed mercaptohexanol molecules in the case of the uncleaved probes (generated by cleavage at the surface). Lower probe coverages would simultaneously provide improved quenching and hybridization efficiencies, due to lower steric and electrostatic repulsions,[44-47] as well as lower total fluorescence intensities, due to the smaller number of TAMRA fluorophores on each wire. The coadsorbed mercaptohexanol in the uncleaved samples may also reduce interactions between the DNA bases or backbone and the wire surface. Beacon probes attached via a single point (the 5' thiol) are more likely to bind to their own stem sequences, allowing them to quench more efficiently, as the stem configuration places the fluorophore in close proximity to the metal surface. The data in Figure 4.2 show that either pre-cleaved or as- received thiolated oligonucleotides can be used for preparation of probe-coated nanowires. For the remainder of the experiments in this paper, we did not pre-cleave probes prior to assembly.

4.3.2. Beacon Probe Design

The beacons used here were designed using mfold, a nucleic acid folding program designed by Michael Zuker.[35] This program offers insight to MB probe secondary structure and predicts binding energies for the folded structures. These structure predictions, however, do not take into consideration the fact that our beacon probes are attached to a surface, nor the impact of adjacent probe molecules. Therefore, the folding program was used primarily as a guide to avoid the use of beacons that contained a great deal of secondary structure in their loop regions, and to provide a means of comparing the relative thermodynamic stabilities of the probes. Solution phase molecular beacon probes are typically designed with 15 to 30 base loop regions and 5 to 7 base pair stem regions. Shorter loops can provide greater discrimination against single base mismatches, while longer loops can provide greater equilibrium binding constants for target sequences. Stem length dictates the stability of the probe secondary structure; probes having longer stems are more difficult to unfold. We anticipated that these general observations from solution phase beacons would hold true; nonetheless, the optimal probe design for surface-based experiments could differ substantially from that for solution studies. To identify design rules for surface-bound beacon probes, we compared the performance of nanowire-bound beacon probes as a function of loop length and stem length.

We had previously observed a decrease in beacon probe performance in nanowire-based assays as loop length was increased from 24 to 34 and 44 bases.[26] In those experiments, we were unable to measure the probe densities the nanowire surface, which complicated interpretation. Here, we compare assay performance and probe density for 24-base loops to that for both shorter (14-base) and longer (34-base) loops,

Figure 4.3 compares mean fluorescence intensities for these nanowire-bound beacon probes in the presence and absence of target DNA (target length = loop length). The stem region was 5 base pairs long for each probe. As we reported previously,[27] fluorescence intensity in the presence of target increases as probe length increases from 24 to 34 bases (i.e., 14 to 24 base loops) due to a combination of decreased quenching by the metal surface and increased hybridization efficiency due to the increased stability of the probe-target duplex. For the 38 base loop, intensity decreases despite the fact that quenching should be further reduced for this longer probe, and the thermodynamic stability of the solution phase analogue of this duplex should be increased. We attribute this to decreased hybridization efficiency for the longer strands, due to increased steric and electrostatic repulsions between probe molecules on the surface. [27] The surface coverage was between 1.2 and 2.5 x 10^{11} probes/cm^2 for all three of the probes, with the highest value coming from the 24-base loop probe. Fluorescence signal in the absence of target is lowest for the probe having the 24-base loop, which, combined with the higher signal in the presence of target, gives optimal quenching efficiency for this intermediate length probe.

The effect of stem length was investigated using a series of probes with a 21-base loop region designed to recognize 16 strains of dengue virus subtype 2 (DENV-2), which is the most serious pathogenic variation of DV. Four stem lengths (sequences *DENV-2(4)*, *DENV-2(5), DENV-2(6)*, and *DENV-2(7)*, corresponding to stem lengths of 4, 5, 6, and 7 base pairs, respectively) were predicted by mfold nucleic acid folding software to form secondary structures with ΔG between –2 and –9 kcal/mol in 0.5 M NaCl (the salt concentration used for these experiments). Fluorescence intensities for these probe

sequences after incubation at 25 ^{o}C in the presence and absence of target oligonucleotides are shown in Figure 4.4A. As expected, the shorter stems (i.e. least stable hairpin structures) led to higher fluorescence signals both in the presence and absence of complementary target DNA strands. This is consistent with less stable hairpin secondary structure formation. Longer stems led to greatly decreased intensity for the complementary target, slightly decreased intensities for the no target samples, but essentially no improvement in the noncomplementary controls. Quenching efficiencies were somewhat similar for all four probes, ranging from ~90 % for the 5 base pair stem to ~75 % for the 7 base pair stem. Repeating the experiment at higher hybridization temperatures (40 ^{o}C and 60 ^{o}C) decreased the QE, particularly for the longest stem probes (Figure 4.4*B;* fluorescence intensities for the 40 ^{o}C and 60 ^{o}C experiments are plotted in Figure 4.5). We note that QE determination is less accurate for lower intensity samples, and that the apparently anomalous QE for the 7 base pair probe at 40^{o}C is most likely the result of variability rather than a physical phenomenon unique to this temperature.

Our results thus far indicate that probes having approximately 24-base loops and 5-base pair stems are optimal under the conditions of these assays (300-500 mM NaCl, 20-60 ^{o}C). Performing the hybridizations at room temperature provided the best QE for all four *DV* stem lengths tested. Changes in either ionic strength or temperature are expected to alter the optimum probe design. For example, if substantially lower ionic strength buffer or higher hybridization temperatures are used, it may be necessary to go to longer stems to maintain quenching efficiency.

4.3.3. The Effects of Ionic Strength on MB-Target Duplexes

Salt-dependent electrostatic effects are a major factor in determining the secondary structure and hybridization thermodynamics of nucleic acids. The high density of probe oligonucleotides can be expected to the increase electrostatic repulsions that must be overcome for probe secondary structures or probe-target binding to occur. We compared the performance of the MB-coated nanowires in a triplexed assay format where each of three different MB probes (*HIV*, *SARS*, and *HCV*) was attached to a different nanowire barcode pattern (as shown in Figure 4.1, except that all three targets were added). The three probe-coated wires were mixed together and then either all three targets, or no target (for the negative control), was added for hybridization in one of four different buffers. The four buffers tested were: (1) TRIS (100 mM $MgCl_2$, 20 mM TRIS-HCl, pH 8.0, used by Lu and coworkers for molecular beacons immobilized on agarose films),[16] (2), PBS (0.3 M NaCl, 10 mM phosphate, which is commonly used for metal particle-bound DNA hybridization assays),[46,47,49,50] (3) HS114 (a commercial hybridization buffer, the contents of which are proprietary, which we had previously used for nanowire-bound beacon assays),[26] and (4) CAC (0.5 M NaCl, 20 mM cacodylic acid, 0.5 mM EDTA, pH 7.0, which was used by Krauss and coworkers for molecular beacons immobilized on planar Au supports[24]). Hybridization was performed in each buffer at 25 °C and 50 °C.

Figure 4.6 summarizes the results of this experiment. Quenching efficiencies (filled symbols) are plotted on the left axis for all three beacons multiplexed in each buffer formulation at 25 ^{o}C (top panel) and 50 ^{o}C (bottom panel). The corresponding fluorescence intensities (open symbols) in the presence of target strands are plotted on the

right axis. For the 25 ^{o}C hybridization, QE varied substantially with the hybridization buffer used, with the more stringent HS114 buffer resulting in QE as low as 24 % (for HIV probe), and the highest ionic strength CAC buffer providing QE as high as 88 %. (for HCV probe). The high salt content of the CAC buffer enables improved performance by screening the electrostatic repulsions due the high density of negatively charged probe molecules at the nanowire surface. The buffers can be ranked in terms of QE as CAC>TRIS>PBS≈HS114, and in terms of fluorescence intensity as HS114>CAC>PBS>TRIS. The best overall performance was observed for CAC, which had the highest QE and the second highest fluorescence intensity. Some differences between the three beacon probes are apparent in Figure 4.6 (top). For example, the HIV probe is generally the brightest, consistent with the lower thermodynamic stability of this probe's hairpin secondary structure (Table 4.1).

When hybridization was performed at 50 ^{o}C, both fluorescence intensities and QE generally improved (Figure 4.6, bottom panel). We note, however, that QE for CAC decreased slightly at 50 ^{o}C as compared to 25 ^{o}C, in agreement with Figure 4.4B. QE for the four buffers now can be ranked as TRIS≈PBS≈CAC>HS114, and fluorescence intensity as HS114>CAC>PBS>TRIS. Although the QE for the HIV probe is anomalously poor for PBS in this data set, good overall performance is achieved with both CAC and PBS buffers at this temperature. The TRIS buffer gave equally good QE, but low fluorescence intensities. HS114, in contrast, gave the highest intensities, but poor quenching. Based on these findings, we selected either CAC or PBS buffers for our ongoing studies; when PBS was used, hybridization was performed at 50 ^{o}C to avoid the low QE observed at 25 ^{o}C (Figure 4.6, top panel). One advantage of PBS over CAC is

avoiding the use of dimethyl arsenate (i.e. cacodylic acid), which is toxic and carcinogenic and therefore must be handled with care.

The most critical aspect of buffer composition is its ability to screen electrostatic repulsions between probe and target DNA molecules as well as between the two ends of the beacon probes. We compared the performance of nanowire-bound *DENV-2(5)* beacon probes as a function of ionic strength by varying the NaCl concentration between 50 mM and 1.5 M in cacodylate buffer at 25 and 50 ^{o}C (Figure 4.7). At 25 ^{o}C, fluorescence intensity in the presence of target increases from 50 mM NaCl to 500 mM NaCl, and then decreases. Fluorescence intensity in the absence of target is lowest for the lower salt samples; however QE is best for 200 and 500 mM, at 90 %. QE drops to 87 % at 100 mM, and 82 % at 750 mM NaCl. When hybridized at 50 ^{o}C, quenching was nearly complete even in the presence of target for ≤100 mM NaCl. As the salt concentration was increased, fluorescence intensity in the presence of target increased substantially to peak at 500 mM, then decreased at higher salt concentrations. Quenching efficiencies were again optimal for 200 and 500 mM NaCl, at 88 % for both.

The general trends observed in Figure 4.7 are consistent with our understanding of MB probe structure at the metal surface. At very low salt, the beacon probes cannot readily bind target molecules, and are unable to fold as effectively into secondary structures due to electrostatic repulsions. Thus, the quenching observed for ≤100 mM NaCl in Figure 4.7, particularly when hybridized at 50 ^{o}C, arises not from hairpin formation, but rather from conformational flexibility of the single-stranded probes, which prevents their 3' dye molecules from extending far enough away from the metal surface to avoid quenching. The very low intensities for low salt samples could also be explained

by loss of the probes from the surface due to increased intermolecular electrostatic repulsions. To test for this, we measured the surface coverage of probes after being stored under hybridization conditions in buffer containing either 50 mM or 1 M NaCl, in the absence of target DNA. Surface coverages at 50 mM and 1.0 M NaCl were indistinguishable, at $4 \pm 2 \times 10^{11}$ and $3 \pm 1 \times 10^{11}$ probes/cm^2, respectively. Thus, no significant loss of probe DNA occurred at the lower salt concentrations, supporting our interpretation that the low intensities observed in low salt buffers were the result of quenching due to probe flexibility. The surface coverage experiment was performed on samples incubated for 2 hr at 40 ^{o}C. This is a slightly lower temperature than in the lower panel of Figure 4.7, however we also see very low fluorescence intensities in low salt buffers at 40 ^{o}C (Figure 4.8).

The decrease in emission at very high NaCl concentrations in the presence of target observed in Figure 4.7 presumably arises due to stabilization of the probe's hairpin structure, which must remain fluxional to enable hybridization to complementary target strands. The intensity for the negative control samples is relatively low at all salt concentrations, increasing slightly with NaCl concentration up to 750 or 500 mM, for the 25 ^{o}C and 50 ^{o}C data sets, respectively, before leveling off. At both temperatures, the highest intensities in the presence of target are observed in 500 mM NaCl, and optimal QE are observed in both 200 and 500 mM. For the remainder of the work described here, we used either 300 mM or 500 mM NaCl. These are relatively high ionic strengths, required due to strong electrostatic repulsions between the adjacent probes on the nanowire surface.[49-51]

4.3.4. Nanowire MB Assay Sensitivity

The sensitivity of the nanowire beacon assays described here is comparable to other surface-bound molecular beacon assays.[16,21,22,24,25,29] Figure 4.9 shows assay response as a function of target oligonucleotide concentration for *HCV* beacon probes hybridized in 0.3 M PBS at 50 ^{o}C. The y axis is fractional coverage, estimated based on the fluorescence intensity as compared to the maximum intensity. The limit of detection (LOD) for this data was calculated by taking the average fluorescence intensity for the control (background signal) and adding two times its standard deviation.[52] We report a LOD = 38.1 + 2(3.0) = 44.1 mean fluorescence units which translates to a concentration of <100 pM (10 femtomoles in our 100 μL volume), with dynamic range of three to four orders of magnitude in concentration. We note that, although the dynamic range is large, this assay is most sensitive to changes in concentration at low concentrations (see Figure 4.9 inset). The data in Figure 4.9 could be fit to a Sips isotherm,

$$f = (KC)^a/[1+(KC)^a] \qquad (1)$$

where f is the fractional coverage of target binding sites on the beacon probe-coated wire, K is the average equilibrium constant for adsorption, C is the concentration of target in solution, and a is the heterogeneity index.[53,54] The Sips isotherm assumes that the heterogeneity in binding sites takes the form of a Gaussian distribution of affinities. The width of this distribution is determined by the magnitude of a, which varies from 0 to 1 (when a = 1, the equation simplifies to the more familiar Langmuir isotherm). Fitting to equation (1) gave a K_d of 1.7 ± 0.3 nM and a heterogeneity index of 0.57 ± 0.06 for the

nanowire-bound *HCV* beacon probes. We hypothesize that the heterogeneity in binding affinities observed in our experiments could arise from: (1) variations in surface probe density between nanowires or at different points on a single nanowire, which would alter steric and electrostatic contributions to the binding affinity, (2) differences in probe conformation, which would affect accessibility, or (3) differences in the signal observed for binding events occurring on Ag vs. Au segments of the nanowires, which would not change the affinity but would alter the fluorescence intensity per binding event, which would impact our apparent affinity.

These results differ substantially from those reported for molecular beacons on planar Au surfaces (which fitted a two-state model with a K_d of 0.95 μM and a narrow dynamic range),[24] but follow expectations for surface-bound single stranded probes with no secondary structure, which can generally be fit by Langmuir or related surface adsorption isotherms.[55,56] For example, Corn and coworkers fit an thermodynamic date for probes on planar Au to a Langmuir isotherm and report similar K_d values (55 nM for an 18-mer probe/target duplex in a 300 mM NaCl, 100 mM urea PBS buffer).[57] Peterson *et al*. found that perfectly matched duplex formation on an Au surface could be fit to a Langmuir isotherm (with K_d =17 nM for a 25-mer duplex in 1 M NaCl buffer), while mismatched duplexes were better modeled by the Sips isotherm.[58] The preceding examples both used unstructured probe DNA, rather than MB probes. However, we note that MB probes in solution also exhibit several orders of magnitude in dynamic range of fluorescence response to target concentration.[25]

Factors that affect sensitivity include the number of wires in each assay (surface area), surface coverage of beacon probes, hybridization thermodynamics, and beacon

probe quenching efficiency. The highest target concentration tested ($1x10^{-6}$ M) provided $3.0x10^{13}$ target strands/sample, which decreased to $3.0x10^{9}$ /sample for $1x10^{-10}$ M target. For the data shown in Figure 4.9, ~ $3x10^{6}$ nanowires, with $1.3x10^{12}$ beacon probes/cm^2 were used for each sample. This resulted in approximately $2.4x\ 10^{11}$ total beacon probes per sample. The number of target molecules added as compared to the number of probe molecules present on the nanowires can be estimated at 126 % for 10 nM target, 1.3% for 0.1 nM, and 0.13 % for 10 pM target. Reducing the number of wires present in the assay, in principle down to a single wire, could improve sensitivity by reducing the volume of ~0.1 nM target needed to detect a response. However, use of multiple wires simplifies handling and visualization, as well as providing more data points for statistical analysis. Therefore, although it may be possible to improve LOD by reducing the surface available for binding, there are other trade offs that must be considered. Other approaches to increasing LOD include probe design, to improve K_d, and nanowire surface chemistry, to improve quenching efficiency. Nonetheless, we will ultimately be limited by the binding affinity of the target for the probe strand, and therefore we do not anticipate that this sensing approach will rival ultrasensitive methods such as PCR. Rather, it could offer a route to simple, relatively low sensitivity multiplexing under closed-chamber conditions (i.e. with no target labeling, washing, or other addition of reagents, such that ease of use is increased, and contamination risk is reduced).

4.3.5. Single Base Mismatch Detection

Solution-phase MB probes can provide excellent selectivity, due to their intrinsic secondary structure.[4,13] We tested the selectivity of our nanowire-immobilized MBs by

comparing their response after exposure to mismatched or fully complementary targets sequences. An HIV-specific probe with a relatively short 14 base loop region, sequence *SBM*, was used for these experiments in order to increase the energetic difference between binding the matched vs. single base mismatched targets. Figure 4.10 shows the fluorescence results for each of the target sequences after hybridization at 55 ^{o}C for 30 minutes. We note that this experiment was performed under more stringent hybridization and wash conditions than any other in this paper; poor mismatch discrimination was observed when hybridized in 0.5 M NaCl CAC buffer for 2 hrs at room temperature.

The fully complementary target gave a greater response than any of the single base mismatches (the three mismatches shown correspond to all possibilities for replacing a central C in the target). Discrimination was best for the T, which gave a 4.5 fold difference between the fully complementary and mismatched targets. The A and G mismatch sequences gave 3.6 and 2.8 fold differences, respectively. Although the nanowire bound beacon probes were able to differentiate the single base mismatches, they did not provide as large of a difference as was observed by Krauss and coworkers for MBs on planar Au (8-fold difference).[24] We hypothesize that the greater increase in fluorescence signal in the presence of fully complementary DNA, leading to the larger increase in signal, may be due in part to the longer probe used in reference 24, which would help avoid quenching from the metal surface (36 total bases as compared to 25 bases). We have recently reported that 34 base long sequences exhibit higher fluorescence than 24 base long sequences.[27]

4.3.6. Multiplexed, No-wash, Sealed Assays

Diagnostic applications of bioassays under clinical settings must contend with the risk of sample cross-contamination. One advantage of reagentless approaches such as molecular beacons (whether in solution or surface-bound) is that once the sample is added to the beacon probes, no further manipulation (e.g., addition of reagents, washing) should be required. The ability to perform an assay in a sealed container greatly reduces contamination risk. We therefore considered the performance of a sealed assay, where all reagents were sealed on a microscope slide during both reaction and analysis, as the risk of contamination is greatly reduced. A multiplexed, sealed assay was performed as shown in Figure 4.5 by first coating three different MB probes (*HIV*, *SARS*, and *HCV*) on three different patterns of wires (00100, 00001, and 00010, respectively), and then mixing the beacon coated wires with all hybridizing reagents and target in sealed chamber gaskets on glass slides, which were not opened even for imaging. Representative fluorescence and reflectance microscope images for an assay in which *HIV*- and *SARS*-specific targets (but not *HCV*-specific target) have been added are presented in Figure 4.11 *(*the sample was hybridized in PBS at 50 ^{o}C). The nanowires that are visible in the fluorescence image correspond to 00100 and 00001 patterns, as evident in the corresponding reflectivity image, indicating that only nanowires coated with HIV- and SARS-specific MB probes gave a positive response.

Figure 4.12 gives quantification for the assay represented in Figure 4.11 as well as other combinations of targets. Since the individual assays making up this multiplexed experiment exhibited differences in fluorescence response (i.e. the *HIV* probes were always brighter than the *HCV* or *SARS*, as also observed in Figure 4.3), each probe was

normalized independently to simplify interpretation. The quenching efficiencies from this sealed chamber assay were 89, 87, and 92 % for *HIV*, *HCV*, and *SARS*, respectively. There was good discrimination in triplex samples where only one or two targets are present, considering the assays with all three targets present or no targets present as reference points. We note that the background signal is lowest when no targets have been added, as compared to when one or more targets are added. For example, fluorescence response for the *HCV* and *SARS* assays when only *HIV* target was added were larger than when no target had been added. This indicates either nonspecific target binding, or incorrect nanowire identification by software, or some combination of the two. This can be improved by beacon probe design and/or optimization of identification software and nanowire electrodeposition. Nonetheless, the multiplexed, sealed assay in its current form unambiguously identified the correct targets in each sample. These results suggest that the elimination of the rinsing step, and the reduction on mixing due to the sealed chamber geometry did not negatively affect the ability to perform simultaneous assays for three oligonucleotide targets. Indeed, we see no degradation in assay performance between rinsed and unrinsed samples (data not shown). These results are promising in that sealed chamber assays can help eliminate sample contamination, and personnel exposure, as well as simplifying assay performance. Although our prior demonstration of PCR product detection by nanowire-bound MB was rinsed (i.e. not performed in a sealed chamber),[27] the success of solution-phase MB-style probes in the more complex matrices of PCR products, clinical samples, and living cells suggests that the sealed chamber approach used here will be applicable to samples of diagnostic interest.[1,60-63]

4.3.7. Preservation of Assays using Citrate Buffer

Since future clinical applications of the beacon-coated nanowires would likely involve storage of the bioconjugated wires prior to use, we were interested in determining whether the performance of wires pre-coated in beacon probes deteriorated if not used immediately after preparation. In previous studies, we had found that citrate buffer protected the Ag segments of bare or DNA-coated striped nanowires from Ag degradation and DNA loss in oxygenated, PBS buffers over relatively long periods of time (at least months).[64] Therefore, we added 40 mM citrate to the 0.3 M PBS storage buffer for these experiments. Wires were centrifuged and resuspended into 500 mM NaCl CAC buffer prior to hybridization, to avoid any differences in assay performance due to the citrate. Figure 4.13 shows fluorescence intensities from multiplexed assays in which *HIV*-, *HCV*-, and *SARS*-specific beacon probe sequences are used. In Figure 4.13A, samples to which all three targets or no target are compared after 0, 22, 65, and 110 days of storage. To correct from day-to-day variations in lamp intensity (which were substantial, since between days 22 and 65 we installed a new, brighter lamp), we normalized these data such that the intensity of the brightest nanowire population (in every case this corresponded to those with the *HIV*-specific probes) in the presence of target oligonucleotides was defined as 100 %. The quenching efficiency for each of the three nanowire populations improved slightly between days 0 and 22, from 78 to 91 %, 82 to 88 %, and 84 to 93 %, for *HIV*-, *HCV*-, and *SARS*-specific probes, respectively). We interpret this improvement as arising from reorganization or loss of some probe strands leading to improved hybridization at the surface. After day 22, essentially no change in QE was observed.

The relative intensities of the three different beacon probe sequences stayed constant over the 110 day period, with the *HIV*-specific probes in all cases significantly brighter than the other two probes. This can be understood in light of the greater stability of the hairpin structures for the *HCV* and *SARS* probes (Table 4.1); the *HIV* probe has the least negative ΔG of the three probes, and its superior performance under the conditions of this assay (500 mM NaCl, 50 ^{o}C) is consistent with the results of varying probe ΔG by changing stem length shown in Figure 4.3B.

Figure 4.13B shows results for simultaneous assays for *HIV*, *HCV*, and *SARS*-specific target oligonucleotides with all permutations of target combinations (i.e., none, all, and mixtures) using the nanowire bioconjugates that had been stored in citrate-containing PBS for 110 days. To simplify interpretation in the multiplexed assay, each probe was normalized independently, and signal from a no target sample was subtracted from each data point. Despite over three months in storage, it remained possible to determine which target sequences were present in this multiplexed assay, and no loss in assay performance was observed.

4.4. Conclusions

In this manuscript, we have focused on initial optimization of MB probe performance on the encoded Au/Ag striped nanowires. Immobilization of the beacon probes leads to a strong electrostatic repulsion within and between probes on the nanowire surface, such that optimal performance requires high salt buffers (300 to 500 mM NaCl). The length of both the stem and loop regions of the MB probes impacted performance, and relative thermodynamic stabilities predicted for solution-phase

analogies of the probes used here provided useful information despite surface attachment and steric/electrostatic effects. Target binding could be fit to a Sips isotherm, and detection sensitivity for optimum probe stem and loop lengths was on the order of 100 pM. A multiplexed, sealed assay for three viral signature sequences was demonstrated, without reduction in performance as compared to the identical assay performed under non-closed tube conditions with higher mixing volumes. Beacon-coated nanowires could be prepared ahead of time and stored indefinitely prior to use. No reduction in assay performance was observed after storage in citrate containing buffer for 110 days, the longest time tested. Our results suggest the potential of beacon-coated, barcoded metal nanowires for multiplexed detection of target DNA sequences such as viral signatures. While only three sequences were simultaneously detected in this work, larger numbers of identifiable nanowire patterns have been demonstrated and could be used to increase the level of multiplexing.[36,32] No sample manipulations are needed after mixing the molecular beacon probe coated nanowires with the target DNA, reducing assay complexity and the risk of contamination.

4.5. References

1. (a) Mackay, I. M.; Arden, K. E.; Nitsche, A. *Nucl. Acids Res*. **2002**, *30*, 1292-1305. (b) Klein, D. *TRENDS Molec. Med*. **2002**, *8*, 257-260.

2. Nam, J.-M.; Thaxton, C. S.; Mirkin, C. A. *Science* **2003**, *301*, 1884-1886.

3. (a) Rosi, N. L.; Mirkin, C. A. *Chem. Rev*. **2005**, *105*, 1547-1562. (b) Kricka, L. J. *Ann. Clin. Biochem.* **2002**, *39*, 114-129.

4. Bonnet, G.; Tyagi, S.; Libchaber, A.; Kramer, F. R. *Proc. Nat. Acad. Sci. USA* **1999**, *96*, 6171-6176.

5. Park, S.-J.; Taton, T. A. *Science* **2002**, *295*, 1503-1506.

6. Kwok, P.-Y. *Ann. Rev. Genomics Hum. Genet*. **2001**, *2*, 235-258.

7. Tyagi, S. Kramer, F. R. *Nat. Biotech.* **1996**, *14,* 303-308.

8. Fang, X.; Li, J. J.; Perlette, J.; Tan, W.; Wang, T. *Anal. Chem.* **2000**, 747 A-753A.

9. Broude, N. E. *TRENDS Biotechnol*. **2002**, *20*, 249-256.

10. Drake, T. J.; Tan, W. *Appl. Spectrosc*. **2004**, *58*, 269A-280A.

11. Tan, W.; Wang, K.; Drake, T. J. *Curr. Opin. Chem. Biol*. **2004**, *8*, 547-553.

12. Tyagi, S.; Marras, S. A. E.; Kramer, F. R. *Nat. Biotechnol*. **2000**, *18*, 1191-1196.

13. Tyagi, S.; Bratu, D. P.; Kramer, F. R. *Nat. Biotechnol.* **1998**, *16*, 49-53.

14. (a) Vet, J. A. M.; Majithia, A. R.; Marras, S. A. E.; Tyagi, S.; Bube, S.; Poiesz, B.; Kramer, F. R. *Proc. Natl. Acad. Sci. USA* **1999**, *96*, 6394-6399. (b) Sinsimer, D.; Leekha, S.; Park, S.; Marras, S. A. E.; Koreen, L.; Willey, B.; Naidich, S.; Musser, K. A.; Kreiswirth, B. N. *J. Clin. Microbiol.* **2005**, *43*, 4585-4591.

15. Yao, G.; Tan, W. *Anal. Biochem.* **2004**, *331*, 216-223.

16. Wang, H.; Li, J.; Liu, H.; Liu, Q.; Mei, Q.; Wang, Y.; Zhu, J.; He, N.; Lu, Z. *Nucleic Acids Res.* **2002**, *30*, e61.

17. Du, H.; Disney, M. D.; Miller, B. L.; Krauss, T. D. *J. Am. Chem. Soc.* **2003**, *125*, 4012-4013.

18. Palecek, E. *TRENDS Biotechnol*. **2004**, *22*, 55-58.

19. Fang, X.; Tan, W. *Anal. Chem.* **1999**, *71*, 3101-3105.

20. Liu, X.; Farmerie, W.; Schuster, S.; Tan, W. *Anal. Biochem.* **2000**, *283*, 56-63.

21. Steemers, F. J.; Ferguson, J. A.; Walt, D. R. *Nature Biotechnol.* **2000**, *18*, 91-94.

22. Liu, X.; Tan, W. *Anal. Chem.* **1999**, *71*, 5054-5059.

23. Liu, H,; Wang, H.; Shi, Z.; Wang, H.; Yang, C.; Silke, S.; Tan, W.; Lu, Z. *Nucleic Acids Res.* **2006**, *34*, e4.

24. Du, H.; Strohsahl, C. M.; Camera, J.; Miller, B. L.; Krauss, T. D. *J. Am. Chem. Soc.* **2005**, *127*, 7932-7940.

25. Dubertret, B.; Calame, M.; Libchaber, A. J. *Nat. Biotech.* **2001**, *19*, 365-370.

26. Sha, M. Y.; Yamanaka, M.; Walton, I. D.; Norton, S. M.; Stoermer, R. L.; Keating, C. D.; Natan, M. J.; Penn, S. G. *Nanobiotechnology* **2005**, 1, 327-335.

27. Stoermer, R. L.; Keating, C. D. "Distance-dependent Emission from Dye-labeled Oligonucleotides on Striped Au/Ag Nanowires: Effect of Secondary Structure and Hybridization Efficiency." *J. Am. Chem. Soc.* (manuscript accepted Aug **2006**).

28. Marras, S. A. E.; Kramer, F. R.; Tyagi, S. *Nucleic Acids Res.* **2002**, *30*, e122.

29. Maxwell, D. J.; Taylor, J. R.; Nie, S. *J. Am. Chem. Soc.* **2002**, *124*, 9606-9612.

30. Nicewarner-Pena, S. R.; Freeman, R. G.; Reiss, B. D.; He, L.; Pena D. J.; Walton, I. D.; Cromer, R.; Keating, C. D.; Natan, M. J. *Science* **2001**, *294,* 137-141.

31. Keating, C. D.; Natan, M. J. *Adv. Mater.* **2003**, *15,* 451-454.

32. Walton, I. D.; Norton, S. M.; Balasingham, A.; He, L.; Oviso, D. F. Jr.; Gupta, D.; Raju, P. A.; Natan, M. J.; Freeman, R. G. *Anal. Chem.* **2002**, *74*, 2240-2247.

33. (a) Tuerk, C.; Gold, L. *Science* **1990**, *249*, 505-510. (b) Ellington, A. D.; Szostak, J. W. *Nature* **1990**, *346*, 818-822. (c) Navani, N. K.; Li, Y. *Curr. Opin. Chem. Biol.* **2006**, *10*, 272-281.

34. Reiss, B. D.; Freeman, R. G.; Walton, I. D.; Norton, S. M.; Smith, P. C.; Stonas, W. G.; Keating, C. D.; Natan, M. J. *J. Electroanal. Chem.* **2002**, *522*, 95-103.

35. Zuker, M. *Nucleic Acids Res.* **2003**, *31*, 3406-3415.

36. Perrin, A.; Duracher, D.; Perret, M.; Cleuziat, P.; Mandrand, B. *Anal. Biochem.* **2003**, *322*, 148-155.

37. The DENV-2 genomic signature is Orion Integrated Biosciences Inc. proprietary information in pending patent applications filed with the US Trademark and Patent Office.

38. Nicewarner-Pena, S. R.; Carado, A. J.; Shale, K. E.; Keating C. D. *J. Phys. Chem. B* **2003**, *107,* 7360.

39. Enustun, B. V.; Turkevich, J. *J. Am. Chem. Soc*. **1963**, *85*, 3317-3328.

40. Keating, C. D.; Musick, M. D.; Keefe, M. H.; Natan, M J. *J. Chem. Ed*. **1999**, *76*, 949-955.

41. Park, S.; Brown, K. A.; Hamad-Schifferli, K. *Nano Lett*. **2004**, *4*, 1925-1926.

42. Schonherr, H.; Ringsdorf, H. *Langmuir* **1996**, *12*, 3891-3897.

43. Gronbeck, H.; Curioni, A.; Andreoni, W. *J. Am. Chem. Soc.* **2000**, *122*, 3839-3842.

44. (a) Herne, T. A.; Tarlov, M. J. *J. Am. Chem. Soc.* **1997**, *119*, 8916-8920. (b) Steel, A. B.; Levicky, R. L.; Herne, T. M.; Tarlov, M. J. *Biophys. J.* **2000**, *79*, 975-981.

45. (a) Shchepinov, M. S.; Case-Green, S. C.; Southern, E. M. *Nucleic Acids. Res.* **1997**, *25*, 1155-1161. (b) Southern, E.; Mir, K.; Shchepinov, M. *Nature Genetics Supplement* **1999**, *21*, 5-9.

46. Nicewarner-Peña, S. R.; Raina, S.; Goodrich, G. P.; Fedoroff, N. V.; Keating, C.D. *J. Am. Chem. Soc.* **2002**, *124*, 7314-7323.

47. Demers, L. M.; Mirkin, C. A.; Mucic, R. C.; Reynolds III, R. A.; Letsinger, R. L.; Elghanian, R.; Viswanadham, G. *Anal. Chem*. **2000**, *72*, 5535-5541.

48. Fang, X.; Li, J. J.; Perlette, J.; Tan, W.; Wang, T. *Anal. Chem.* **2000**, 747 A-753 A.

49. (a) Storhoff, J. J.; Elghanian, R.; Mucic, R. C.; Mirkin, C. A.; Letsinger, R. L. *J. Am. Chem. Soc*. **1998**, *120*, 1959-1964. (b) Li, H.; Rothberg, L. *Proc. Natl. Acad. Sci. USA* **2004**, *101*, 14036-14039.

50. He, L.; Musick, M. D.; Nicewarner, S. R.; Salinas, F. G.; Benkovic, S. J.; Natan, M. J.; Keating, C. D. *J. Am. Chem. Soc.* **2000**, *122*, 9071-9077.

51. Mirkin, C. A.; Letsinger, R. L.; Mucic, R. C.; Storhoff, J. J. *Nature* **1996**, *382*, 607-609.

52. Harris, D. C. *Quantitative Chemical Analysis*, 4th ed.; W. H. Freeman and Company: New York; 1995.

53. Sips, R. *J. Chem. Phys*. **1948**, *16*, 490-495.

54. Vijayendran, R. A.; Leckband, D. E. *Anal. Chem*. **2001**, *73*, 471-480.

55. (a) Levicky, R.; Horgan, A. *TRENDS Biotechnol*. **2006**, *23*, 143-149. (b) Halperin, A.; Buhot, A.; Zhulina, E. B. *J. Phys.: Condens. Matter* **2006**, *18*, S463-S490.

56. Hekstra, D.; Taussig, A. R.; Magnasco, M.; Naef, F. *Nucleic Acids Res*. **2003**, *31*, 1962-1968.

57. Nelson, B. P.; Grimsrud, T. E.; Liles, M. R.; Goodman, R. M.; Corn, R. M. *Anal. Chem*. **2001**, *73*, 1-7.

58. Peterson, A. W.; Wolf, L. K.; Georgiadis, R. M. *J. Am. Chem. Soc*. **2002**, *124*, 14601-14607.

59. Abravaya, K.; Huff, J.; Marshall, R.; Merchant, B.; Mullen, C.; Schneider, G.; Robinson, J. *Clin. Chem. Lab. Med*. **2003**, *41*, 468-474.

60. Tan, L.; li, Y.; Drake, T. J.; Moroz, L.; Wang, K.; Li, J.; Munteanu, A.; Yang, C. J.; Martinez, K.; Tan, W. *Analyst* **2005**, *130*, 1002-1005.

61. Mhlanga, M. M.; Malmberg, L. *Methods* **2001**, *25*, 463-471.

62. Szuhai, K.; van den Ouweland, J. M.; Dirks, R. W.; Lemaitre, M.; Truffert, J.-C. Janssen, G. M.; Tanke, H. J.; Holme, E.; Maassen, J. A.; Raap, A. K. *Nucleic Acids Res.* **2001**, *29*, e13.

63. (a) Sokol, D.; Zhang, X.; Lu, P.; Gewirth, A. M. *Proc. Natl. Acad. Sci. USA* **1998**, *95*, 11538-11543. (b) Bratu, D. P.; Cha, B.-J.; Mhlanga, M. M.; Kramer, F. R.; Tyagi, S. *Proc. Natl. Acad. Sci. USA* **2003**, *100*, 13308-13313.

64. Stoermer, R. L.; Sioss, J. A.; Keating, C. D. *Chem. Mater.* **2005**, *17*, 4356-4361.

Table 4.1. Probe sequences used in this work.[a]

Name	Sequence (5′-3′)[b]	Predicted ΔG[c] (kcal/mol)	Comments
HCV	thiol-$(CH_2)_6$-GCG AGC ATA GTG GTC TGC GGA ACC GGT GAC TCG C- TAMRA	–6.26	probe specific for a 24-base region of HCV
SARS	thiol$(CH_2)_6$-GCG AGA GAT GCT GTG GGT ACT AAC CTA CCT CTC GC-TAMRA	–9.77	probe specific for a 25-base region of SARS; extends the stem from 5 to 7 bases due to self complementarity
HIV	thiol$(CH_2)_6$-GCG AGT GTT AAA AGA GAC CAT CAA TGA GCT CGC-TAMRA	–3.97	probe specific for a 23-base region of HIV
SBM	thiol-GCG AGA TAG TG**G** TCT GCG GAC TCG C-TAMRA	–4.50	probe used for mismatch assay; position of mismatch is **bold**
L14	thiol$(CH_2)_6$-GCG AGA TCA ATG AGG AAG CCT CGC-TAMRA	–4.24	probe with 14-base loop; specific for HIV
L24	thiol$(CH_2)_6$-GCG AGG AGA CCA TCA ATG AGG AAG CTG CACT CGC-TAMRA	–3.57	probe with 24-base loop; specific for HIV
L38	thiol$(CH_2)_6$-GCG AGA AAA GAG ACC ATC AAT GAG GAA GCT GCA GAA TGG GAT ACT CGC-TAMRA	–4.95	probe with 38-base loop; specific for HIV
DENV-2(4)	thiol$(CH_2)_6$-GCG AGT GTC TGT TAC CAA GGA TCT GTC GC-TAMRA	–1.80	probe with 4 base pair stem; specific for DENV-2
DENV-2(5)	thiol$(CH_2)_6$-GCG AGG TGT CTG TTA CCA AGG ATC TGC TCG C-TAMRA	–4.00	probe with 5 base pair stem; specific for DENV-2
DENV-2(6)	thiol$(CH_2)_6$-GCG AGC GTG TCT GTT ACC AAG GAT CTG GCT CGC-TAMRA	–6.27	probe with 6 base pair stem; specific for DENV-2
DENV-2(7)	thiol$(CH_2)_6$-GCG AGC GGT GTC TGT TAC CAA GGA TCT GCG CTC GC-TAMRA	–8.88	probe with 7 base pair stem; specific for DENV-2

[a] Targets were synthetic oligonucleotides fully complementary to the loop region of each probe.
[b] The underlined portions of the sequences indicate complementary stem regions.
[c] Generated by mfold for most stable secondary structure in 500 mM NaCl at 25 °C.

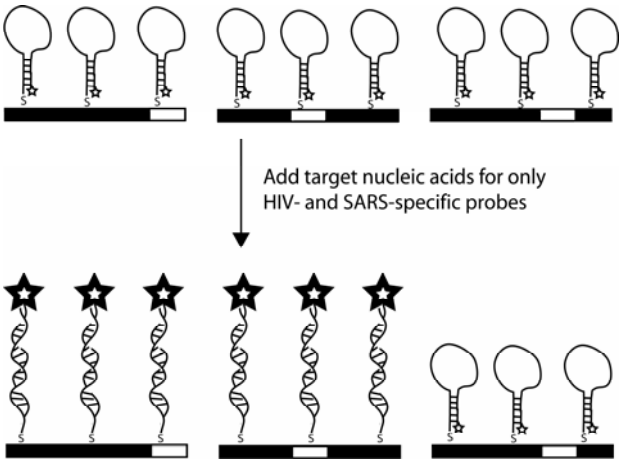

Figure 4.1. Illustration of multiplexed detection of nucleic acid targets by encoded nanowires functionalized with molecular beacon probes. In this illustration, wires patterned 00001 (left), 00100 (middle), and 00010 (right) are coated with MB probes *SARS*, *HIV*, and *HCV*, respectively, and complementary target sequences have been added for *SARS* and *HIV* only.

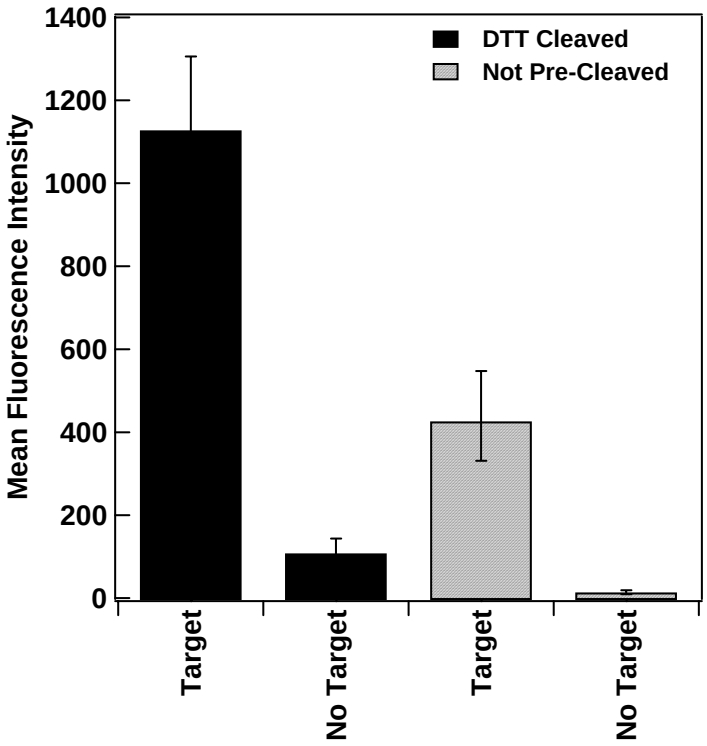

Figure 4.2. Assays for HCV beacon when pre-cleaved using DTT versus the same beacon not pre-cleaved in the presence and absence of complementary target. Error bars shown are the 95 % confidence intervals.

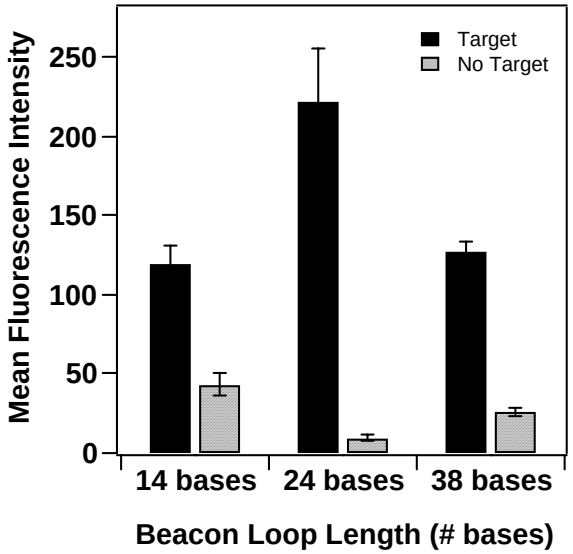

Figure 4.3. Effect of loop length on fluorescence intensity for molecular beacon probes bound to Ag/Au striped nanowires in the presence and absence of complementary target strands. Stem length was held constant at 5 base pairs. Error bars are the 95 % confidence interval.

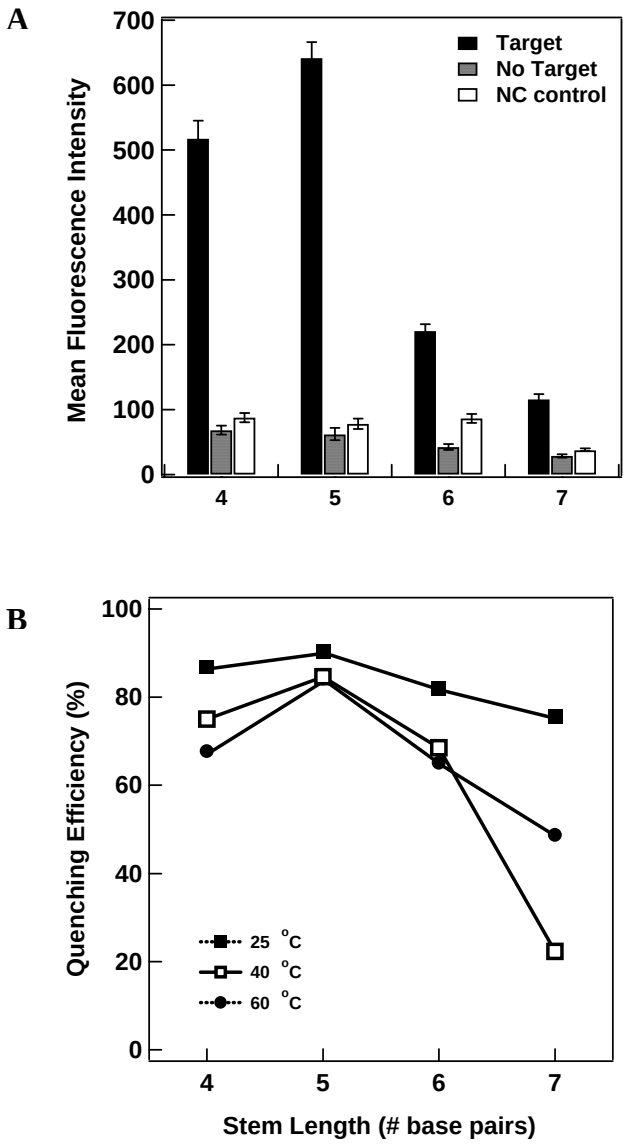

Figure 4.4. (*A*) Effect of stem length on fluorescence intensity for *DENV-2* molecular beacon probes bound to Ag/Au striped nanowires in the presence and absence of complementary target strands. Hybridization was performed at 25 ^{o}C in 500 mM NaCl CAC buffer. Loop length was held constant at 21 bases. Error bars are 95 % confidence intervals. (*B*) Effect of hybridization temperature on quenching efficiency for four stem lengths. Lines connecting the points are present only to guide the eye.

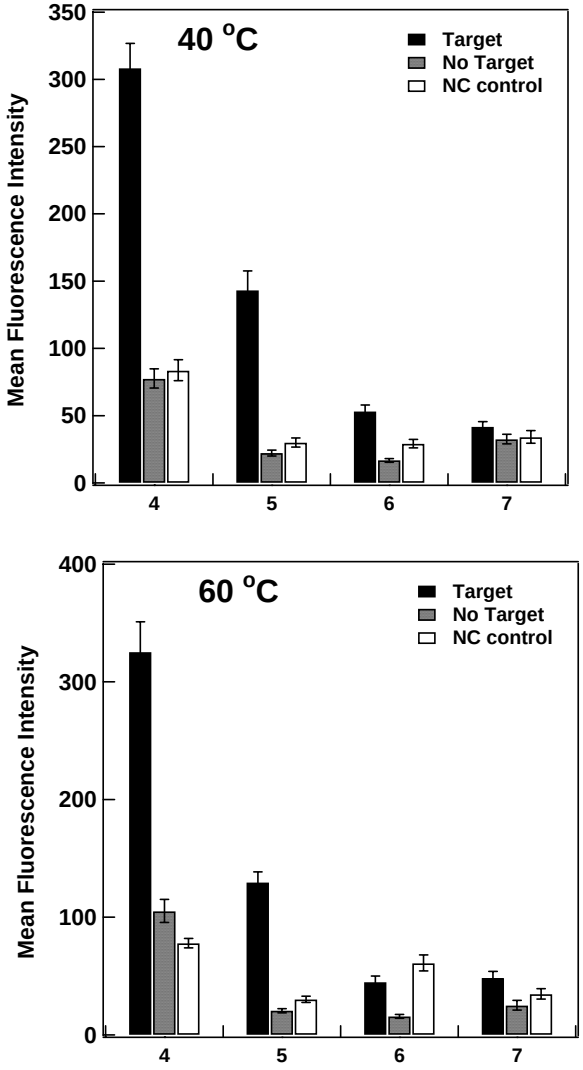

Figure 4.5. Effect of stem length on fluorescence intensity for *DENV-2* molecular beacon probes bound to Ag/Au striped nanowires in the presence and absence of complementary target strands. Hybridization was performed at 40 °C (top panel) and 60 °C (bottom panel) in 500 mM NaCl CAC buffer. Loop length was held constant at 21 bases. Error bars are 95 % confidence intervals.

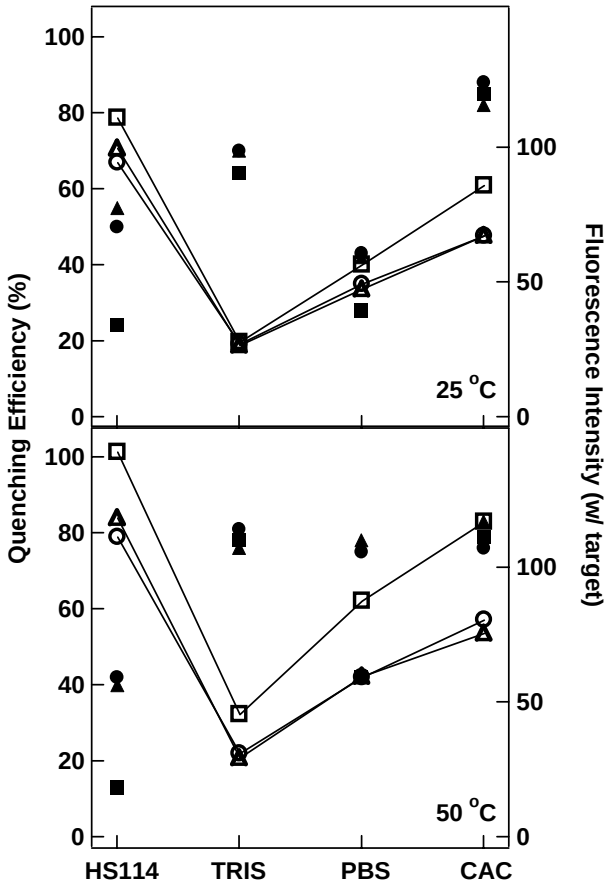

Figure 4.6. Comparison of assay performance in four different hybridization buffers at 25 °C (top) and 50 °C (bottom). Filled symbols are quenching efficiencies for (■) *HIV*, (▲) *SARS*, and (●) *HCV*. Open symbols are mean fluorescence intensities in the presence of target oligonucleotides for (□) *HIV*, (Δ) *SARS*, and (○) *HCV*. The lines connecting the fluorescence intensity points are present only to guide the eye.

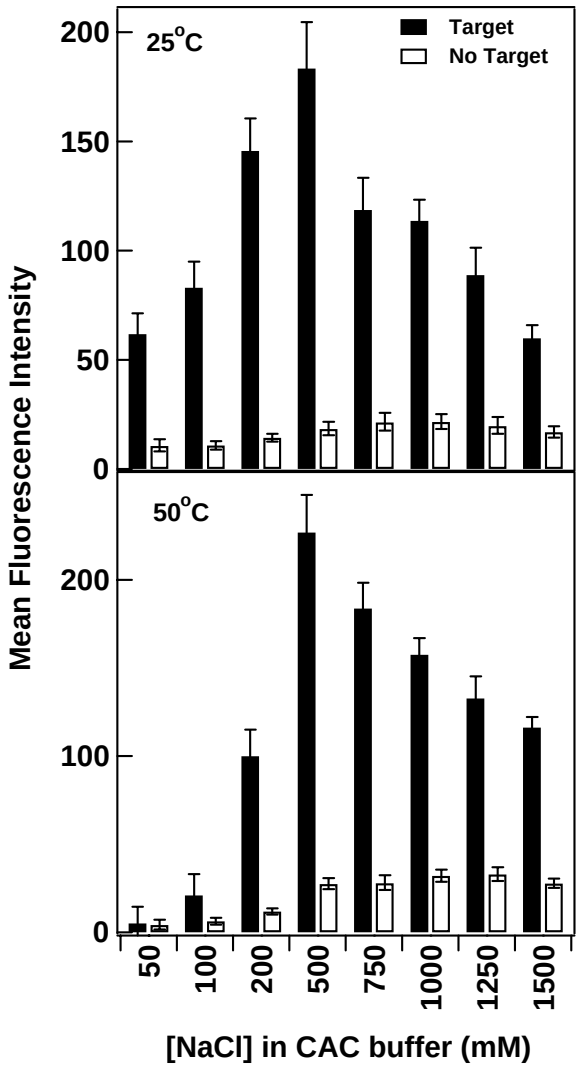

Figure 4.7. Effect of NaCl concentration on performance of nanowire-bound *DENV-2(5)* probes. Intensities are shown in the presence (filled bars) and absence (open bars) of complementary target sequence at room temperature and 50 ^{o}C. Error bars shown are the 95 % confidence intervals.

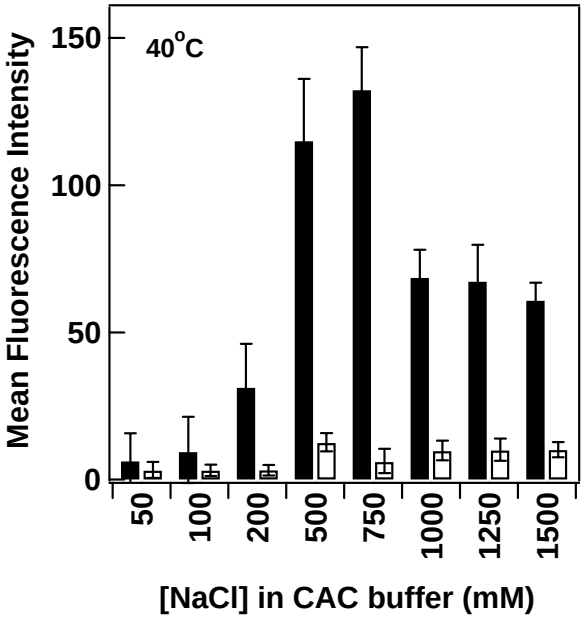

Figure 4.8. Effect of NaCl concentration on performance of nanowire-bound *DENV-2(5)* probes. Intensities are shown in the presence (filled bars) and absence (open bars) of complementary target sequence. The low intensities observed even in the presence of target for low [NaCl] are similar in this experiment at 40 °C to what is shown in Figure 4.7 at 50 °C. Please note that the probes in this experiment were attached to the nanowire surface following a slightly different protocol than in Figure 4.7, such that the density of probes on the surface was considerably higher, shifting the optimal [NaCl] to higher values. Error bars shown are the 95 % confidence intervals.

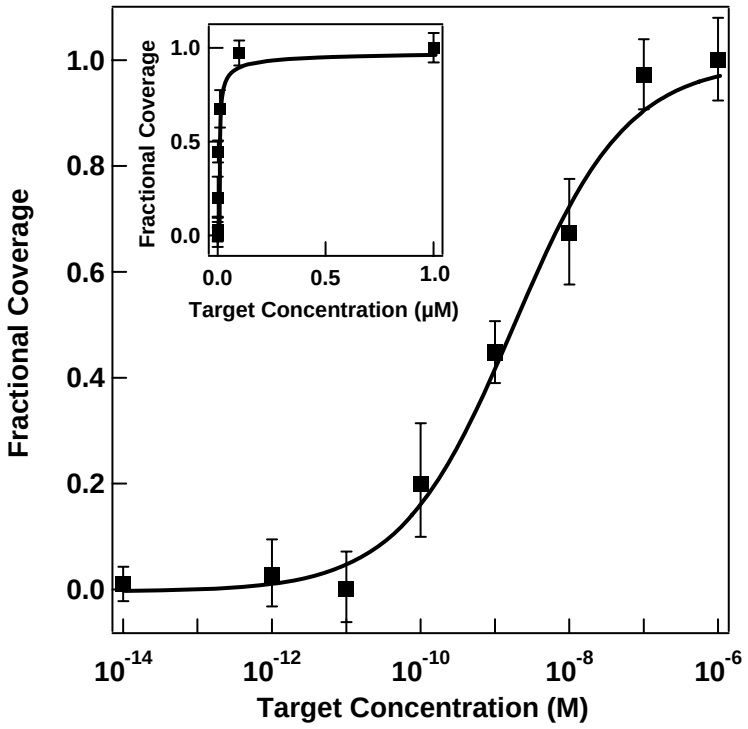

Figure 4.9. Hybridization adsorption isotherm for target binding to HCV beacons on metal nanowires. Fractional coverage was determined based on fluorescence intensity compared to intensity at saturation (1 μM). Dotted line is a fit to the Sips isotherm. Inset shows the same data on a linear concentration scale. The error bars are the 95 % confidence intervals.

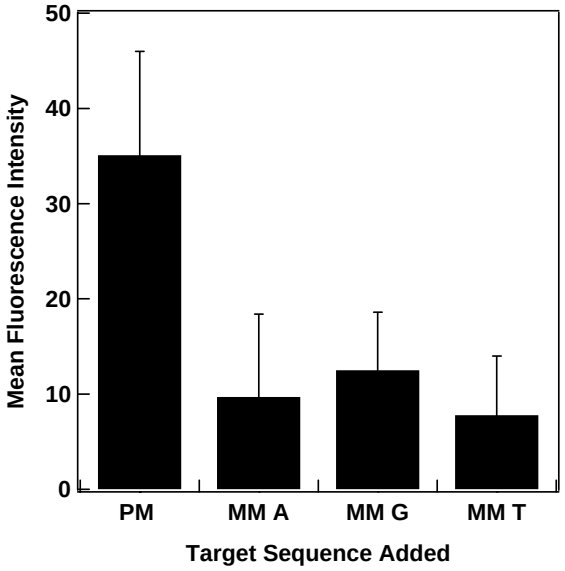

Figure 4.10. Comparison of response from fully complementary and mismatched target sequences binding to HIV MB probe *SBM* on the nanowire surface. PM indicates the perfectly matched target; mismatched targets (MM) for each of the bases in place of the C base in the PM are shown. The fluorescence intensity of a sample containing no target was subtracted from each sample. Error bars shown are the 95 % confidence intervals.

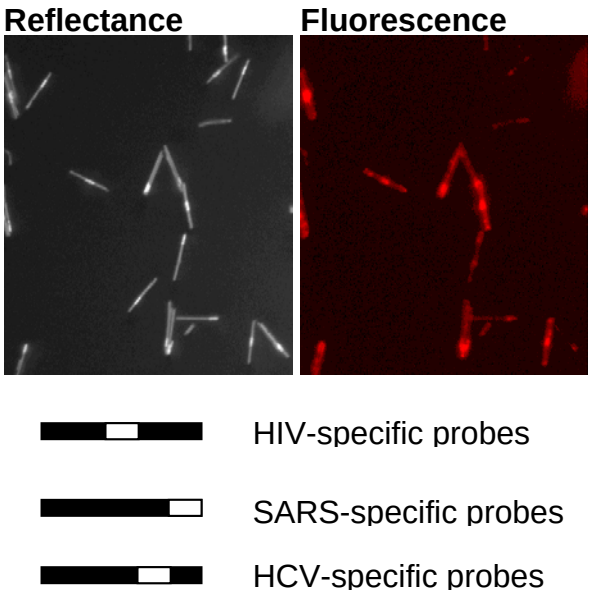

Figure 4.11. Reflectance and corresponding fluorescence microscopy images of triplexed, sealed chamber assay for HIV, SARS, and HCV target sequences. In this assay, only HIV and SARS targets were added. Thus, while all three nanowire patterns are visible in the reflectance image, only the HIV and SARS-specific nanowires should be visible in the fluorescence image. Nanowire patterns and corresponding probe specificities are given below the images.

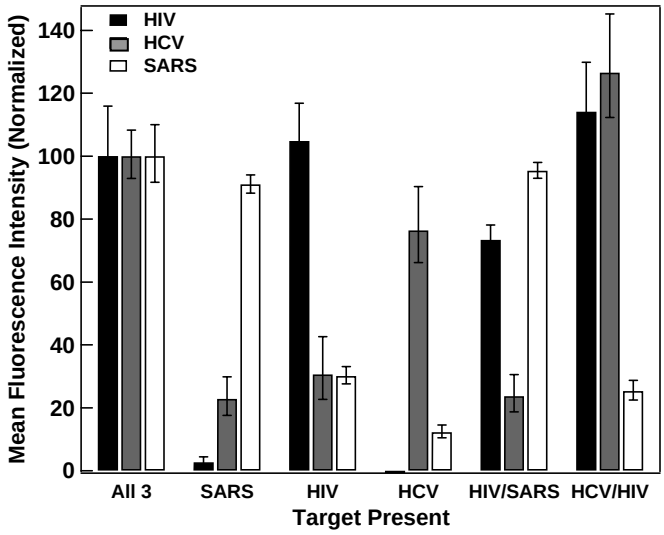

Figure 4.12. Triplex beacon assays performed and analyzed in a sealed chamber. The labels below the bar graphs indicate which target/targets are present in each assay. Background from a negative control (no targets added) has been subtracted from the data, and the intensity for each probe has been normalized to its intensity in the sample containing all three targets. The error bars shown are the 95 % confidence intervals.

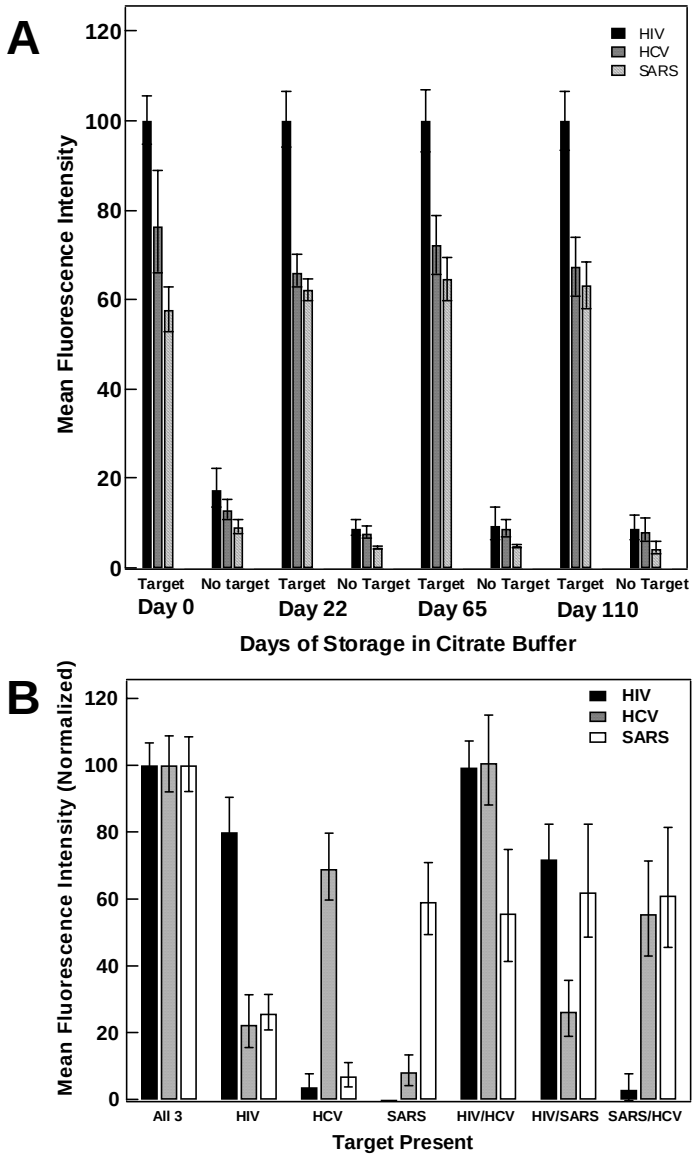

Figure 4.13. Triplex beacon assay using wires pre-coated in beacons and stored in citrate buffer for different lengths of time. Graph (*A*) shows target versus no target data for days of storage up to 110 days. Intensities for all three probes on each day have been normalized to the HIV intensity at day 0. Graph (*B*) shows multiple triplexed assays in the presence of various targets (targets added are indicated under the bars on the graph) after 110 day storage in citrate buffer. Intensities have been normalized for each probe, and the no target background has been subtracted. Error bars shown are the 95 % confidence intervals.

Chapter 5

DNA-directed Assembly of Barcoded Nanowires onto Glass Slides for Biosensing Applications

5.1. Introduction

The detection of specific DNA and RNA sequences has become increasingly important as we learn more about both genomics and gene expression. Nucleic acids are used in disease diagnosis, identification of pathogenic organisms (such as those in foods), and in functional genomic analyses. As the desire to simultaneously measure ever-increasing numbers of species grows, multiplexing has become a frontier theme in bioanalysis. Functional genomics illustrates one such application, where changes in gene expression are monitored via fluorescence on planar microarrays.[1,2] The use of microarrays for multiplexing permits detection of entire genomes at once, while conserving time and reagents. However, drawbacks of using conventional microarrays can include variations in fluorescence signals between arrays, difficulty in maintaining the stability of fluorescent dyes, and costly detection of the fluorescent tags. The use of fluorescence also limits the number of species that can be detected simultaneously, as the spectral bandwidths of the fluorescent peaks are large and oftentimes overlap. Replacing molecular dyes with semiconductor quantum dots prevents photobleaching and decreases the spectral bandwidth limitations;[3-8] however, detection still relies on fluorescence emission, which ultimately limits the number of species that can be simultaneously detected.

Barcoded nanowires are an attractive alternative to fluorescent tags in multiplexing applications because they do not photobleach, reflective read-out is inexpensive and simple, and many tags (in the form of different striping patterns) are simultaneously detectable. Prepared by sequential electrochemical deposition of metal ions into templates with uniformly sized pores, barcoded nanowires are intrinsically patterned based on the sequence of metals used and number of stripes added at the time of fabrication. The possibility of using barcoded nanowires for multiplexing assays was first reported in 2001.[9] The striping pattern is deciphered based on reflectance differences of adjacent metal stripes using reflectance optical microscopy. Due to this simple means of detection and the large number of possible tags, these nanowires are attractive for multiplexing bioassays.

We have previously shown that barcoded nanowires can be used for multiplexed sandwich hybridization assays in suspension, where detection was accomplished by fluorescent tags and the nanowire striping patterns were used to identify the DNA sequences detected.[9] It should be possible to perform multiplexed hybridization assays without fluorescent dyes by coupling the barcoded nanowires to planar supports. Planar supports such as glass slides are commonly used in DNA arrays. Typically, DNA microchips have individual regions of unique DNA sequences (probes) spotted onto them.[10-15] Fluorescently labeled target sequences then bind via complementarity to the immobilized probes and the fluorescence at each spot is measured to determine quantitatively the amount of DNA that hybridized. With barcoded nanowires, it will be possible to make a single DNA spot containing multiple DNA sequences on a surface and identify the hybridization binding events by simple optical detection of the barcoded

nanowire tags. Barcoded nanowires are employed here as a replacement for fluorescent tags and will report not only on the presence of target, but also on its identity. Nanowire tags could also be used on surfaces having multiple DNA spots, such as DNA macro- or microarrays. In this latter case, comparative functional genomics experiments could test for alterations in gene expression in response to multiple stimuli at the same time.

In the envisioned barcode-based microchip, a glass surface is silanized and is spotted with a mixture of different sequences of DNA through the use of a NeutrAvidin™-biotin linkage.[16] Separate strands of DNA are attached to nanowires, again using NeutrAvidin™ (NA) and biotin. The DNA on the wires is then attached to the DNA on the glass surface using a complementary linker DNA strand (Figure 5.1).

By using single stranded DNA complements, nanowires with different, optically distinguishable striping patterns bind to their complements on the glass surface. When wires of a specific barcoded pattern are attached to the glass through sandwich-type DNA binding (three strand system), the detection of a particular linker sequence is possible. In a biological application, the linker strand would be the species being sought, and the rest of the sensor would be designed to be complementary to that sequence. By using wires with different striping patterns, multiple linkers can be detected simultaneously.

Here, we present steps towards this surface-based nanowire biosensor. We report a method of attaching DNA to glass slides using a carboxy-terminated silane. The amount of nonspecific binding associated with the binding of one type of nanowire to a specific sequence of DNA was studied and determined to be 5.0 %. When two types of nanowires were mixed and allowed to bind competitively to a glass surface coated only

with the DNA necessary to bind one type of wire, the amount of nonspecific binding was also ~ 5 % (5.6 %).

5.2. Materials and Methods

5.2.1. Materials

Gold (Orotemp 24-1 troy oz/gal) and silver (Silver 1025-4.5 troy oz/gal) plating solutions were purchased from Technic, Inc. for nanowire synthesis. Alumina membranes (25 mm) were purchased from Whatman. Ag wire for evaporating the backside of alumina membranes was purchased from Acros. Glass microscope slides were purchased from Fisher (cat. no. 12-544-1). Carboxyethylsilanetriol was purchased form Gelest. EDC [1-ethyl-3-(3-dimethylaminopropyl)carbodiimide hydrochloride], NHS [*N*-hydroxysuccinimide] and NeutrAvidin™ were purchased from Pierce. All water used was distilled and purified to 18.2 MΩ using a Barnstead Nanopure system.

5.2.2. DNA Synthesis

DNA sequences were synthesized on an 8909 Expidite DNA synthesizer (from Applied Biosystems) using reagents purchased from Glen Research. Concentrated ammonium hydroxide was used to cleave the oligo from the column, and the strands were detritylated overnight on a heat block at 55 °C. The sequences were purified using PolyPak™ purification cartridges and modified protocols from Glen Research. Table 5.1 lists the DNA sequences used in these experiments.

5.2.3. Nanowire Synthesis

Anodisc aluminum membranes with membrane pores having average diameters of 318 ± 50 nm[17] were used as templates for the synthesis of barcoded nanowires. The synthesis of striped nanowires is reported in detail elsewhere.[18] Briefly, the backside of an alumina membrane was coated with ~500 nm of Ag by thermal evaporation and then was placed into an electrochemical cell where another ~1 μm of silver was electrodeposited onto the evaporated layer. This step was done as a preventative measure to ensure thorough coverage of the pores and prevent leaks during electrodeposition. The membrane was then removed from the cell, turned over and placed back into the cell so that more Ag could be deposited into the pores. This Ag layer is to reduce template irregularities (i.e. smaller, flared pores) by filling the bottoms of each pore with silver. The nanowires were then grown galvanostatically into the pores of the membrane. To get the desired metal striping patterns, the metal solutions were changed at defined intervals to the metal of choice. In this work, wires synthesized were either entirely Au or patterned AuAgAu, and were ~3-4 μm in length and ~320 nm in diameter. When the synthesis was complete, the cell was disassembled and the membrane was removed and rinsed with water. The silver backing was removed by dissolution in 4 M HNO_3, and then the membrane was rinsed in water. The alumina membrane was dissolved using 3M NaOH for 30 min and then the nanowire suspension was centrifuged at 2000 *g* for 2 min to collect the wires. They were then rinsed several times in water to remove any remaining NaOH. Au wires were stored in water and silver containing wires were stored in ethanol until ready for use.

5.2.4. Derivatization of Glass for DNA Attachment

Extruded glass microscope slides (1" x 3") were either cut to fit into 1-dram vials (1 cm x 1 cm) or left whole. The glass was first cleaned with aqua regia (3:1 HCl:HNO_3) for 15 min and then was rinsed 3 times with water and cleaned in piranha solution (3:2 H_2SO_4:H_2O_2) for 20 min. It was then rinsed with distilled water, sonicated in methanol for 10 min, and stored in methanol until use.[19]

The glass surfaces were rinsed with water prior to use and were silanized with a 2 % mixture of carboxyethylsilanetriol (CEST) in water (pH adjusted to 5.5 with acetic acid) for 15 min at room temperature. Slides were stirred in either 1 dram vials (for small slides 1 cm x 1 cm) or in square plastic Petri dishes (for full size slides) on an orbit shaker at 200 rpm to allow the silane to attach. Silane solution was poured off of the slides and they were rinsed three times with water. The slides were transferred to new vials/beakers, and then were cured in an oven at 120 °C for 20 min.

To link the carboxy-terminated silane to the amines of NeutrAvidin™ (NA), a solution of EDC/NHS ([1-ethyl-3-(3-dimethylaminopropyl)carbodiimide hydrochloride]/Sulfo-*N*-hydroxysuccinimide) was used. It is necessary to have more NHS than EDC in the EDC/NHS solution mixture because EDC reacts with a carboxyl group first and forms an amine reactive intermediate, an *o*-acylisourea. This intermediate is unstable in aqueous solution and therefore must be stabilized through the use of NHS.[20-22] For this reason, a solution consisting of 2 mM EDC/5 mM NHS was reacted for 30 min with each slide at room temperature on an orbit shaker. The slides were then rinsed 3 times with water.

To incorporate NA onto the slides, 0.05 mg/ml NA in water was added to the glass slides and was allowed to react 2 hrs at room temperature while being stirred on an orbit shaker at 200 rpm before being rinsed 3 times with water. This concentration is in great excess to the amount that can possibly attach to the surface, but ensures that the NA concentration is not a factor in wire attachment and coverage on the surface. A 10 mM solution of hydroxylamine was allowed to react for 30 min with each slide in an effort to reduce nonspecific binding of DNA to the activated surface. The slides were then rinsed three times in water.

5.2.5. DNA Attachment to Glass and Nanowires

For the smaller slides, 0.3 μM F-21B biotinylated DNA in water was added to each slide. The DNA was allowed to react ca. 4 hours on an orbit shaker at 200 rpm at room temperature. The slides were then rinsed 3 times with water. For the experiments done on full size glass slides, 5 mm glass joints with O-ring seals (from Ace Glass) were clamped to the slides to make chimneys for isolated DNA attachment to specific areas of each slide. To each chimney, 10 μM BS-6 DNA in 0.3M NaCl/10 mM phosphate buffer (pH 7.0) was added and allowed to react on the benchtop at room temperature over night.

The second sequence of DNA added was the linker sequence. On the smaller slides, F-12 DNA was used for the linker strand and 31mer was used as the control sequence, added at a concentration of 0.3 μM in hybridization buffer (0.3 M NaCl/10 mM Phos, pH 7.0). These sequences were allowed to hybridize at room temperature on the orbit shaker at 300 rpm for 4 hrs. They were then rinsed three times in the same

buffer. For the full size slides, 10 μM BS-8 DNA linker in hybridization buffer was added to the chimney and allowed to react at room temperature overnight.

The third DNA sequence was first attached to the nanowires, and then attached to the linker sequences. To attach the DNA to the nanowires, the wires were soaked in 0.1 mg/ml NA for 2 hours, rinsed three times in water, and then DNA was added. Au nanowires used on the small glass slides had F-18B DNA attached to them (30 μl of 10 μM F-18B DNA was added in 1 ml water and allowed to react 4 hours). Nanowires were then rinsed 3 times in water and then they were mixed with the DNA coated glass slides in 1 ml hybridization buffer and allowed to react overnight. For the large slides, Au nanowires were reacted with 10 μM BS-7 DNA and AuAgAu wires were reacted with BS-9 DNA overnight in hybridization buffer. Once the DNA was attached to the wires, 20 μl of each type of DNA coated wire was added to each chimney and allowed to attach overnight at 37 °C. The slides were then rinsed three times in hybridization buffer before imaging.

5.2.6. Optical Microscopy

Brightfield reflectance images were acquired using a Nikon TE-300 inverted microscope equipped with a 12-bit high resolution Coolsnap HQ camera (Photometrics). A CFI plan fluor 60x oil immersion lens (NA = 1.3) was used in conjunction with Image-Pro Plus software (version 4.5) to image the samples. The light source was a 175 W ozone free Xe lamp, and a Sutter Instruments filter wheel (Lambda 10-2) allowed for wavelength selection. Samples were prepared by sandwiching the nanowires on the glass

slides between a glass coverslip (Fisher 12-542-C) with a10 μl drop of water to adhere the coverslip to the slide. All reflectance images were taken at 430 nm, which is the wavelength that gives the biggest reflectance contrast between Au and Ag.[23]

5.3. Results and Discussion

For biosensing applications, it is desirable to have high nanowire coverages in the presence of specific target sequences, and no attachment for noncomplementary strands. In our previous work on DNA-directed nanowire attachment to planar Au surfaces,[24] we observed high nonspecific binding (~25 %). In those experiments, thiol self-assembled monolayer chemistry was employed both on the nanowire surfaces and on the planar Au supports. We hypothesized that moving from Au to SiO_2 and changing the DNA attachment chemistry from thiol to NA-biotin might decrease the nonspecific attraction between the particles and the surface. Two types of experiments were performed: Au nanowire assembly and competitive Au and Au-Ag-Au nanowire assembly experiments.

5.3.1 Single Nanowire Attachment

For Au nanowire assembly, nonspecific binding was determined by preparing two sets of glass slides. Both Au nanowires and small glass slides were derivatized with DNA. To some of the slides, the correct complementary linker was added such that the nanowires should have attached to the glass, and to other slides, the noncomplementary DNA linker was added such that nanowire attachment on these slides would be a result of nonspecific binding. Figure 5.2a shows reflectance optical microscopy images of the nanowires attached via complementary DNA hybridization. Figure 5.2b shows

representative images of samples containing noncomplementary DNA, and here the presence of the nanowires is a result of nonspecific attachment. From this experiment, nanowire coverages for samples containing complementary DNA were $2.4\pm0.9\text{x}10^5$ wires/cm^2. Samples containing non-complementary DNA had wire coverages of $1.2\pm 0.5\text{x}10^4$ wires/cm^2. Overall, these show 5.0 % nonspecific binding for samples containing noncomplementary DNA linkers. These data are very encouraging, as they show a dramatic improvement in the specificity of nanowire assembly as compared to our previous work on Au surfaces.[24] The surface coverage of nanowires here is lower than observed for attachment to Au surfaces (~1 x 10^6/cm^2).

5.3.2. Competitive Nanowire Attachment

The sensing applications we envision will require competitive binding of nanowires with complementary DNA strands in the presence of other nanowires having noncomplementary DNA. To demonstrate competitive nanowire attachment, two types of nanowires Au and AuAgAu were both derivatized with different sequences of DNA. Large glass slides with glass chimney chambers were used for DNA substrates and mixing vessels. The DNA applied to the glass substrate and the linker DNA were complementary to each other; however, only the DNA on the Au wires was complementary to the linker sequence. Both the DNA-coated Au and AuAgAu wires were mixed together and added to the chimney for attachment to the glass. Since only the Au wires had DNA complementary to the linker strand, only Au wires should have bound to the surface and the AuAgAu wires should have remained detached. Figure 5.3 shows optical reflectance images of these samples. Averages of $8.9\pm4.9\text{x}10^5$ Au

wires/cm^2 and 5.0± 3.4x10^4 AuAgAu wires/cm^2 are given by this data. These results lead to 5.6 % nonspecific binding, similar to that observed for the attachment of Au wires alone, and still very encouraging as compared to our earlier results using Au surfaces.[24]

Some variation is observed in both the coverage and the degree of nonspecific binding from experiment to experiment. In large part, these differences appear to result from the manner in which the wire suspension is mixed during assembly. The mixing methods between the two experiments outlined above are different (one using small pieces of glass in vials, the other using full size slides with chimneys) in an attempt to get more uniform wires coverages across the surface of the glass. A variety of mixing methods have been tested, with the glass chimneys thus far providing the best results.

5.4. Conclusions

In these experiments, a protocol was developed using a carboxy-terminated silane to derivatize glass slides for DNA attachment. Demonstrated here was the efficiency of nanowire attachment to glass via complementary DNA hybridization. The selectivity of competitive nanowire binding to the DNA coated glass substrate was shown to be discriminatory with an average of about 5 % nonspecific binding reported. With improvements in surface blocking, it is foreseen that greater numbers of assays could be simultaneously assayed using barcoded metal nanowires.

5.5. References

1. Schena, M. *DNA Arrays: A Practical Approach*; University Press: Oxford, **1999**.
2. McBeath, G.; Schreiber, S. L. *Science* **2000**, *289*, 1760-1762.
3. Bruchez, M.; Moronne, M.; Gin, P.; Weiss, S.; Alivisatos, A. P. *Science* **1998**, *281*, 2013-2018.
4. Han, M.; Gao, X.; Su, J. Z.; Nie, S. *Nat. Biotechnol.* **2001**, *19*, 631-635.
5. Alivisatos, A. P. *J. Phys. Chem.* **1996**, *100*, 13226-13239.
6. Colvin, V. L.; Schlamp, M. C.; Alivisatos, A. P. *Nature* **1994**, *370*, 354-357.
7. Alivisatos, A. P. *Science* **1996**, *271*, 933-937.
8. Gerion, D.; Pinaud, F.; Williams, S. C.; Parak, W. J.; Zanchet, D.; Weiss, S.; Alivisatos, A. P. *J. Phys. Chem. B* **2001**, *105*, 8861-8871.
9. Nicewarner-Pena, S. R.; Freeman, R.; Reiss, B. D.; He, L.; Pena, D. J.; Walton, I. D.; Cromer, R.; Keating, C. D.; Natan, M. J. *Science* **2001**, *294*, 137-141.
10. Marshall, A.; Hodgson, J. *Nat. Biotechnol.* **1998**, *16*, 27-31.
11. Lemieux, B.; Aharoni, A.; Schena, M. *Molec. Breeding* **1998**, *4*, 277-289.
12. Lipshutz, R. J.; Fodor, S. P. A.; Gingeras, T. R.; Lockhart, D. J. *Nat. Gen. Supp.* **1999**, *21*, 20-24.
13. Pidgeon, A. *Nature* **2001**, *410*, 860-861.
14. Ramsey, G. *Nat. Biotechnol.* **1998**, *16*, 40-44.
15. Wang, J. *Nucleic Acids. Res.* **2000**, *16*, 3011-3016.
16. Page, J. S.; Rubakhin, S. S.; Sweedler, J. S. *Clin. Chem*. **1991**, *37*, 625-636.
17. Martin, C. R. *Chem. Mater.* **1996**, *8*, 1739-1746.

18. Reiss, B. D.; Freeman, R. G.; Walton, I. D.; Norton, S. M.; Smith, P. C.; Stonas, W. G.; Keating, C. D.; Natan, M. J. *J. Electroanal. Chem.* **2002**, *522*, 95-103.

19. Zammatteo, N., Jeanmart, L., Hamels, S., Courtois, S., Louette, P., Hevesi, L., Remacle, J. *Anal. Biochem.* **2000**, *280*, 143-150.

20. Grabarek, Z.; Gergely, J. *Anal. Biochem.* **1990**, *185*, 131-135.

21. Staros, J. V.; Wright, R. W.; Swingle, D. M. *Anal. Biochem.* **1986**, *156*, 220-222.

22. Timkovich, R. *Anal. Biochem.* **1977**, *79*, 135-143.

23. Nicewarner-Pena, S. R.; Carado, A. J.; Shale, K. E.; Keating C. D. *J. Phys. Chem. B* **2003**,*107,* 7360-7367.

24. Mbindyo, J. K. N.; Reiss, B. R.; Martin, B. R.; Keating, C. D.; Natan, M. J.; Mallouk, T. E. *Adv. Mater.* **2001**, *13*, 249-254.

Table 5.1. DNA sequences used in experiments.

Sequence Name	Sequence 5'-3'
F-21B	AAT TTT TGA CGC ACG-biotin 3'
F-18B	5’-biotin-AAA AAA AAC TCC BTTG CGC ACG T
31mer	AGC CAT TAA GCC TAT CGG TAC GGT AAT TAG C
F-12	CGT GCG TCA AAA ATT ACG TGC GCA AGG AGT T
BS-6	5’-biotin- TTT TTT CGC ATT GAC GAT TGC TAT
BS-7	GAT TCT ACC GTA TAG ACG TTT TTT-biotin 3’
BS-8	CGT CTA TAC GGT AGA ATC ATA GCA ATC GTC AAT GCG
BS-9	GCT ATG AAC TTC GAG CTA TTT TTT-biotin 3’

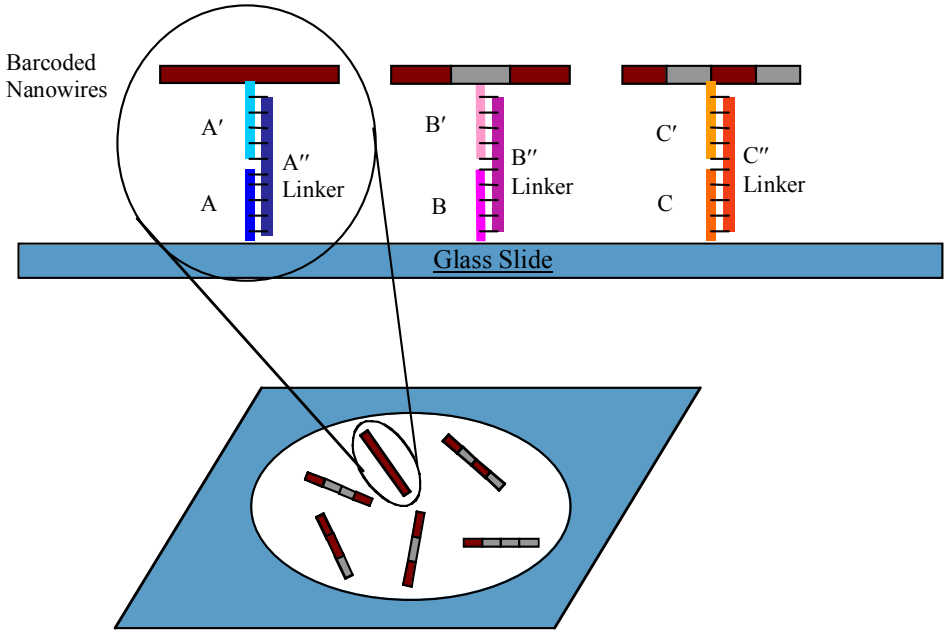

Figure 5.1. Schematic of nanowires attached to a mixture of DNA sequences on a glass slide via a DNA sandwich assay. Each spot contains the DNA necessary to bind multiple types of wires. The wires are attached to the glass slides via DNA complementarity. Not drawn to scale.

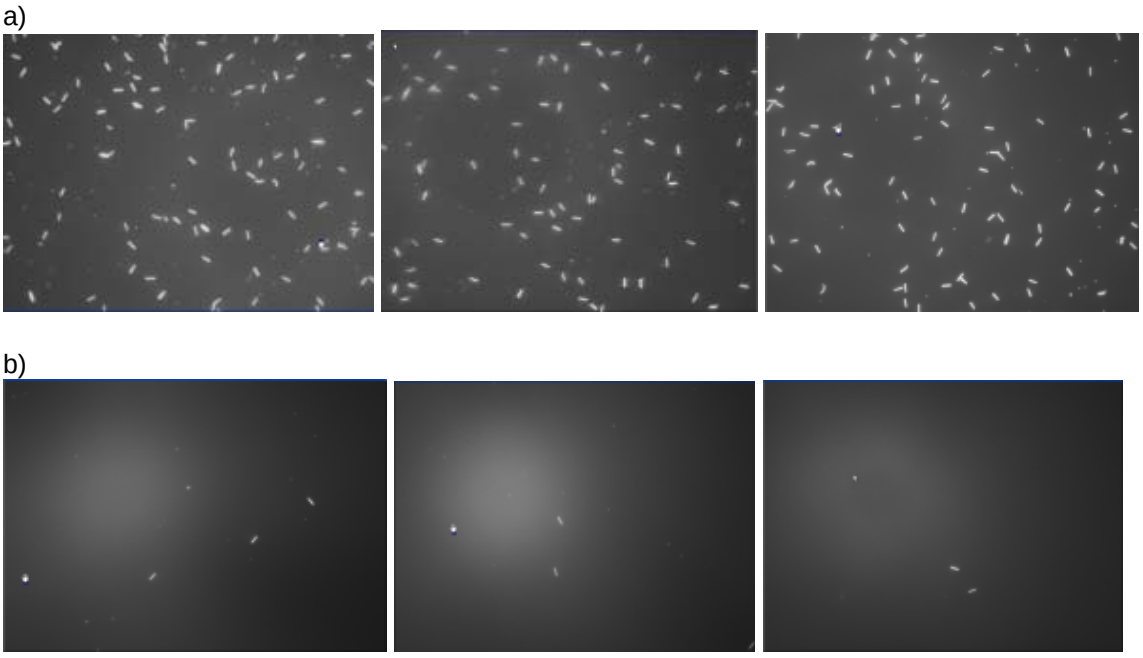

Figure 5.2. (a) Reflectance optical microscopy images of Au nanowires on glass bound by DNA complementarity, and (b) controls containing non-complementary DNA.

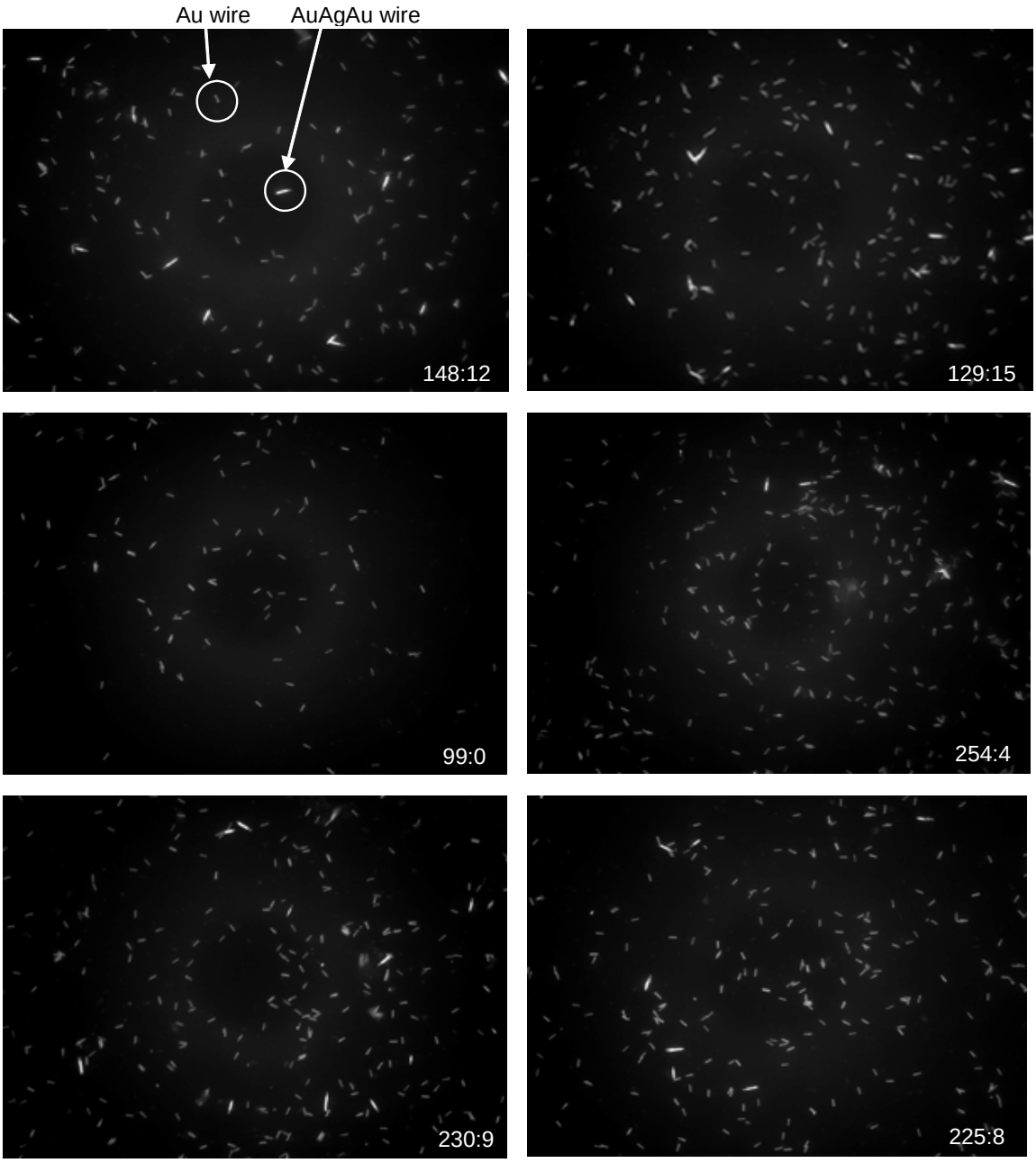

Figure 5.3. Reflectance images of competitive nanowire attachment to glass. Samples were illuminated with 430 nm light. At this wavelength, Ag segments appear much brighter than Au, allowing the two wire types to be distinguished. Both Au and AuAgAu nanowires were added to the slide, but only Au wires had complementary DNA to bind to the glass surface. AuAgAu wires had a noncomplementary DNA strand and should not attach. The ratios in the bottom corners of each image list the number of Au:AuAgAu wires in each image.

Chapter 6

Glass-Coated Striped Metal Nanowires for Improved Fluorescent Bioassays

6.1. Introduction

Multiplexing capabilities have become increasingly important, particularly due to the rapidly growing interest in gene detection and discrimination. Several techniques have been developed that detect multiple binding events simultaneously that utilize different substrates. Such techniques include microarrays,[1-6] encoded particles such as polystyrene microbeads embedded with ratios of red and infrared fluorescent dyes,[7-10] and barcoded metal nanowires.[11-15] However, only the use of barcoded metal nanowires allows for both ease of adding or subtracting probe sequences by incorporating or removing wires coated in different probes and does not rely on fluorophores for identification of the tagged bioassay. Fluorescence is used in these assays to signal that a binding event has occurred, but the striping pattern of the wire is relied on for identification of particular assays instead of the fluorophore. It is ideal to avoid relying on fluorescence for identification of particular assays because the use of fluorescence as an identifying tag limits the number of species that can be detected simultaneously, as the spectral bandwidths of the fluorescence peaks tend to overlap.

The ability to encode a large number of metal nanowires with distinct patterns of different striped metals allows them to have great potential in multiplexed bioanalyses. They are easily synthesized by electrodeposition of metals into porous aluminum oxide membranes. These barcoded metal nanowires in conjunction with fluorophores have in

the past been used in multiplexed bioassays for detection of antibody-antigen binding,[12] and DNA binding interactions.[12,14] In fact, the metal nanowire surfaces have also been employed as quenchers for fluorescence in multiplexed molecular beacon based bioassays.[11,16] Because the fluorescence is used here to identify binding events and not as tags, more possible binding events could be detected over techniques that multiplex assays using fluorescence for identification of particular species. Although there are many benefits to utilizing the metal surfaces of barcoded metal nanowires, for instance for fluorophore quenching and enhancement, the metal surfaces do introduce interesting effects on different fluorophores, or on the same fluorophores placed at different distances from the surface.[11,16] Occasional pits in the nanowire surfaces have also been shown to enhance the fluorescence at those locations, leading to greater deviation in the uniformity of the overall fluorescence intensity. Also affecting the fluorescence intensities are the identities of the underlying metals.[14,16] Under some experimental conditions, a particular fluorophore will be brighter on Ag segments, for example, over Au. A separate set of conditions may make the same fluorophore appear brighter on the Au. This is primarily due to the distance effects of the fluorophores from the surface as a result of hybridization efficiency.[16]

To avoid the effects of fluorophore-metal interactions, but take advantage of the multiplexing capabilities of metal nanowires, we glass-coated nanowires prior to use in bioassays. We report on fluorophore behavior when attached to wires coated with on different glass thicknesses. In this work, the stability of the glass-coated nanowires was also investigated and has proven to prevent oxidation of silver segments in the wires. Because glass-coated nanowires also provided more uniform fluorescence and resistance

to oxidation, we were interested in using such substrates to develop multiplexed DNA hybridization assays. Therefore, a 2-plex simultaneous assay was performed towards the identification of a single nucleotide polymorphism (SNP), which causes mutations in a P53 cancer gene.[17,18] A SNP is a single base mismatch in the DNA sequence. This SNP assay was performed using different attachment chemistries to both metal nanowires with no glass coating and to nanowires with glass coating, since bioassays on bare metal wires have been well studied and would provide a means of comparison for the assay performed on glass-coated wires.

6.2. Materials and Methods

6.2.1. Materials

Nanobarcodes™ obtained from Nanoplex, Inc. (Mountain View, CA), were patterned 010100, 010010, 00010110100, 000100110000, 00000100010 and 00000111000 where 0 represents a 0.75 μm segment of Au and 1 represents a 0.75 μm segment of Ag. Nanobarcodes were received in a 1 ml solution of mercaptoundecanoic acid (MUA), which aids in the prevention of NBC clumping. A 1 ml batch of the wires contains ~ 1x 10^9 NBCs. In all experiments the MUA coating was left on the wires prior to any functionalization. Tetraethylorthosilicate (TEOS) and aminopropyltrimethoxysilane (APTMS) were purchased from Aldrich. Reagents for buffers used in these experiments were 10 mM PBS (0.138 M NaCl; 0.0027 M KCl; pH 7.4, from Sigma), MES (T. J. Baker), TMAC (tetramethyl-ammonium chloride) purchased from Sigma, and SSPE (Promega). Sodium dodecyl sulfate (SDS) was purchased from Aldrich, and BSA (bovine serum albumin) and EDC were purchased from Pierce. Streptavidin-Cy5 (SA) was purchased from e(BioScience) (San Diego, CA). Samples were sent to Accurel (Sunnyvale, CA) to obtain TEM images of glass coating on the nanowires.

6.2.2. Glass Coating of NBCs

(Thin Coating)- NBCs were glass coated with a thin glass coating using modified procedures.[19-20] A 1 ml batch of wires was rinsed two times in ethanol to remove some of the residual MUA and then was resuspended in 490 µl ethanol, 160 µl water, 40 µl tetraethylorthosilicate (TEOS), and 10 µl 28 % ammonium hydroxide. The solution was sonicated for 1 min to suspend and mix all materials and then was allowed to react at room temperature with gentle rotation for 45 min. The NBCs were then rinsed three times in ethanol and stored in 1000 µl of ethanol until use.

(Thick Coating)- NBCs were coated with a thick coating of glass by rinsing the wires in ethanol and dividing each batch of NBCs in half, resulting in 2-500 µl aliquots. To each aliquot containing 500 µl ethanol, 160 µl water, 40 µl TEOS, and 10µl 28 % ammonium hydroxide were added. The samples were sonicated for 30 seconds and allowed to react at room temperature for 1 hour while tumbling. The NBCs were rinsed 3 times in ethanol, and then the entire procedure was repeated a second time. These samples were rinsed and stored in 1 ml ethanol until future use.

6.2.3. Glass Coating as a Protective Barrier against Silver Oxidation

Nanowires with no glass coating, thin glass coating (13.5 nm), and thick glass coating (100 nm) were continuously sonicated (2 µl of each batch of wires) in 50 µl of 20 % nitric acid for 5, 10, 15, and 30 min. After the indicated length of time, the samples were rinsed two times in 100 µl water and were resuspended in 50 µl water for imaging.

The rinsing step was only necessary here to avoid the nitric acid from destroying the well tray used for imaging.

6.2.4. SNP Assays (Probe Conjugation to Wire Surfaces)

(Glass Coated) Wires patterned 00010110100, and 000100110000 were glass coated with a 40-nm-thick layer of silicon oxide by following the procedure above for thin glass coating with the exception of using only 300 µl of wires in each batch. The coated wires were rinsed three times in ethanol and resuspended in 930 µl ethanol, 50 µl water, and 20 µl APTMS. Nanowires were allowed to react at room temperature with gentle rotation for 1 hr, then were then rinsed two times in ethanol, two times in DMSO, and were resuspended in 1 ml DMSO. To achieve carboxyl functionalization, a succinic anhydride (SSA) solution was then made by dissolving 0.04 g SSA in 1000 µl DMSO. Added to the APTMS functionalized NBCs was 10 µl of the SSA solution, which was allowed to react for 1 hr at room temperature while rotating, after which an additional 10 µl of SSA was added and allowed to react at room temperature for another hour. The samples were then rinsed three times in MES buffer (pH 4.5) and resuspended in 300 µl of the same buffer.

To functionalize both glass-coated and non-glass coated wires with DNA, 100 µl of each pattern wire was used. Non-glass-coated wires patterned 00000100010 and 00000111000 were rinsed two times in 50 mM MES buffer (pH 4.5) to remove any residual MUA before use. The samples were each resuspended in 320 µl of 50 mM MES buffer (pH 4.5), to which 3 µl 100 µM DNA probe (either N21A or N21B) was added. The DNA probes used in this assay were synthetic oligos purchased from Bio Source

International (Camarillo, CA), and they mimic gene regions in DNA that affect the function of P53, which is a tumor suppressor protein. A one-base mismatch in the DNA sequence can lead to improper function of P53 and can thus cause the formation of tumors. We have tested here two probes that are related to one of the places in the DNA sequence that is susceptible to SNP mutation, and they differ in sequence by only one base difference. The sequences used are called N21A and B because N refers to the amino acid in the protein that is affected by this SNP (N is the abbreviation for asparagine), and 21 refers to the position in the chromosome sequence where this SNP may occur. The sequences A and B are the wildtype (A) and mutant (B) forms of the DNA that exist. The DNA sequences used are presented in Table 6.1. After the DNA probe was added, the samples were placed on ice until a 20 % EDC solution was prepared in 50 mM MES (pH 7.0), of which 30 µl was added to each sample and allowed to react for 1 hour at 4 °C. The samples were then washed four times by centrifugation in 10 mM PBS, resuspended in 100 µl of the same buffer, and stored at 4 °C until use.

6.2.5. SNP Assays -Hybridization of Target(s) and Dye Labeling

For hybridization of target(s) in each SNP assay, 34 µl of 2xTMAC hybridization buffer was added to new tubes along with 3 µl of 2 µM each oligo target. The targets were boiled for 1 min to dehybridize any strands that may have been interacting with each other as a result of frozen storage, and then were placed on ice for 30 sec before use. Probe-coated wires were added (3 µl of each type (N21A and N21B)) to the DNA target(s) (N21A-T and/or N21B-T). Samples that contained no targets (control samples) were prepared the same as above except in place of adding DNA target, 3 µl of water was

added. The samples were allowed to incubate at 55 °C for 30 min, then were centrifuged to remove the supernatant and were resuspended in 500 µl 1xSSPE-0.1 % SDS buffer. The samples were rotated at room temperature in this buffer for 10 min, before removing the supernatant and resuspending the samples in 500 µl 0.1xSSPE-0.05 % SDS buffer. These samples were sonicated for 10 sec, incubated at 55 °C for 7 min, centrifuged, and then resuspended in 100 µl of 10 mM PBS buffer. As a stock solution, 3 µl of streptavidin-Cy5 was diluted in 1.1 ml of water. From this stock solution of diluted streptavidin, 100 µl was removed and added to each SNP assay. It is important to note that the samples were not sonicated after adding the streptavidin, so as not to denature the protein. The samples were allowed to mix at room temperature for 30 min while undergoing gentle rotation, after being covered in foil to protect the Cy5 dye from photobleaching. The samples were then centrifuged and washed one time with 500 µl 10 mM PBS and were resuspended in 50 µl PBS for imaging (see below). Later SNP assays with less non-specific binding were obtained by adding 1 % BSA into the 0.1xSSPE-0.05 % SDS wash buffer and also adding 1 % BSA to the streptavidin-Cy5 before conjugation to the biotin terminated probes.

6.2.6. Reflectance and Fluorescence Microscopy

Samples for imaging were prepared by adding 50 µl of each assay to particular wells of a 100 well glass-bottom microscope tray, and allowing the wires to settle to the bottom of the tray for at least 2 min before imaging. Microscope images were acquired using an automated Zeiss Axiovert 100 microscope outfitted with a Prior H107 stage, Sutter Instruments 300 W Xe lamp with liquid light guide, Physik Instrumente 400

micron travel objective positioner, and Photometrics CoolSnap HQ camera. A 63x objective was used with a NA=1.4. Reflectance images were acquired using a bandpass filter allowing for illumination using 406 nm light, as this wavelength gives good contrast between silver and gold metals. The fluorescence images were obtained using a filter cube selective for the excitation and emission preferences of Cy 5 dye. NBSee software was used to quantitate the amount of fluorescence on the wires present in each sample, as it identifies the wires using the reflectance image and quantifies the amount of fluorescence in the corresponding fluorescence images.[21]

6.3. Results and Discussion

The use of striped metal nanowires as substrates for multiplexed bioanalysis has many promising aspects such as ease of detection, ease of incorporating different assays together without substantial pre-planning, and potential for highly multiplexed testing. Although the metal surfaces have beneficial aspects in bioassays in terms of fluorescence quenching and enhancement, in order to avoid the complicated effects associated with metal-fluorophore interactions, we explored the potential of performing bioassays on glass-coated NBCs. The glass coating was expected to shield the fluorophores from the effects of the underlying metals and provide a more uniform fluorescence response across the entire striped nanowire surface.

6.3.1. Different Glass Thicknesses

To study the fundamental differences between wires with different thickness of glass coated on their surfaces, separate batches of NBCs (Nanobarcodes™) were coated with silicon dioxide to two different thicknesses by repeating a glass coating protocol multiple times to achieve thicker layers. Figure 6.1A shows TEM images of the glass coatings at two different thicknesses, ~13.5 nm and ~100 nm. Wires with coatings of both thicknesses of glass were derivatized with fluorescently labeled DNA to compare the fluorescence intensity and uniformity on each surface. Presented in Figures 6.1B and C, are reflectance and corresponding fluorescence images of both thickness of glass-coated nanowires with fluorescent DNA probes attached. When fluorescently labeled oligos were attached to the wires containing a thin glass layer, the fluorescence appeared non-uniform with concentrated bright spots along the nanowires (Figure 6.1), presumably a result of electromagnetic interactions due to unevenness of both surface molecules and metal substrate. We have noted in the past that pits in the metal wire surfaces have lead to fluorescence enhancements at those pits.[16] Since surface-enhanced fluorescence generally occurs at tens of nanometers from the surface and is sensitive to the nanoscale roughness of the metal, [22-37] it is feasible that with a thin, uneven glass coating, the fluorophores are still experiencing effects from the underlying metals. However, when using fewer NBCs per batch and coating them twice, a much thicker, more uniform glass coating resulted, which led to uniform fluorescence coverage across the wires when used in an assay with fluorescence labeling (Figure 6.1). Also, at this greater distance, the fluorophores are not subjected to quenching or enhancing phenomena exhibited by the metal surfaces, allowing the fluorescence to be more consistent.[22-26] It is also important

to note that the glass coating does not inhibit the identification of the wire's striping pattern, and typical reflectance microscopy conditions allow for the detection of the pattern (see reflectance images in Figure 6.1).

6.3.2. Glass Coating as Protection against Oxidation

We have previously reported that the stability of silver segments in NBCs is poor after incorporation of biomolecules onto the surfaces and storage in a buffered saline solution due to oxidation.[14,38] We anticipated that the glass coating would also aid in protecting the Ag segments in the nanowires. In this work, we glass coated separate batches of NBCs with two different thicknesses of glass and attached fluorescently labeled DNA to compare the fluorescence intensity and uniformity of each. To test whether or not the glass coating at each thickness protected the Ag segments, these wires as well as a sample of wires containing no glass coating were exposed to solutions of nitric acid while sonicating for different lengths of time. Nitric acid is known to dissolve silver; therefore, we were able to get an idea of whether or not the glass coating provided any benefits against silver oxidation. Figure 6.2 illustrates the stability of all three samples (thin glass coated, thick glass coated, and non-glass coated) when subjected to continual sonication in 20 % nitric acid for different amounts of time (Figure 6.2). All of the wire batches retained their integrity for 5 min of sonication, however, for the non-glass-coated sample after 10 min exposure, the wires were no longer identifiable. The wires with ~13.5 nm thickness of glass were still whole (not broken) after 30 min, with only small amounts of wire breakage (Figure 6.2). Wires with ~100 nm thick coating of glass withstood the sonication for 30 minutes without any visible degradation of the

silver. This suggests that the glass coating does in fact help to preserve the integrity of the nanowires under harsh conditions, preventing oxidation of the silver segments. This experiment also provides a technique for determining whether or not the glass coating is present in the event that a TEM is not readily available to analyze the coating. Wires with silver segments that do not show degradation after 30 min of sonication in nitric acid are glass coated. This method of determining if the glass coating is present is not quantitative and does not allow the precise thickness of the glass to be known, however, if the samples cannot be analyzed via TEM, this method can be used to check that the glass in fact coated the wires. A separate technique was also performed to determine if nanowires had been coated in glass; however, it was more complicated than the method just described. The other method involved attaching APTMS to the glass on the wires and then adding a Cy5 Mono NHS ester dye, which would bind to the amine groups on the APTMS. Controls were done on wires that were not glass coated where both APTMS and the Cy5 dye were added. There was a 4.5 times increase in fluorescence intensity for the samples containing glass-coated wires over those not glass coated. Although this method provided discrimination between wires with glass coating and wires without glass, this method was more time consuming and expensive than the one previously described.

It was also noted in conducting experiments using 11-segment glass-coated wires that little to no wires were broken or bent, which is very unusual for wires without glass coating at such lengths. The stability and improved uniformity in fluorescence coverage of these glass-coated wires over their non-glass coated counterparts provides further cause for their use in future bioanalytical assays.

6.3.3. SNP Assay on Glass-Coated Wires

To investigate further the use of glass coated wires in the development of an actual assay, a 2-plex SNP assay was performed on both glass-coated and non-glass-coated NBCs. For this assay, DNA probes were attached to the glass surfaces using succinic anhydride to achieve carboxyl functionalization on the surface, which was then linked using EDC to amine-terminated DNA probes. Biotin-terminated target sequences, which may or may not have contained a DNA SNP, were then hybridized to the anchored probes. Following hybridization of target, fluorescently labeled streptavidin protein, which binds to the biotin molecule appended to the end of the target sequence, was added (Figure 6.3). If DNA that is not fully complementary to the probe sequence is added (in this case, a SNP sequence), this SNP DNA is not expected to bind, causing there to be no biotin present for streptavidin binding, and thus no fluorescence on the wire. The SNP sequence detected in this work is a region of chromosome 17, which is susceptible to mutations and can lead to cancer tumor formation. The wildtype (or non-mutated) region of the chromosome has the sequence of the DNA probe labeled N21A in this work. The mutated region of this chromosome leads to the SNP sequence called N21B in this work. This one-base mutation can lead to the formation of cancer by way of affecting the function of the P53 tumor suppressor gene. P53 is a protein with activity to stop the formation of tumors. In the cell, P53 protein binds DNA, which in turn stimulates another gene to produce a protein called P21 (given this name because it is a protein with the molecular weight of 21). P21 interacts with a cell division stimulating protein (cdk2) to form a complex that cannot pass through the next stage of cell division and therefore acts as a “stop signal” for cell division. If a DNA SNP is present, the P53 protein binds

differently and no longer binds DNA in an effective way, which does not allow for the production of P21. Therefore the P21 is not made available to act as the "stop signal" for cell division, leading to uncontrolled division of the cells and thus formation of tumors. In the 2-plex assay studied here, the probe for the wild-type DNA sequence (N21A) was bound to a batch of wires patterned differently than the wires to which the mutant SNP DNA (N21B) was attached. The two wire batches were mixed after probe attachment and before binding of target sequences. It was of interest to determine the selectivity of these two probes for target binding although they differ by only 1 base from each other in order to determine if glass-coated substrates were suitable for such selective assays.

Reported in Figure 6.4 are two separate sets of assays performed on both glass-coated and non-glass-coated wires. On the graphs, the x-axis indicates which target sequences were added to each assay. Although the surface chemistry of probe attachment is different between the two sample sets (due to the nature of the surfaces being different), these data show reasonable discrimination between the presence of one SNP sequence (A), over another (B), with little non specific binding (as seen in the no target sample). Comparable results between the two assays on different substrates (glass coated vs non-glass coated) suggest that it is feasible to use either substrate for this type of SNP detection assay.

To ensure that the fluorescently labeled streptavidin did not bind to non-specific interactions to the surface, many rinsing and blocking strategies were attempted. The data presented in Figure 6.4 were later improved for the glass-coated assays by adding 1 % BSA to the 0.1xSSPE-0.05 % SDS rinse buffer and adding 1% BSA to the fluorescently labeled SA during attachment. Figure 6.5 shows the data for the improved

assay on glass-coated wires. Experiments were also conducted where BSA was added only to the wash buffer and separate experiments were done where BSA was added only with the SA (data not shown), which yielded improvements in the specificity of the assay. However, the best discrimination between appropriate target binding came with combined use of adding BSA both in the rinse buffer and along with SA during attachment. The outcome of this set of experiments suggests that using wires coated in silicon dioxide is promising for bioassay performance. In fact, because the fluorescence signal was relatively uniform on these glass-coated wires, the error bars are smaller for these samples than for those performed on wires with no glass coating.

6.4. Conclusions

Barcoded metal nanowires were coated in glass and tested for use in DNA hybridization assays. We note here that the glass coating not only provides a means for covalent DNA attachment, but also helps to preserve the silver segments in the nanowires as they are typically susceptible to oxidation.[13,16] Also, when coated in a thick glass coating (100 nm), fluorescence patterning noted previously[13] as a result of fluorophore quenching and enhancement effects on the different metals is no longer present. We show that the thick glass coating provides protection against metal quenching and enhancing effects, resulting in uniform fluorescence coverage across the nanowire surfaces. Also, in this work we were able to achieve successful discrimination between two DNA sequences in a 2-plex assay when the sequences differed by only a one-base mismatch. Glass coating metal nanowires has proven to protect against Ag etching, to allow for more uniform and consistent fluorescence coverage, to prevent the wires from

bending, and to allow a multiplexed assay to work. All of these benefits suggest that whenever the metal surface is not participating directly in the assay readout, (as it does for the beacon experiments reported in Chapters 3 and 4), then glass coatings should routinely be used.

6.5. References

1. Marshall, A.; Hodgson, J. *Nat. Biotechnol.* **1998**, *16*, 27-31.

2. Lemieux, B.; Aharoni, A.; Schena, M. *Molec. Breeding* **1998**, *4*, 277-289.

3. Lipshutz, R. J.; Fodor, S. P. A.; Gingeras, T. R.; Lockhart, D. J. *Nat. Gen. Supp.* **1999**, *21*, 20-24.

4. Pidgeon, A. *Nature* **2001**, *410*, 860-861.

5. Ramsey, G. *Nat. Biotechnol.* **1998**, *16*, 40-44.

6. Wang, J. *Nucleic Acids Res.* **2000**, *16*, 3011-3016.

7. Walt, D. R. *Science* **2000**, *287*, 451-452.

8. McBride, M. T.; Gammon, S.; Pitesky, M.; O'Brien, T. W.; Smith,T.; Aldrich, J.; Langlois, R. G.; Colston, B.; Venkateswaran, K. S. *Anal. Chem.* **2003**, *75*, 1924-1930.

9. Stitzel, S. E.; Sein, D. R.; Walt, D. R. *J. Am. Chem. Soc.* **2003**, *125*, 3684-3685.

10. Albert, K. J.; Walt, D. R. *Anal. Chem.* **2000**, 72, 1947-1955.

11. Sha, M. Y.; Yamanaka, M.; Walton, I. D.; Norton, S. M.; Stoermer, R. L.; Keating, C. D.; Natan, M. J.; Penn S. G. *Nanobiotechnology* **2005**, *1*, 327-335.

12. Nicewarner-Pena, S. R.; Freeman, R. G.; Reiss, B. D.; He, L.; Pena D. J.; Walton, I. D.; Cromer, R.; Keating, C. D.; Natan, M. J. *Science* **2001**, *294*, 137-141.

13. Keating, C. D.; Natan, M. J. *Adv. Mater.* **2003**, *15*, 451-454.

14. Nicewarner-Pena, S. R.; Carado, A.J.; Shale, K. E.; and Keating C.D. *J. Phys. Chem. B* **2003**, *107*, 7360-7367.

15. Stoermer, R. L.; Keating, C. D. *Proceed. SPIE* **2004**, *5588*, 51-58.

16. Stoermer, R. L.; Keating, C. D. "Distance-dependent Emission from Dye-labeled Oligonucleotides on Striped Au/Ag Nanowires: Effect of Secondary Structure and Hybridization Efficiency." *J. Am. Chem. Soc.* (manuscript accepted Aug **2006**).

17. Janus, F.; Albrechtsen, N.; Dornreiter, I.; Wiesmuller, L.; Grosse, F.; Deppert, W. *Cell. Mol. Life Sci.* **1999**, *55*, 12-27.

18. Jayaraman, L.; Prives, C. *Cell. Mol. Life Sci.* **1999**, 76-87.

19. Sioss, J. A., Keating, C. D. *Nano Lett.* **2005**, *5*, 1779-1783.

20. Yin, Y.; Lu, Y.; Sun, Y.; Xia, Y. *Nano Lett.* **2002**, *2*, 427-430.

21. Walton, I. D.; Norton, S. M.; Balasingham, A.; He, L.; Oviso, D. F. Jr.; Gupta, D.; Raju, P. A.; Natan, M. J.; Freeman, R. G. *Anal. Chem.* **2002**, *74*, 2240.

22. Moskovits, M. *Rev. Mod. Phys.* **1985**, *57*, 783-826.

23. Chance, R. R.; Prock, A.; Silbey, R. *Adv. Chem. Phys.* **1978**, *37*, 1-65.

24. (a) Lakowicz, J. R. *Anal. Biochem.* **2001**, *298*, 1-24. (b) Lakowicz, J .R. *Anal. Biochem.* **2005**, *337*, 171-194.

25. Meitiu, H. *Prog. Surf. Sci.* **1984**, *17*, 153-320.

26. Neumann, T.; Johansson, M.-L.; Kambhampati, D.; Knoll, W. *Adv. Funct. Mater*. **2002**, *12*, 575-586.

27. Weitz, D. A.; Garoff, S.; Gersten, J. I.; Nitzan, A. *J. Chem. Phys.* **1983**, *78*, 5324-5338.

28. Corni, S.; Tomasi, J. *J. Chem. Phys.* **2003**, *118*, 6481-6494.

29. (a) Sokolov, K.; Chumanov, G.; Cotton, T. M. *Anal. Chem.* **1998**, *70*, 3898-3905. (b) Chumanov, G.; Sokolov, K.; Gregory, B. W.; Cotton, T. M. *J. Phys. Chem.* **1995**, *99*, 9466-9471.

30. Whitmore, P. M.; Robata, H. J.; Harris, C. B. *J. Phys. Chem.* **1982**, *77*, 1560-1568.

31. Yokota, H.; Saito, K.; Yanagida, T. *Phys. Rev. Lett.* **1998**, *80*, 4606-4609.

32. Knobloch, H.; Brunner, H.; Leitner, A.; Aussenegg, F.; Knoll, W. *J. Phys. Chem.* **1993**, *98*, 10093-10095.

33. (a) Huang, X.; Lee, K. T.; George, T. F. *J. Phys. Chem.* **1986**, *85*, 567-572. (b) Glass, A. M.; Liao, P. F.; Bergman, J. G.; Olson, D. H. *Optic. Lett.* **1980**, *5*, 368-370. (c) Wokaun, A.; Lutz, H. P.; King, A. P.; Wild, U. P.; Ernst, R. R. *J. Phys. Chem.* **1983**, *79*, 509-514. (a) Amos, R. M.; Barnes, W. L. *Phys. Rev. B.* **1999**, *59*, 7708-7714. (d) Alivisatos, A. P.; Waldeck, D. H.; Harris, C. B. *J. Chem. Phys.* **1985**, *82*, 541-547. (e) Zhang, J.; Malicka, J.; Gryczynski, I.; Lakowicz, J. R. *J. Phys. Chem. B* **2005**, *109*, 7643-7648.

34. Aslan, K.; Lakowicz, J. R.; Geddes, C. D. *Anal. Bioanal. Chem.* **2005**, *382*, 926-933.

35. Kummerlen, J.; Leitner, A.; Brunner, H.; Aussenegg, F. R.; Wokaun, A. *Molec. Phys.* **1993**, *80, 1031-1046*.

36. Tarcha, P. J.; DeSaja-Gonzalez, J.; Rodriguez-Llorente, S.; Aroca, R. *Appl. Spec.* **1999**, *53*, 43-48.

37. Schneider, G.; Decher, G.; Nerambourg, N.; Praho, R.; Werts, M. H. V.; Blanchard-Desce, M. *Nano Lett*. **2006**, *6*, 530-536.

38. Stoermer, R. L.; Sioss, J. A.; Keating, C. D. *Chem. Mater*. **2005**, *17*, 4356-4361.

Table 6.1. DNA sequences used in this work.

Sequence Name	Sequence (5'-3')	Comments
N21A	Amine-C_{12}-TTT TTT TTT TTT TTT TTT TGT GAG GC**G** CTG CCC	Wild-type probe with 18-base poly T spacer. The bolded, underlined base is the position of the SNP.
N21A-T	Biotin-GGG CAG CGC CTC ACA	Complement to N21A
N21B	Amine-C_{12}-TTT TTT TTT TTT TTT TTT TGT GAG GC**A** CTG CCC	Mutant probe with 18-base poly T spacer. The bolded, underlined base is the position of the SNP.
N21B-T	Biotin-GGG CAG TGC CTC ACA	Complement to N21B

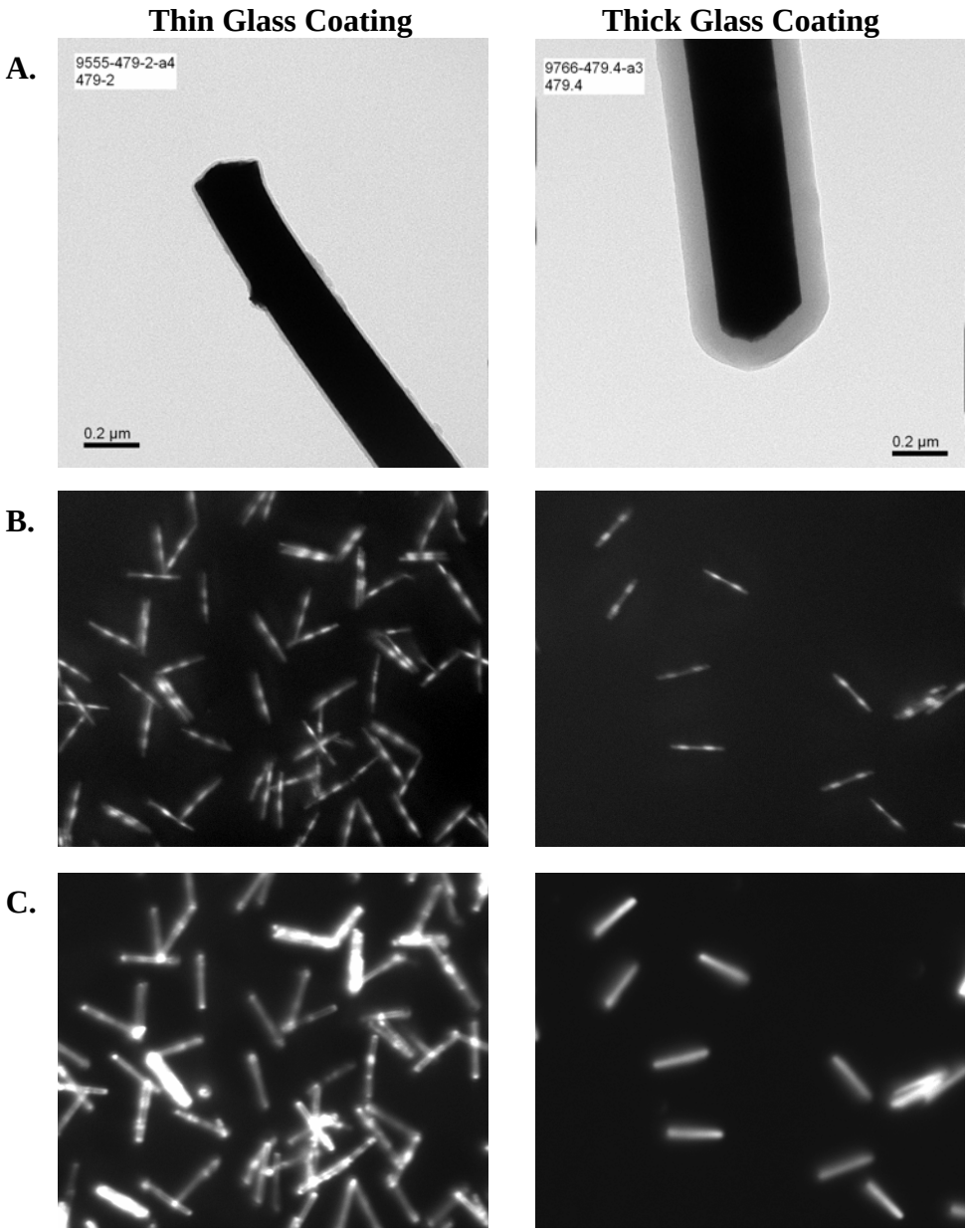

Figure 6.1. Comparison between thin (13.5 nm) and thick (100 nm) glass coating on NBCs. A) TEM images of glass coated NBCs. B) Reflectance images of glass coated NBCs coated in fluorescently labeled probe. C) Corresponding fluorescence images for glass-coated wires coated in probe.

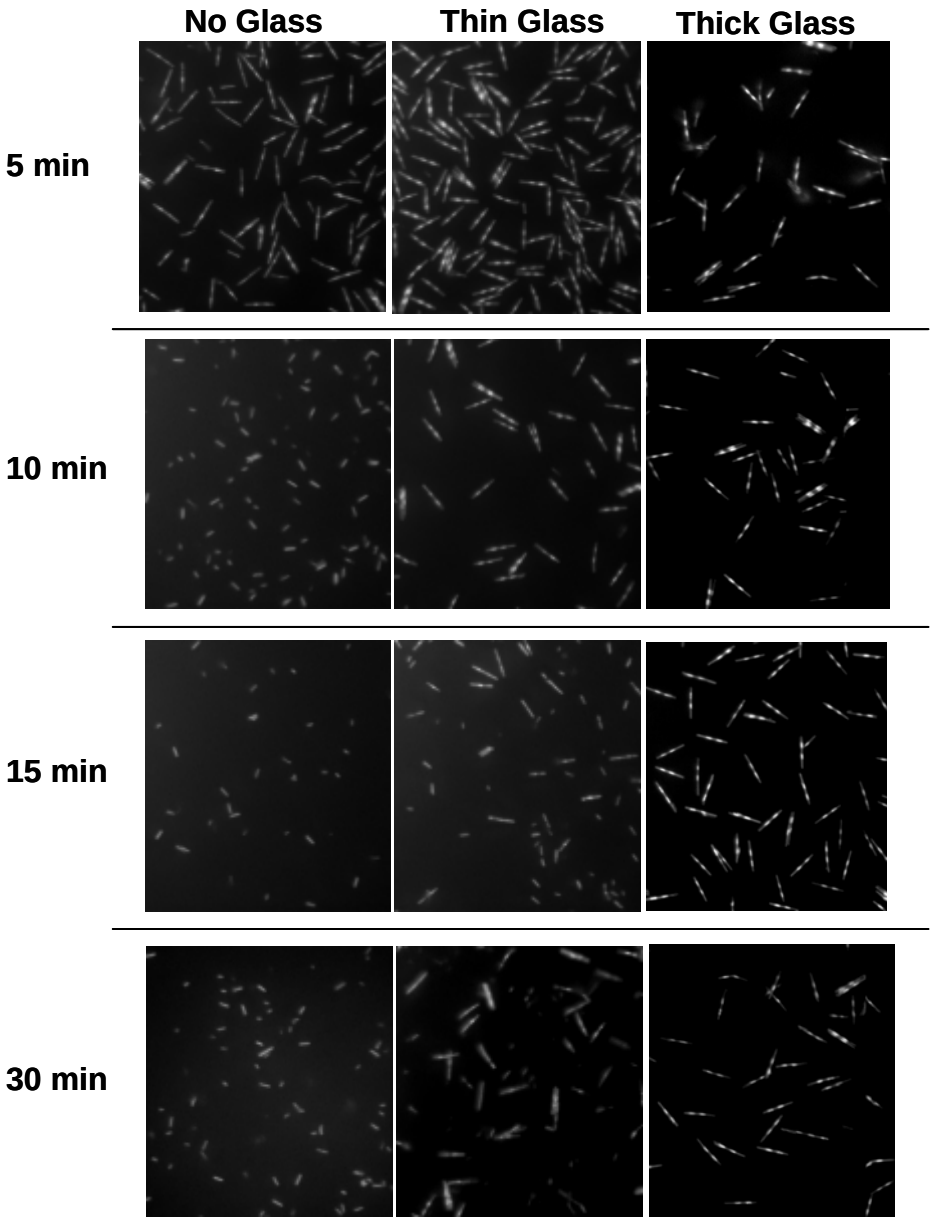

Figure 6.2. Optical reflectance images of nanowires with no glass coating, a thin glass coating (13.5 nm), and a thick glass coating (100 nm) when sonicated in nitric acid from 0-30 min.

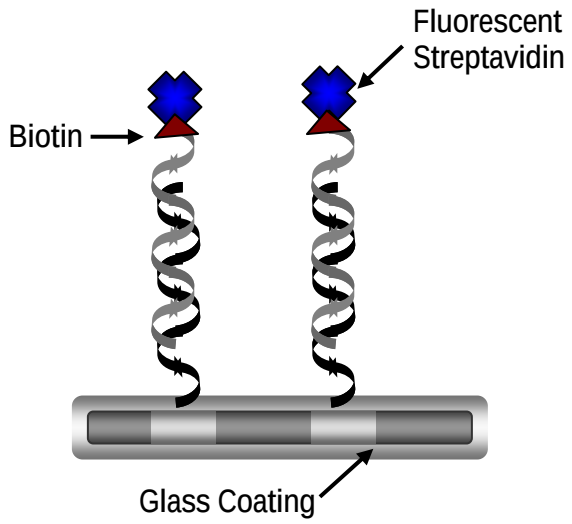

Figure 6.3. Scheme of DNA SNP assay on glass-coated nanowires. Light gray biotin-terminated DNA strand contains the SNP (if applicable). After hybridization of target strands, fluorescently labeled streptavidin protein was added, which binds to the biotin if present.

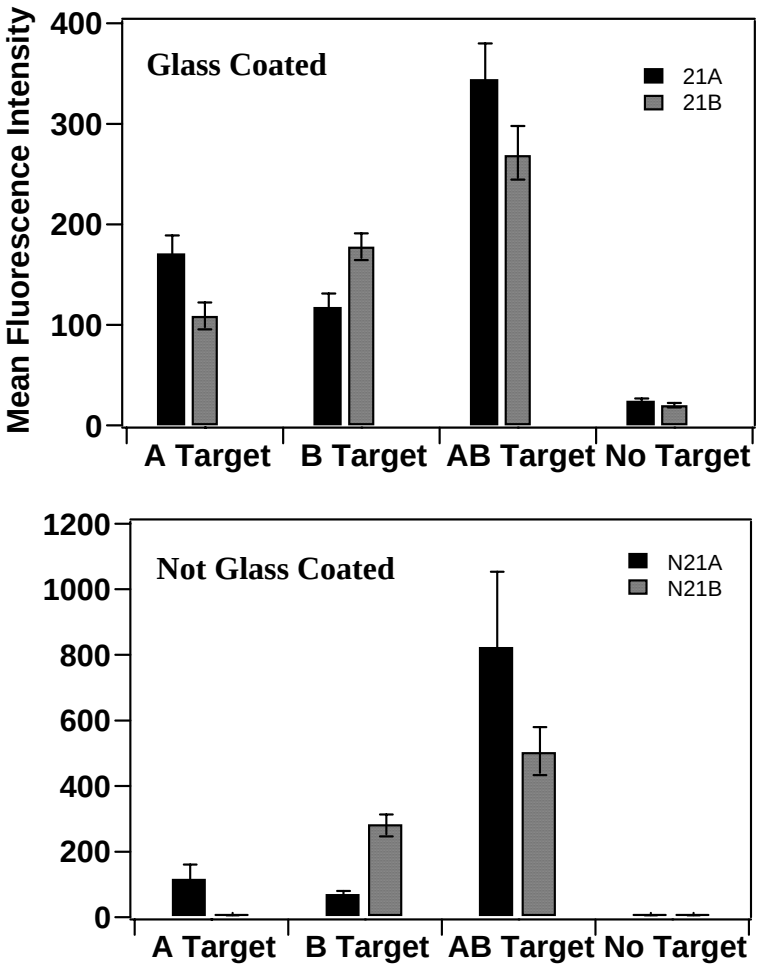

Figure 6.4. 2-plex SNP assay on glass-coated wires (top) and the same assay performed on non glass-coated wires (bottom). The x-axis indicates which target(s) were added to each assay. The error bars shown are the 95 % confidence intervals.

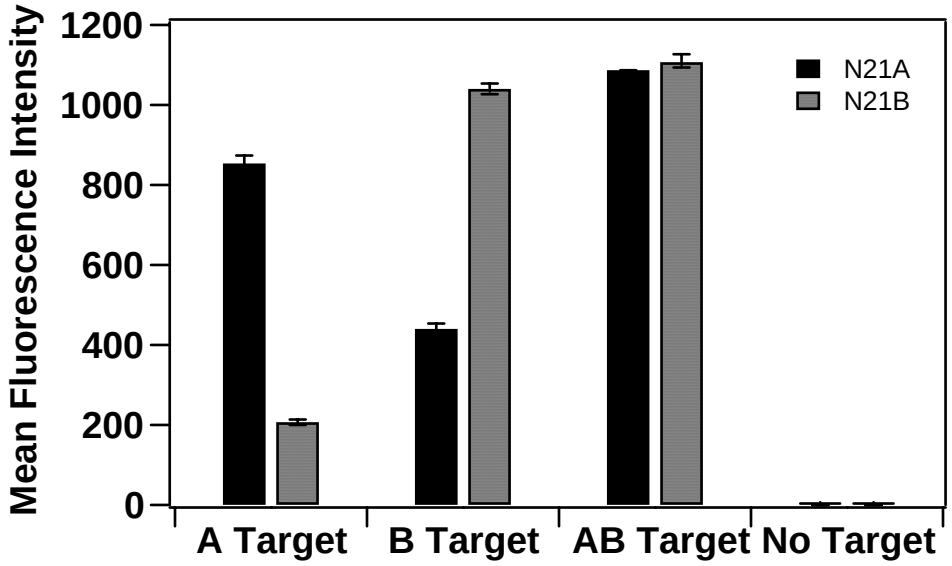

Figure 6.5. 2-plex SNP assay performed on glass-coated wires after optimization of assay conditions. The x-axis indicates which target(s) were added to each assay. The error bars shown are the 95 % confidence intervals.

Chapter 7

Conclusions

Presented in Chapter 2 are data on preserving Ag segments in barcoded metal nanowires after the attachment of biomolecules. This work was important in order to determine if after bioassays are performed on the wires the samples could be retained and re-analyzed at some future time. Also, this research allows for illustration of potential marketing of pre-derivatized barcodes, where probe molecules are already attached, and a clinician would simply hybridize potential targets to multiplexed samples. Without discovering that citrate buffer preserved the Ag segments and still retained the integrity of the bioassay for at least months, pre-derivatized wires would have lasted only about one week before failed performance. This finding has also helped in performing the research presented in Chapters 3 and 4 where molecular beacon probes were attached to metal nanowires. Instead of attaching beacons to nanowires before every experiment, a batch of wires could be coated and stored in citrate buffer for future use without decrease in assay performance or breakage of wires (Chapter 4). The finding of citrate reducing the oxidation of silver and retaining bioactivity is not only useful for our research, but has potential for use in other applications where biomolecules are studied on Ag surfaces (i.e., SERS studies). Because there is potential interest in using citrate buffer to prevent oxidation of Ag in the presence of biological molecules, we have published a paper in *Chemistry of Materials* on this topic.[1]

Chapter 3 revealed data on the distance-dependent effects of metal quenching and unquenching on fluorophores bound to DNA sequences. Here presented were interesting

fluorescence intensity trends dependent upon hybridization efficiency. Hybridization allows DNA to become rigid (not as flexible as when it is single stranded), and therefore moves a fluorophore appended near the end of a DNA sequence further from the metal surface. The difference in proximity to the metal resulted in different fluorescence intensities. It was shown in Chapter 3 that different hybridization efficiencies lead to different trends in fluorescence. Also, since these experiments were conducted on wires containing both Ag and Au, we were able to compare directly the fluorescence trends as a function of distance from the metal on two different metals. Noted here was a reversal in fluorescence patterning on Ag and Au as the fluorophore was positioned further from the surface. Also, reversals in fluorescence patterning were noted when using different dyes positioned at the same distances from the surface. We were able to outline several trends dependent on fluorophore identity, position, and characteristics of the underlying metals. These data have proven useful in designing multiplexed molecular-beacon-style assays where barcoded metal nanowires are used as both distinguishable substrates and quenchers for fluorescence (Chapters 3 and 4). The findings of this study have been accepted for publication in the *Journal of the American Chemical Society*.[2]

Chapter 4 utilizes many of the concepts discovered and explained in Chapter 3, towards the development of nanowire-bound molecular beacon assays. This research, however, was focused on assay performance and molecular beacon design rather than investigating further metal dependent fluorescence trends. Here, distance effects were considered when designing beacon sequence lengths. Surface attachment mechanisms were investigated, as well as effects of hybridization buffer with varying salt content for improved performance. Also shown is a triplexed sealed chamber assay where all targets

and buffer reagents were added at one time along with wires pre-derivatized with beacon probes. The contents were reacted (hybridized) and analyzed without opening the chamber. Discrimination between samples containing targets versus those without targets were practically identical to the same assay performed in a tube with larger mixing volume and opened and transferred to slides for analysis. The advantage of doing closed container analysis is that the risk of contamination is greatly reduced if the sample is not opened for handling or analysis. To eliminate having to coat wires in beacon probes before every experiment, wires were coated and stored in citrate buffer (explained in Chapter 2), for varying lengths of time up to 110 days. Assays performed on these citrate-stored wires showed that there was not a significant decrease in assay performance over time. Therefore, when conducting beacon experiments, it is ideal to coat a large batch of wires in beacon probe and store them in citrate for use in future experiments. The data reported in Chapter 4 have been submitted to the *Journal of the American Chemical Society* for review.[3] A collaborative project on the designed nanowire-bound molecular beacon assays was executed resulting in a publication in *Nanobiotechnology*.[4]

Chapter 5 presents a method of using barcoded nanowires, not as substrates (as reported in previous chapters) but as identifying tags to be attached to glass through complementary DNA binding. The proposed idea was to use striped metal nanowires in a microarray format, which takes the place of fluorophores in traditional multiplexed microarray assays. Shown in Chapter 5 are data suggesting that the discrimination between fully complementary DNA and non-complementary DNA was feasible with ~5 % non-specific binding of wires that were not intended to attach. This level of selectivity for wire binding was achieved by investigating blocking chemistries to avoid the non-

specific interactions. A report containing this proposed microarray format and preliminary data has been published in the *Proceedings of SPIE*.[5] Difficulty in developing these arrays came with the gravitational diffusion of the nanowires to the glass surface, making it challenging not to have wires stick to the surface if they did not have complementary DNA attached. Much effort was employed in trying to avoid these non-selective interactions. A method towards improving such an assay may be to construct a surface that could be electrically charged and to apply a current to drive the nanowires to the surface. Once the wires are allowed to hybridize, it could be imagined that the electrical charge could be reversed to drive the wires that did not hybridize to complementary DNA strands back off of the surface.

Detailed in Chapter 6, are protocols for glass-coating striped metal nanowires to different glass thicknesses. Here it is shown that fluorescence intensity is uniform on wires with a ~100-nm-thick silicon dioxide layer, and the signal effects caused by the underlying metal (explained in Chapter 3) were diminished. The glass coating was shown to provide a barrier against Ag oxidation in the wires and was noted to prevent long wires from bending during use in bioassays. Also in this chapter, a 2-plex assay for selectivity over a DNA sequence differing by only a one base mismatch was shown to perform well on glass-coated wires with little deviation in the fluorescence signal within sample batches (due to eliminating the metal effects on the fluorescence). Since there are numerous advantages to using glass-coated nanowires that improve many of the complicated effects bare metal wires impose on fluorescence, these glass-coated wires should be used in all assays that do not require the use of the metal surface for analysis. The beacon assays presented in Chapter 3 would require the use of bare wires for

quenching. However, it could be imagined that traditional molecular beacons containing both a fluorophore and a quencher molecule could be attached to barcoded metal nanowires for improved multiplexing capabilities.

7.1. References

1. Stoermer, R. L.; Sioss, J. A.; Keating, C. D. *Chem. Mater*. **2005**, *17*, 4356-4361.

2. Stoermer, R. L.; Keating, C. D. "Distance-dependent Emission from Dye-labeled Oligonucleotides on Striped Au/Ag Nanowires: Effect of Secondary Structure and Hybridization Efficiency." *J. Am. Chem. Soc.* (manuscript accepted Aug **2006**).

3. Stoermer, R. L; Cederquist, K. B.; McFarland, S. K. ; Sha, M. Y.; Penn, S. G.; Keating, C. D. "Coupling Molecular Beacons to Barcoded Metal Nanowires for Multiplexed, Sealed Chamber DNA Bioassays." *J. Am. Chem. Soc.* (manuscript submitted Aug **2006**).

4. Sha, M. Y.; Yamanaka, M.; Walton, I. D.; Norton, S. M.; Stoermer, R. L.; Keating, C. D.; Natan, M. J.; Penn S. G. *Nanobiotechnology* **2005**, *1*, 327-335.

5. Stoermer, R. L.; Keating, C. D. *Proceed. SPIE* **2004**, *5588*, 51-58.

VITA

Rebecca L. Stoermer

Education

Ph. D. 2006 The Pennsylvania State University, (University Park, PA), **Chemistry**
B.A. 2001 McDaniel College, (Westminster, MD), **ACS Certified Chemistry**

Selected Award

2005 Braucher Research Award, Penn State University

Experience (Penn State University)

2003 Teaching Assistant - Inorganic Chemistry
2002-2003 Supervisor TA - General Chemistry Labs
2001 TA - General Chemistry Lab

Professional Service (Penn State University)

2004-2005 Graduate Student Think Tank Committee
2004 Student Outreach Programs for Chemistry
2003-2004 Graduate Student Advisory Committee

Publications

1. **Stoermer, R. L.**; Keating, C. D. "Barcoded Nanowires." In *Encyclopedia of Nanoscience and Nanotechnology*, Edition 1; Schwarz, J. A., Marcel Dekker: NY, **2004**; vol 1, pp 205-212.
2. **Stoermer, R. L**.; Keating, C. D. "DNA-directed Assembly of Barcoded Nanowires onto Glass Slides for Biosensing Applications." *Proceedings of SPIE* **2004**, *5588*, 51-58.
3. **Stoermer, R. L.**; Sioss, J. A.; Keating, C. D. "Stabilization of Silver Metal in Citrate Buffer: Barcoded Nanowires and their Bioconjugates." *Chem. Mater.* **2005**, *17*, 4356-4361.
4. Sha, M. Y.; Yamanaka, M.; Walton, I. D.; Norton, S. M.; **Stoermer, R. L.**; Keating, C. D.; Natan, M. J.; Penn, S. G. "Encoded Metal Nanoparticle-Based Molecular Beacons for Multiplexed Detection of DNA." *Nanobiotechnology* **2005**, *1*, 327-335.
5. **Stoermer, R. L.**; Keating, C. D. "Distance-dependent Emission from Dye-labeled Oligonucleotides on Striped Au/Ag Nanowires: Effect of Secondary Structure and Hybridization Efficiency." *J. Am. Chem. Soc.* (manuscript accepted August **2006**).
6. **Stoermer. R. L**.; Cederquist, K. B.; McFarland, S. K.; Sha, M. Y.; Penn, S. G.; Keating, C. D. "Coupling Molecular Beacons to Barcoded Metal Nanowires for Multiplexed, Sealed Chamber DNA Bioassays." *J. Am. Chem. Soc.* (manuscript submitted August **2006**).